POLITECNICO DI TORINO

Collegio di Ingegneria Chimica e dei Materiali

Master of Science Course
in Materials Engineering

Master of Science Thesis

Photocurable vanillin and isosorbide resins for digital light processing 3D printing of reprocessable and recyclable thermosets

Politecnico
di Torino

Supervisors

Professor Marco Sangermano
Professor Minna Hakkarainen
Doctor Anna Liguori

Candidate

Eugenia Oliva

July 2023

Contents

Summary

Al giorno d'oggi, i materiali polimerici costituiscono uno dei pilastri fondamentali della vita moderna dell'uomo. La loro versatilità li rende idonei all'impiego in diversi settori: produzione di imballaggi, elettronica, edilizia, automotive e tanto altro ancora. Per questo motivo il consumo globale di materiali polimerici risulta essere alquanto elevato: 8.3 miliardi di tonnellate sono state prodotte in questo secolo, di cui la metà è stata generata negli ultimi 15 anni. Nello specifico, 390.7 milioni di tonnellate sono state prodotte solo nel 2021. Non sorprende perciò che, come conseguenza, questo abbia portato a un inquinamento da plastica tale da minacciare l'intero ecosistema, compromettendo la biodiversità terrestre e marina. Nel tentativo di risolvere questo problema, gli stati membri delle Nazioni Unite nel 2015 hanno approvato 17 obiettivi di sviluppo sostenibile, noti come Sustainable Development Goals (SDG), e tra questi, in particolare, il dodicesimo obiettivo richiede modelli sostenibili di produzione e consumo. Pertanto, negli ultimi decenni, diversi sforzi sono stati rivolti allo sviluppo di polimeri sostenibili. Molti scienziati hanno accettato la sfida di creare nuovi materiali a partire da fonti bio-rinnovabili. Inoltre, nuove strategie di riciclo sono state introdotte per cercare di raggiungere la circolarità dei materiali prodotti e ridurre lo smaltimento della plastica. Si può infatti parlare di processi di riciclaggio meccanico (riciclaggio secondario) e chimico (riciclaggio terziario). In particolare l'ultimo approccio può coinvolgere la depolimerizzazione dei rifiuti polimerici in specifiche condizioni, con lo scopo di ripolimerizzarli in materiali polimerici con qualità pari ai materiali iniziali (vergini), oppure può mirare alla conversione dei rifiuti polimerici nei building blocks di partenza.

I termoindurenti sono una classe di materiali polimerici, dotati di una struttura reticolata permanentemente, che conferisce loro grandi proprietà meccaniche e termiche. Se però da un lato l'alto grado di reticolazione rende le prestazioni di questi materiali incredibili, dall'altro la struttura chimica ne impedisce un facile riciclaggio. Tuttavia, negli ultimi anni, sono stati effettuati passi in avanti nello sviluppo di termoindurenti riprocessabili e chimicamente riciclabili. In particolare, grande attenzione è stata attirata da una nuova classe di materiali, noti come covalent adaptable network polymers (CANs), in cui si ha l'incorporazione di legami covalenti dinamici all'interno del reticolo polimerico. La capacità di questi legami covalenti reversibili di essere scissi e riformati sotto l'azione di uno stimolo esterno, permette ai CANs di combinare le eccellenti proprietà attribuibili ai termoindurenti con la riprocessabilità dei termoplastici, aprendo nuovi orizzonti verso il riciclaggio di questi materiali.

La presente tesi si pone come obiettivo il design, la sintesi e la caratterizzazione di quattro nuovi termoindurenti ottenuti da fonti bio-rinnovabili, contenenti legami esteri e/o imminici adoperati nella

fase di degradazione e riciclaggio. In particolare, i polimeri sintetizzati sono stati fotopolimerizzati impiegando digital light processing (DLP) come tecnologia di stampa 3D.

Tutti i termoindurenti sono stati prodotti a partire da due building blocks rinnovabili: vanillina e isosorbide. La vanillina è un composto naturale, estratto direttamente dalle piante o sintetizzato a partire dalla lignina; l'isosorbide è un derivato del glucosio.

In una prima fase sono stati introdotti, tramite reazione con anidride metacrilica, dei legami vinilici nei network polimerici dell'isosorbide e della vanillina, ottenendo come prodotti finali isosorbide metacrilato (MI) e vanillina metacrilata (MV) (Schema 2.1 e Schema 2.2 rispettivamente).

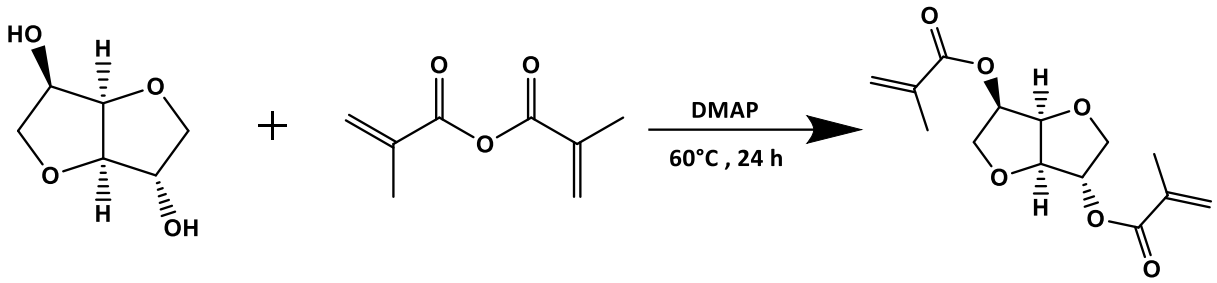

Schema 2.1 Sintesi isosorbide metacrilato.

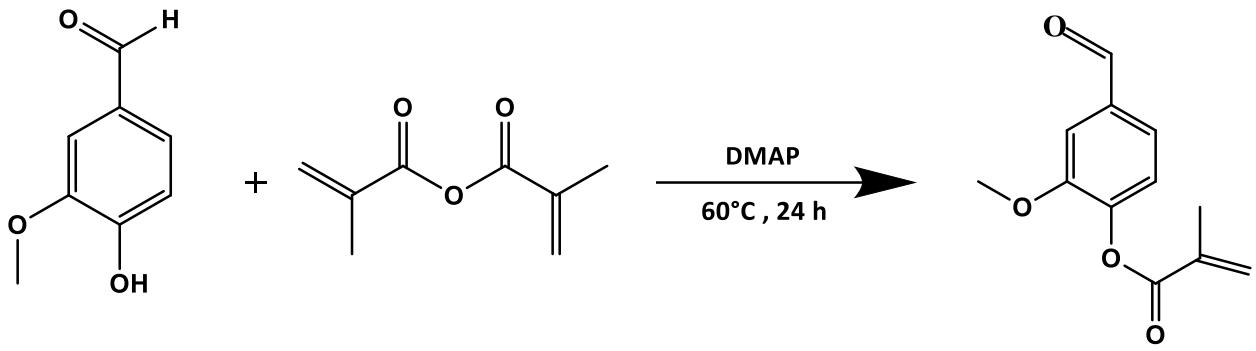

Schema 2.2 Sintesi vanillina metacrilata.

In un secondo momento è stata preparata una resina Schiff base (SB) tramite una reazione di policondensazione tra la vanillina metacrilata e una diammina (Dom) (Schema 2.3).

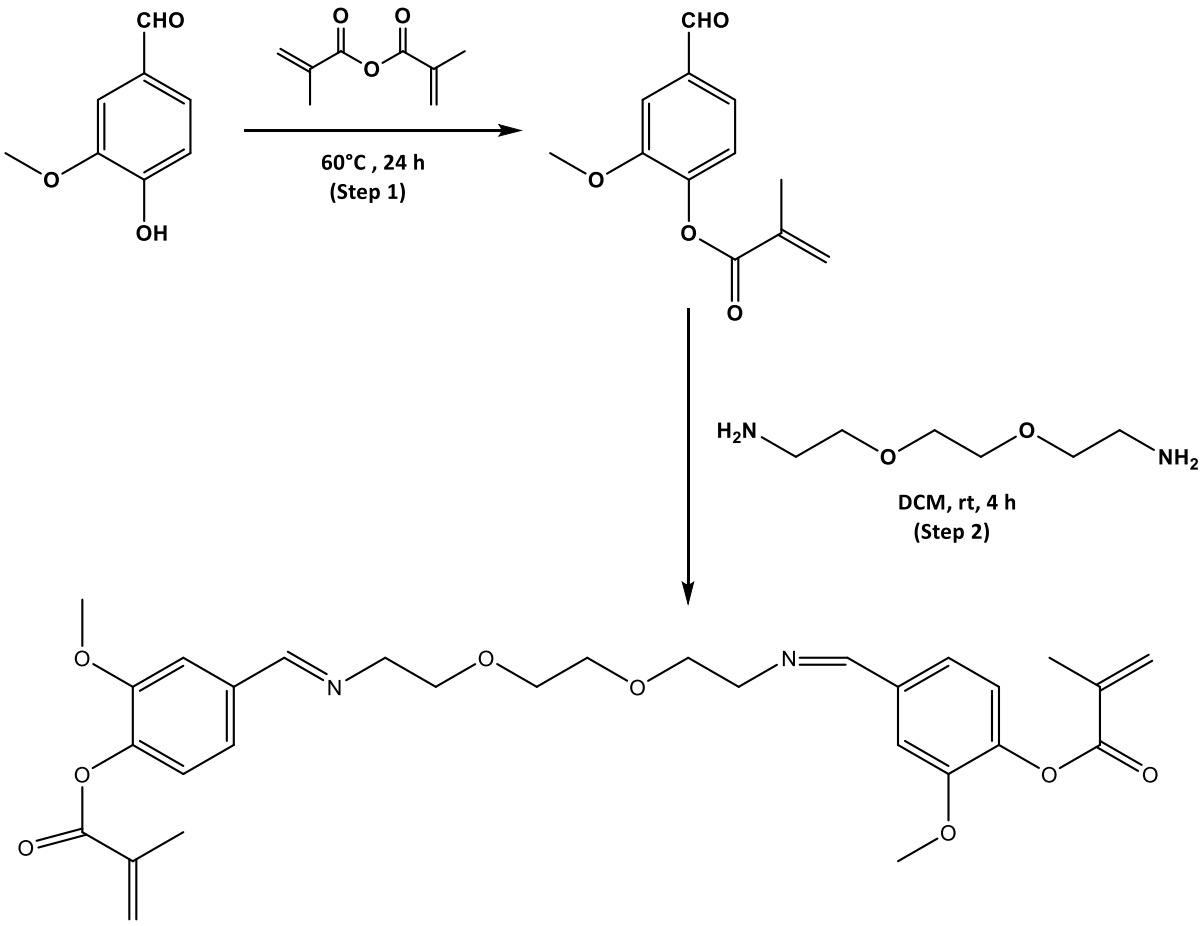

Schema 2.3 Sintesi di resina Schiff base (SB).

La struttura chimica e i gruppi funzionali dei tre monomeri MI, MV e SB sono stati confermati dalle analisi ^{1}H NMR (Figure 3.1, 3.3) e dall'analisi FTIR (Figure 3.2, 3.4). La funzionalizzazione mediante metacrilazione ha reso i polimeri sintetizzati idonei alla stampa 3D tramite DLP.

In seguito sono state formulate tre resine vinilestere mediante miscelazione di MI e MV in diverse concentrazioni: MI50 (50% MI – 50% MV), MI75 (75% MI – 25% MV) e MI100 (100% MI – 0% MV). Una quarta resina imminica, SB_MI50, è stata invece preparata tramite miscelazione di SB (50%) e MI (50%).

La preparazione delle quattro formulazioni impiegate nel processo di stampa 3D ha visto l'aggiunta di un foto-iniziatore (BAPO) e di un diluente reattivo (diclorometano) alle resine di partenza. La capacità, da parte delle resine testate, di essere sottoposte a un processo di fotoreticolazione, è stata valutata tramite l'implementazione delle curve di Jacobs, un importante strumento di caratterizzazione per fotopolimeri altamente reticolati e capaci di subire il processo di polimerizzazione (curing) in maniera rapida. Questo modello determina le proprietà ottiche di una resina quali la profondità di penetrazione (D_p), definita come la distanza che i fotoni percorrono prima dell'assorbimento, e la dose critica (E_c), ovvero l'energia necessaria per indurre la

fotopolimerizzazione e ottenere così un materiale solido. Tali parametri sono ottenuti mediante misurazioni sperimentali: ogni resina viene esposta, tramite l'impiego di una stampante 3D, a dosi di energia crescente, aumentando il tempo di esposizione (90, 95, 98 e 100 secondi) (Figura 3.5). Lo spessore della resina indurita (C_d) viene poi misurato, ed espresso come funzione della dose di irradiazione luminosa (E_{max}) in un grafico semilogaritmico, noto come curva di Jacobs. Tra le curve di lavoro delle resine testate (Figura 3.6), MI75 ha mostrato la pendenza maggiore, corrispondente ad un alto valore della profondità di penetrazione D_p. Questo significa che MI75 mostrerà una maggiore tendenza verso l'overcuring. Invece, SB_MI50 ha esibito, dopo MI100, il valore di dose critica E_c più basso, corrispondente all'intersezione della curva di lavoro con l'asse delle ascisse, ed equivalente a una maggiore efficienza del processo di polimerizzazione (Tabella 3.1).

Una volta stabilita la stampabilità delle resine, queste ultime sono state stampante mediante digital light processing 3D printing nella forma di barre rettangolari e film (Figura 3.7 a,b). I termoindurenti con un maggior contenuto di MI hanno mostrato la tendenza a rompersi più facilmente. Questo è dovuto alla struttura chimica dell'isosorbide, che con il suo anello biciclico e i suoi dioli chirali, conferisce rigidità ai termoindurenti formati. In particolare per MI100 non è stato possibile ottenere dei campioni coerenti a causa del suo comportamento fragile. Dall'altra parte, SB_MI50 ha dimostrato una maggiore flessibilità, dovuta all'introduzione della diammina nel processo di sintesi, che non solo ha consentito la formazione di una resina Schiff-base ma che ha anche svolto il ruolo di spaziatore tra gli anelli aromatici, più rigidi, della vanillina.

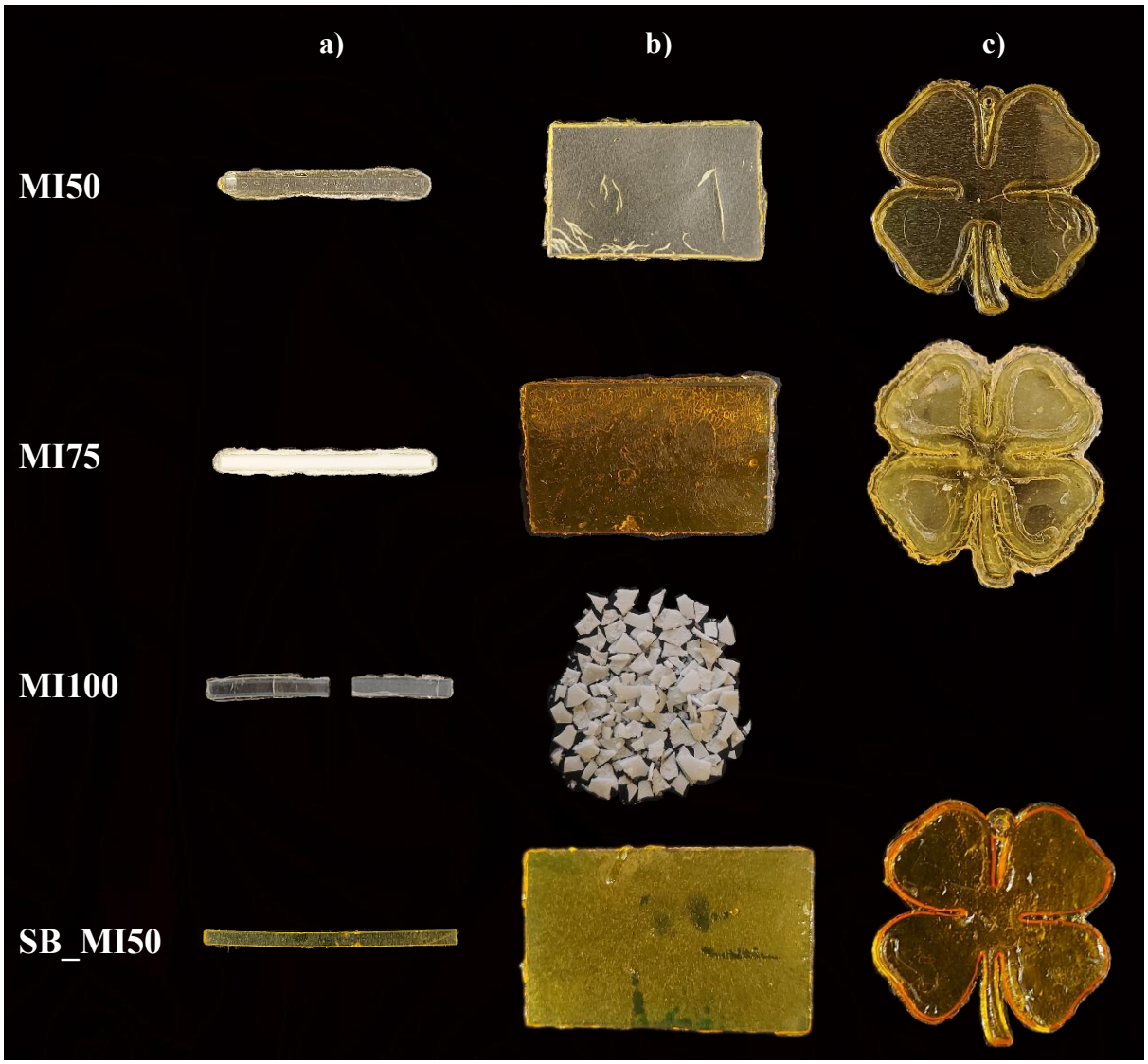

Figura 3.7 Oggetti stampati tramite DLP: a) barre rettangolari, b) film, c) quadrifogli.

L'accuratezza e la precisione di stampa sono state ulteriormente studiate mediante la fabbricazione di campioni a forma di quadrifoglio per tutte le resine, fatta eccezione per MI100 a causa del suo comportamento fragile (Figura 3.7 c). MI75 ha mostrato una tendenza verso l'overcuring, come previsto dalle curve di Jacobs. Dettagli più chiari e nitidi caratterizzano i termoindurenti MI50 e SB_MI50, come il cerchio presente tra le due foglie superiori del quadrifoglio stampato, poco evidente nel termoindurente MI75.

La struttura chimica dei termoindurenti fotopolimerizzati è stata studiata mediante analisi FTIR (Figura 3.8). La riduzione del segnale relativo ai legami vinilici dopo l'irradiazione UV, ha confermato l'avvenuta reticolazione.

L'analisi TGA ha mostrato una buona resistenza termica dei termoindurenti, con una temperatura iniziale di degradazione al di sopra dei 150°C (Figura 3.9a, Tabella 3.2). Dai dati analitici è stato

evidenziato come l'aumento del contenuto di MI influenzi la stabilità termica dei termoindurenti, comportando un aumento della temperatura iniziale di degradazione ($T_{5\%}$) e dell'indice di resistenza al calore (T_s) (Equazione 2.3, Tabella 3.2). Questo risultato può essere spiegato dalla minore densità di reticolazione attribuibile al reticolo polimerico di MI50, e dal fatto che un maggiore contenuto di unità di vanillina, e quindi di gruppi aldeidici, comporti una diminuzione nella resistenza termica. Infatti, mentre il monomero MI ha mostrato una $T_{5\%}$ di ~ 177°C, il monomero MV possiede una $T_{5\%}$ di ~ 138°C. SB_MI50 ha esibito una stabilità termica leggermente più bassa degli altri termoindurenti ($T_{5\%}$ di 159.4°C), dovuta alla minore resistenza termica del monomero SB ($T_{5\%}$ di ~ 120°C). Inoltre una percentuale maggiore di residuo carbonioso (24% circa) è stata riscontrata per il termoindurente contenente legami imminici (SB_MI50), probabilmente dovuta alla maggiore presenza di gruppi aromatici nella struttura. Le analisi termogravimetriche hanno mostrato per tutti i termoindurenti dei picchi di massima velocità di degradazione intorno ai 420°C (Figura 3.9 b, Tabella 3.2).

Le temperature di transizione vetrosa sono state ricavate dall'analisi DSC (Figura 3.10, Tabella 3.3). SB_MI50 ha esibito una T_g di circa 93°C, la più alta tra tutti i termoindurenti. Questo è dovuto alla maggiore flessibilità del monomero di partenza, che ha comportato un grado di reticolazione maggiore. Tra MI50, MI75 e MI100 invece, MI100 ha mostrato la temperatura di transizione più elevata (T_g di circa 64°C), dovuta alla maggiore presenza delle unità rigide dell'isosorbide.

È stato inoltre eseguito il gel content test immergendo i campioni in soluzioni di acetone (Ace), etanolo (EtOH) e diclorometano (DCM) per tre giorni a temperatura ambiente. Tra i quattro termoindurenti testati, solo MI100 è stato leggermente influenzato dalla presenza del solvente (Figura 3.11). La prova ha restituito valori medi di gel content superiori al 87% (Tabella 3.4). Nonostante il minore grado di reticolazione, anche MI50 ha ottenuto sorprendentemente alti valori di gel content (> 92.8%). D'altra parte, MI100 ha mostrato una minore stabilità, con un gel content tra l'88 e il 92%. Questo risultato può essere spiegato dalla minore mobilità della resina, dovuta alla maggiore presenza di unità rigide di isosorbide metacrilato. Infatti durante la polimerizzazione un gruppo metacrilico si lega al reticolo polimerico in formazione, impartendo la fine della catena, dotata di un sito reattivo disponibile (C=C), con una minore mobilità. Maggiore è la conversione di questi siti reattivi, più la catena diventerà statica, fino al punto in cui il sistema sarà bloccato. SB_MI50 ha mostrato i più alti valori di frazione insolubile (> 96.5%), suggerendo un alto grado di reticolazione, con valori di gel content simili a quelli ottenuti in lavori precedenti per un termoindurente formato solo da unità del monomero SB, dimostrando che le unità di MI non hanno influenzato la resistenza finale al solvente.

Le analisi di caratterizzazione meccanica hanno previsto prove di trazione per i termoindurenti MI50, MI75 e SB_MI50. MI100 non è stato soggetto a tale caratterizzazione a causa del suo comportamento fragile e dell'impossibilità di ottenere dei provini integri per effettuare la prova. Le curve

rappresentative sforzo deformazione per i materiali testati sono mostrate in Figura 3.12, e i valori di modulo elastico, sforzo e deformazione a trazione sono riportati nella Tabella 3.5. Alti valori di modulo elastico sono stati ottenuti per tutti i termoindurenti, e in particolare per MI50 e MI75 (2026.8 e 1925.0 MPa rispettivamente). Le proprietà meccaniche dei covalent adoptable network (CANs) può essere definita come funzione della densità di reticolazione, della struttura del monomero di partenza, e della natura dei legami covalenti dinamici presenti nel reticolo. Per questo i monomeri più rigidi dei termoindurenti MI50 e MI75 hanno portato al raggiungimento di sforzi a trazione più elevati (47.0 e 58.2 MPa rispettivamente), oltre che a maggiori valori di modulo elastico. La struttura chimica di SB_MI50, e in particolare la maggiore flessibilità del suo monomero di partenza SB, impartita dalla catena derivata dalla diammina nel processo di sintesi, può essere ritenuta responsabile per il modulo elastico minore ottenuto (1163.8 MPa). SB_MI50 ha inoltre esibito una maggiore deformazione a rottura rispetto agli altri termoindurenti.

MI50, MI75 e SB_MI50 sono stati riprocessati meccanicamente. Il riprocessamento è stato realizzato effettuando in un primo step la riduzione dei film termoindurenti mediante macinazione. In un secondo momento è stato aggiunto un catalizzatore di transesterificazione, acetato di zinco ($Zn(OAc)_2$), con una concentrazione del 5%. Quest'ultimo è stato successivamente miscelato insieme ai frammenti dei termoindurenti, e il mix risultante è stato posto in uno stampo e riprocessato mediante pressatura a caldo a 180°C per 30 minuti, sotto l'azione di 3 MPa. L'aggiunta del catalizzatore è stato un parametro determinante per la formazione di un nuovo film omogeneo, specialmente nel caso di MI50 e MI75. Per questi due termoindurenti infatti, una prima strategia per il riciclaggio meccanico ha previsto la riduzione dei campioni in frammenti più piccoli (senza l'uso di un mortaio), e il successivo riprocessamento mediante pressatura a caldo, in assenza di catalizzatore. Utilizzando questa procedura non è stato possibile ottenere dei nuovi film termoindurenti omogenei. La presenza di $Zn(OAc)_2$ facilita, nel caso di MI50 e MI75, le reazioni di scambio tra i legami esteri (transesterificazione), ottenendo la ridistribuzione della connettività delle catene polimeriche, e come dimostrato precedentemente, l'assenza di gruppi idrossili liberi non impedisce la realizzazione di queste reazioni. Nel caso di SB_MI50 invece, i legami che rendono il termoindurente in esame riprocessabile, oltre a quelli esteri, sono quelli imminici, mediante una reazione di metatesi.

Per quanto riguarda il riprocessamento di MI50 e MI75 a 180°C, sono stati provati due diversi tempi di lavorazione: un'ora e 30 minuti. Dato il successo nell'ottenere un nuovo film termoindurente dopo riprocessamento per un'ora, è stato provato un tempo inferiore, sia per constatare la fattibilità del riprocessamento in tali condizioni, sia per cercare di diminuire il rischio di degradazione del materiale. Come è possibile vedere infatti in Figura 3.13, i film ottenuti dopo 30 minuti possiedono

un colore più chiaro rispetto a quelli riprocessati per un'ora, suggerendo un minor danneggiamento del materiale e una maggiore preservazione della struttura chimica del reticolo polimerico. A questo punto è stato interessante osservare come il tempo di lavorazione abbia influito sulle proprietà meccaniche del materiale. In Figura 3.14 si può notare come il primo ciclo di riciclaggio meccanico abbia comportato in entrambi i casi (un'ora, 30 minuti) una diminuzione generale delle proprietà meccaniche. Tuttavia, questa riduzione risulta essere più evidente nel caso dei campioni riprocessati per un tempo maggiore. In particolare, MI50 ha esibito un modulo di Young di 392.7 MPa dopo un'ora di riprocessamento, e di 624.3 MPa dopo 30 minuti. Inoltre, con un tempo di lavorazione più breve il processo risulta essere meno energivoro.

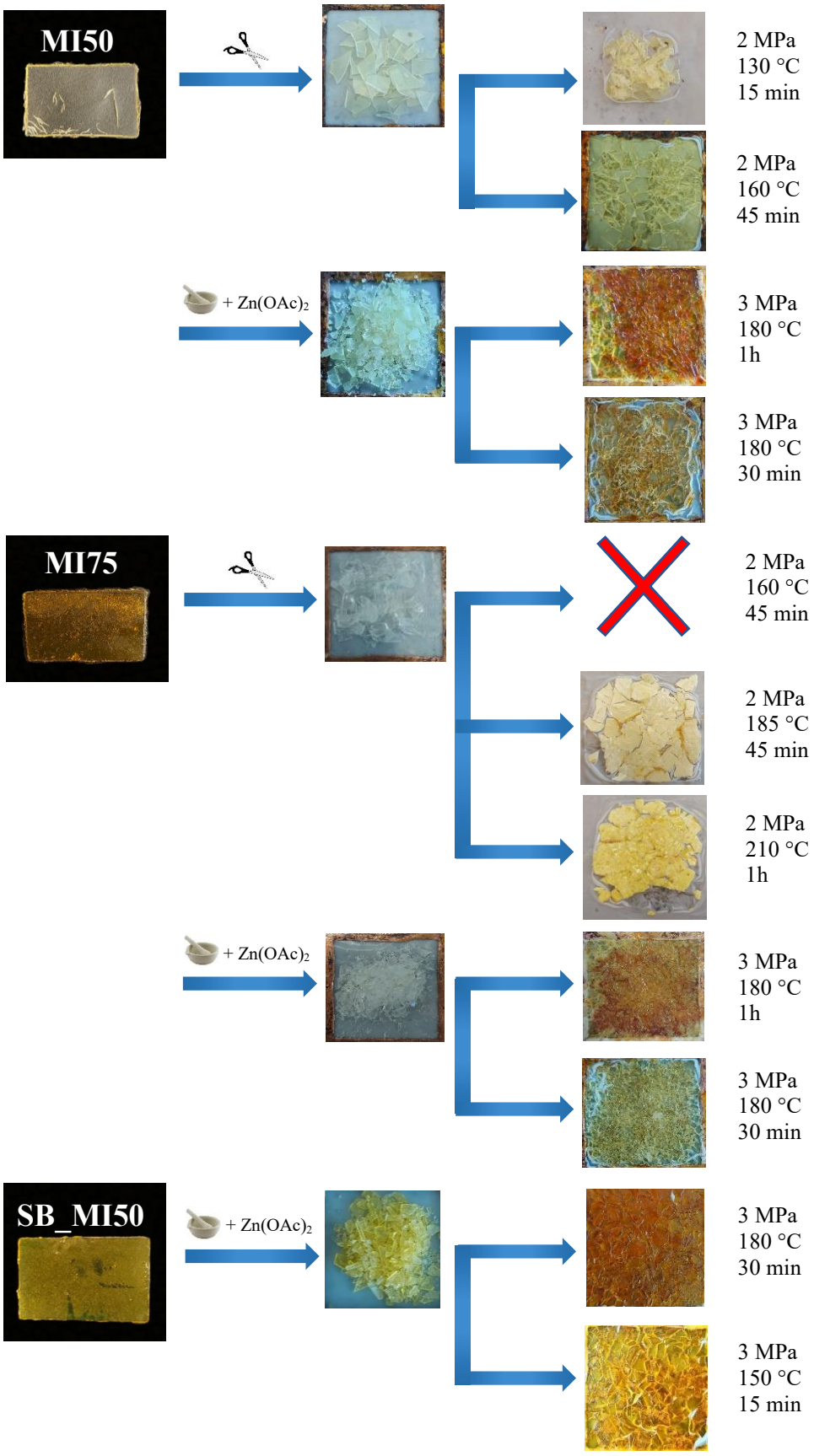

Figura 3.13 Procedura per il primo ciclo di riciclaggio meccanico di MI50, MI75 e SB_MI50.

Nel caso di SB_MI50 invece, il riciclaggio meccanico è stato eseguito non solo a 180°C, ma anche ad una temperatura inferiore pari a 150°C. In entrambi i casi è stato possibile ottenere un film omogeneo, e, ancora una volta, un cambiamento di colore è stato osservato impiegando una temperatura maggiore, indicando un maggior danneggiamento del materiale (Figura 3.13). La possibilità di ottenere un film termoindurente riprocessando il materiale a 150°C, dimostra la possibilità di attivare lo scambio tra i legami imminici a temperature più basse. La stessa cosa non può essere detta per le reazioni di transesterificazione, che richiedono temperature più elevate, come confermato da lavori precedenti. Infatti, in questo progetto, i tentativi di riprocessare MI50 a 130°C e a 160°C, e MI75 a 160°C, 185°C e 210°C, (senza l'uso di un catalizzatore), sono falliti, come visibile in Figura 3.13. Il modulo elastico di SB_MI50 è stato preservato dopo un primo ciclo di riciclaggio meccanico, sia a 180°C che a 150°C, esibendo un valore di 1088.8 MPa e 1229.7 MPa rispettivamente (Figura 3.15). Tuttavia una riduzione è stata osservata sia nello sforzo a trazione che nella deformazione a rottura.

Facendo un confronto tra tutti i campioni riprocessati dopo un ciclo, si può dire che SB_MI50 sia non solo il materiale con il più alto modulo elastico dopo riprocessamento, ma anche l'unico che sia stato in grado di conservare il modulo elastico originale. Una riduzione nel modulo di Young pari al 69% e 78% è stata infatti osservata nel caso DI MI50 e MI75 rispettivamente, mentre SB_MI50 ha mostrato una diminuzione del 6%. Questo significativo calo nelle proprietà meccaniche dei termoindurenti riprocessati MI50 e MI75 può essere spiegato dalla ristretta mobilità delle catene polimeriche, che ha implicato una inadeguata fusione tra i frammenti macinati, come osservato in lavori precedenti. D'altra parte, la maggiore flessibilità delle catene nel network polimerico di SB_MI50 e la minore energia di attivazione, correlata alla natura della reazione di scambio chimico, possono essere considerate responsabili del minore modulo elastico iniziale e della sua maggiore conservazione dopo riprocessamento.

Un secondo ciclo di riciclaggio meccanico è stato eseguito sui termoindurenti testati. La procedura impiegata è la medesima adottata nel primo ciclo: macinazione dei campioni, aggiunta del catalizzatore $Zn(OAc)_2$, successivo trasferimento della miscela in uno stampo e sua pressatura a caldo. Poiché le proprietà meccaniche di MI50 e MI75 dopo un primo riprocessamento per un'ora, sono risultate meno performanti rispetto ai campioni riprocessati per 30 minuti, il secondo ciclo di riciclaggio meccanico per questi materiali è stato direttamente eseguito a 180°C per 30 minuti, sotto l'azione di 3 MPa. Per SB_MI50 invece è stato effettuato un secondo ciclo sia a 180°C che a 150°C. I film riprocessati meccanicamente sono mostrati in Figura 3.16, mentre le curve di sforzo e deformazione e le proprietà meccaniche ottenute dopo prove di trazione sono visibili in Figura 3.17.

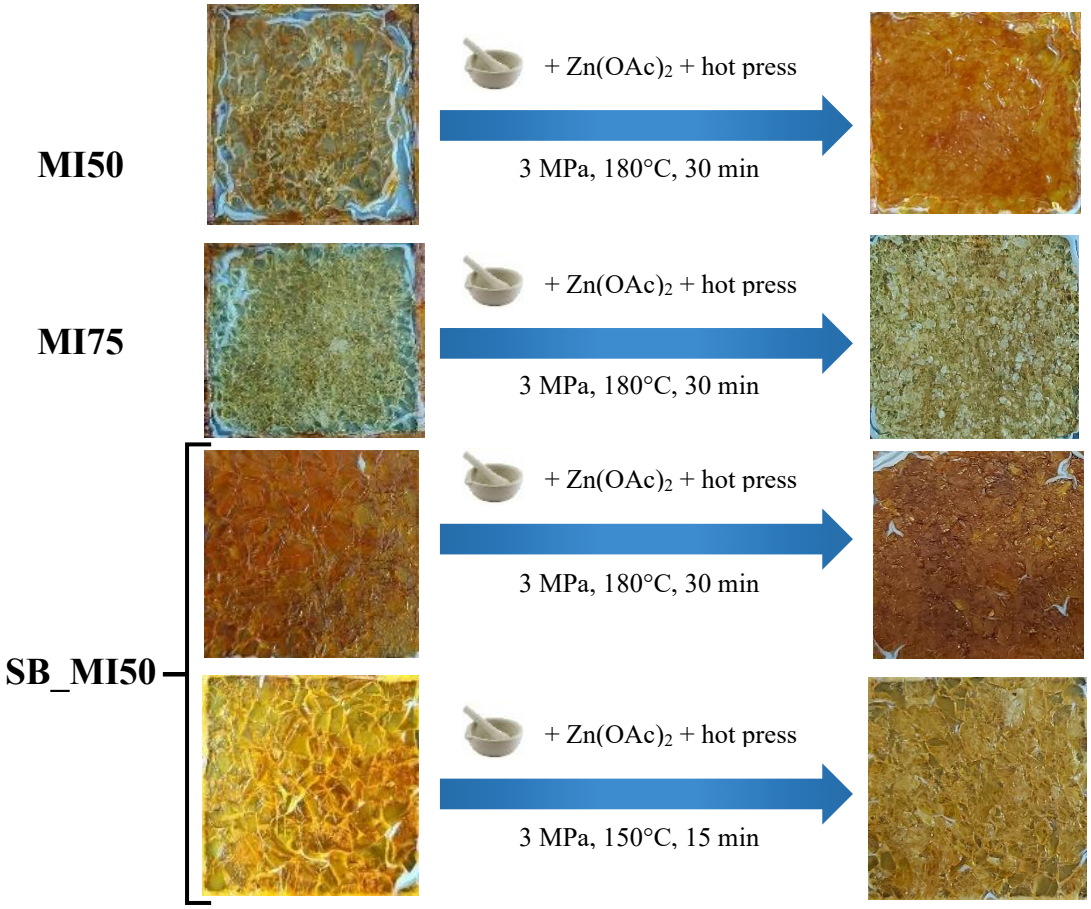

Figura 3.16 Procedura per il secondo ciclo di riciclaggio meccanico di MI50, MI75 e SB_MI50.

Nel caso di MI50 e MI75, un leggero incremento del modulo elastico è stato osservato, raggiungendo 681.3 MPa e e 562.0 MPa rispettivamente. Questo risultato è dovuto alla presenza di un piccolo numero di siti ancora reattivi all'interno del reticolo polimerico che hanno subito, durante il riprocessamento nella pressa a caldo, una reazione di polimerizzazione (post-curing). Tutti i campioni riprocessati due volte hanno inoltre mostrato valori di sforzo a trazione simili a quelli dei campioni riprocessati una volta. Una riduzione nella deformazione a rottura è stata invece riscontrata per tutti i campioni fatta eccezione per SB_MI50 riprocessato a 150°C.

Un'analisi FTIR è stata condotta sui campioni riprocessati due volte (Figura 3.18). Negli spettri di MI50 e MI75 sono stati individuati a 1721 cm^{-1} i picchi relativi ai gruppi esteri (C=O). Inoltre è stato possibile osservare alcuni cambiamenti dovuti alla presenza di $Zn(OAc)_2$. Il picco a 1595 cm^{-1}, associato ai legami aromatici C=C, presenta una piccola spalla (picco supplementare), dovuto probabilmente alla formazione di un complesso del carbossilato di zinco (Figura 3.19), con una banda di assorbimento tra 1560 e 1520 cm^{-1} e un picco a 1408 cm^{-1}. Inoltre, è stata osservata la comparsa di una banda di assorbimento relativa ai gruppi ossidrilici (OH), e la riduzione del segnale degli esteri negli spettri dei termoindurenti MI50 e MI75 dopo due cicli di riciclaggio. Per il campione

riprocessato di SB_MI50 è stato individuato il segnale relativo ai gruppi esteri, e quello correlato alle vibrazioni aromatiche. Alcuni cambiamenti sono stati osservati, come l'apparizione di un picco a 1674 cm^{-1} che potrebbe essere dovuto ad uno shift del segnale imminico o del gruppo aldeidico, suggerendo la probabile avvenuta apertura di una parte del materiale.

La degradazione dei termoindurenti è stata valutata immergendo i campioni in diversi solventi.

MI50 e MI75 sono stati immersi in metanolo, NaOH 0.5M e NaOH 1M. La soluzione NaOH ha portato alla solubilizzazione dei campioni dopo circa 3 ore alla temperatura di 100°C. In questo caso quindi, è stata impiegata una soluzione alcalina per depolimerizzare il materiale mediante clivaggio di legami covalenti, e nello specifico di legami esteri secondari scindibili tramite l'applicazione di uno stimolo esterno, quale l'aumento di temperatura. La soluzione così ottenuta è stata acidificata mediante aggiunta di HCl, fino al raggiungimento di un pH pari a 2. Dopodiché, il solvente è stato evaporato, ed è stato aggiunto dell'etanolo in agitazione al materiale recuperato, in modo da rendere possibile una filtrazione del sale formatosi nel processo. Alla polvere così ottenuta è stato aggiunto il catalizzatore $Zn(OAc)_2$ con una concentrazione del 5% e il mix risultate è stato riprocessato mediante pressatura a caldo a 120°C per 30 minuti, sotto l'azione di 3 MPa. Il riciclaggio chimico di MI75 ha avuto successo, permettendo la formazione di un nuovo film, come visibile in Figura 3.20. Per MI50 invece non è stato possibile riformare un nuovo film, in quanto il materiale è risultato essere molto colloso.

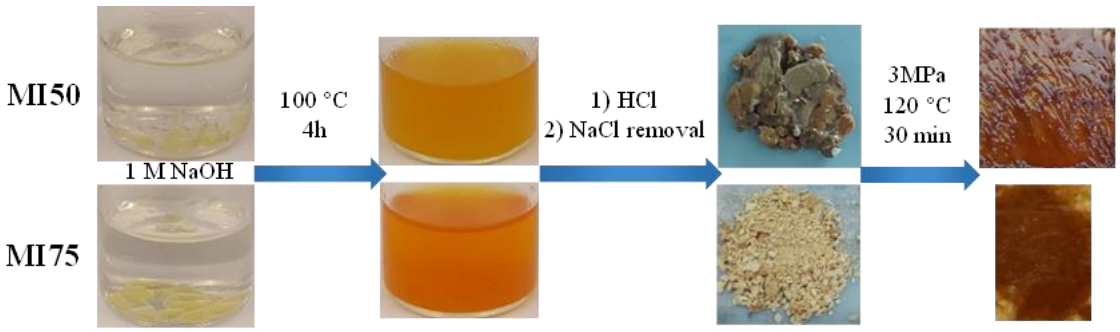

Figura 3.20 Procedura di riciclaggio chimico per MI50 e MI75.

Un'analisi FTIR ha mostrato negli spettri del materiale ottenuto dopo degradazione chimica di MI75 (MI75 deg), e dopo riprocessamento (MI75 CR), la conservazione dei legami esteri (Figura 3.21). Per MI50 invece l'analisi FTIR del materiale ottenuto dopo degradazione è risultata in due spettri diversi (MI50 deg1 e MI50 deg2) (Figura 3.22). Nello spettro di MI50 deg1, la presenza di picchi nelle stesse bande di assorbimento della vanillina suggerisce la presenza di questo building block. Sia in MI50 deg1 che MI50 deg2 è stata rilevata una banda di assorbimento, ascrivibile ai gruppi OH, mentre il segnale relativo alle funzioni estere è risultato assente o presente con una bassa concentrazione, implicando una completa depolimerizzazione del termoindurente in soluzione alcalina. L'inabilità di

MI50 ad essere chimicamente riciclato in un nuovo film può essere dovuta alla minore presenza di unità di isosorbide metacrilato (MI) rispetto a MI75, e quindi ad un numero inferiore di siti reattivi disponibili per il riprocessamento.

Il film ottenuto dal riciclaggio chimico di MI75 è stato sottoposto ad una prova di trazione. Le curve di sforzo e deformazione, e le proprietà meccaniche sono illustrate in Figura 3.23. Tale materiale ha esibito un modulo elastico di 393.7 MPa, comparabile a quello del termoindurente dopo uno e due cicli di riciclaggio meccanico. Inoltre si è osservato un elevato valore di deformazione a rottura, comparabile con quello del materiale originale. La diminuzione delle proprietà meccaniche rispetto al termoindurente di partenza può essere dovuta a una incompleta reazione di esterificazione tra i gruppi idrossilici e gli acidi carbossilici.

Per quanto riguarda il termoindurente contenente legami imminici, SB_MI50, la degradazione chimica è stata valutata immergendo i campioni in HCl 0.1 M, NaOH 1 M e diammina (Dom). Come visibile in Figura 3.24, nessuna degradazione è stata osservata nella soluzione HCl 0.1 M, nonostante la presenza nel reticolo polimerico di legami imminici, che in precedenti lavori sono risultati sensibili a solventi acidi. Questo è probabilmente dovuto all'alto grado di reticolazione del materiale e alla maggiore presenza di gruppi aromatici. La soluzione alcalina NaOH 1 M ha invece portato ad una parziale degradazione, agendo probabilmente sui legami esteri. Con l'impiego della diammina come solvente, è stato infine possibile ottenere una completa depolimerizzazione del materiale dopo 6h a 80°C. Questo risultato è stato conseguito grazie alla sensibilità dei legami imminici alle ammine, tra cui avviene una reazione di transaminazione. La soluzione così ottenuta è stata precipitata in acqua, e dopo una filtrazione sottovuoto, è stato possibile raccogliere una polvere, mostrata in Figura 3.24c. Gli oligomeri ottenuti, contenenti gruppi amminici finali, sono stati impiegati per la preparazione di una nuova resina, tramite aggiunta di vanillina metacrilata (MV) e fotoiniziatore (BAPO). Questo mix di reazione è stato riprocessato mediante pressatura a caldo a 140°C per 30 minuti, sotto l'azione di 3 MPa, ottenendo come risultato finale un film omogeneo, mostrato in Figura 3.26.

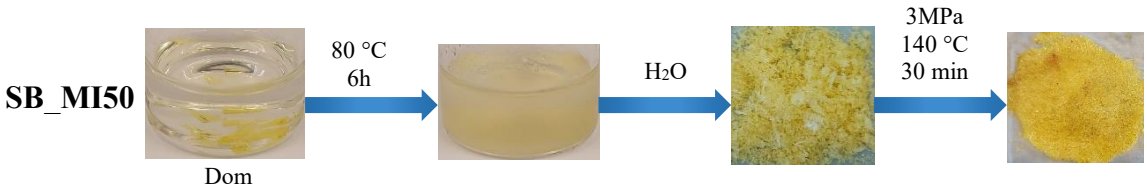

Figura 3.26 Procedura di riciclaggio chimico per SB_MI50.

Un'analisi FTIR è stata condotta su SB_MI50 in seguito a degradazione chimica (SB_MI50 deg), e in seguito a riprocessamento (SB_MI50 CR). Nello spettro di SB_MI50 deg, mostrato in Figura 3.25, è stato possibile individuare i picchi a 1721 e 1645 cm^{-1}, relativi rispettivamente ai gruppi esteri e

imminici. Inoltre la comparsa di una banda di assorbimento a 3500 cm^{-1} (relativa alle ammine primarie) conferma l'avvenuta reazione di transaminazione. In seguito a riprocessamento, non si è riscontrata la presenza del gruppo aldeidico della vanillina metacrilata, dimostrando che quest'ultima ha reagito interamente con il materiale riciclato. Ciononostante, si è potuta ancora osservare una banda di assorbimento, seppur ridotta, a 3500 cm^{-1}; questo significa che i gruppi amminici rimanenti nel reticolo polimerico potenzialmente avrebbero potuto reagire ulteriormente in presenza di vanillina metacrilata.

Le proprietà meccaniche di SB_MI50 CR sono state determinate ancora una volta tramite prove di trazione, e il modulo elastico risultante (1045 MPa) si è dimostrato essere comparabile con quello del materiale vergine (1163.8 MPa) (Figura 3.27).

In conclusione, a partire da fonti rinnovabili è stato possibile sintetizzare con successo quattro resine fotopolimerizzabili termoindurenti, tre delle quali contenenti legami esteri, e la quarta contenente legami sia esteri che imminici. Queste resine sono state successivamente stampante mediante digital light processing 3D printing. Tutti i termoindurenti hanno mostrato una buona stabilità termica ed eccellente resistenza solvente, indicatrice di un alto grado di reticolazione. La presenza di legami covalenti dinamici, esteri e/o imminici, all'interno del reticolo polimerico, ha consentito la realizzazione di due cicli di riciclaggio meccanico. Quest'ultimo ha comportato una diminuzione delle proprietà meccaniche nei termoindurenti MI50 e MI75. Il termoindurente contenente legami imminici, SB_MI50, ha invece mostrato la conservazione del modulo elastico iniziale. Inoltre è stato possibile realizzare il riciclaggio chimico di MI75 e SB_MI50, ottenendo dal materiale depolimerizzato dei nuovi film omogenei tramite pressatura a caldo. I termoindurenti fotopolimerizzabili, termicamente riprocessabili e chimicamente riciclabili, sintetizzati in questo lavoro, rappresentano un'attraente alternativa ai polimeri derivati da risorse petrolifere, ma richiedono ulteriori indagini per il raggiungimento della scalabilità del processo a livello industriale.

Introduction

1.1 Plastics

Polymers, ordinarily referred to as “plastics”, are one of the fundamental materials on which human daily life is based. Many benefits support their usage: they are affordable, versatile, resilient, formable and lightweight materials with both good thermal and mechanical properties. They are widely employed in food packaging, construction, electronic appliances, transport industries, and many other fields. For these reasons, the global plastic production turned out to be quite staggering: 390.7 million tonnes (Mt) of plastic were consumed only in 2021 (Figure 1.1a)[1].Among the 8.3 billion tons of plastic waste cumulated over the last century[2], half of it has been generated just in the past 15 years.[3] The gigantic amounts of plastic pollution represent a threat to the human health and the ecosystem, affecting both terrestrial and freshwater biodiversity. As a matter of fact, a new microbial habitat, known as plastisphere, has been formed, and this is only one of the several negative impacts of plastics on the planet.[4] Furthermore, the foundation of this material can be found in fossil feedstock, and nowadays the global production capacity of bio-based/bio-attributed plastics is only about 1.5% of the total amount of plastic generated (Figure 1.1b).

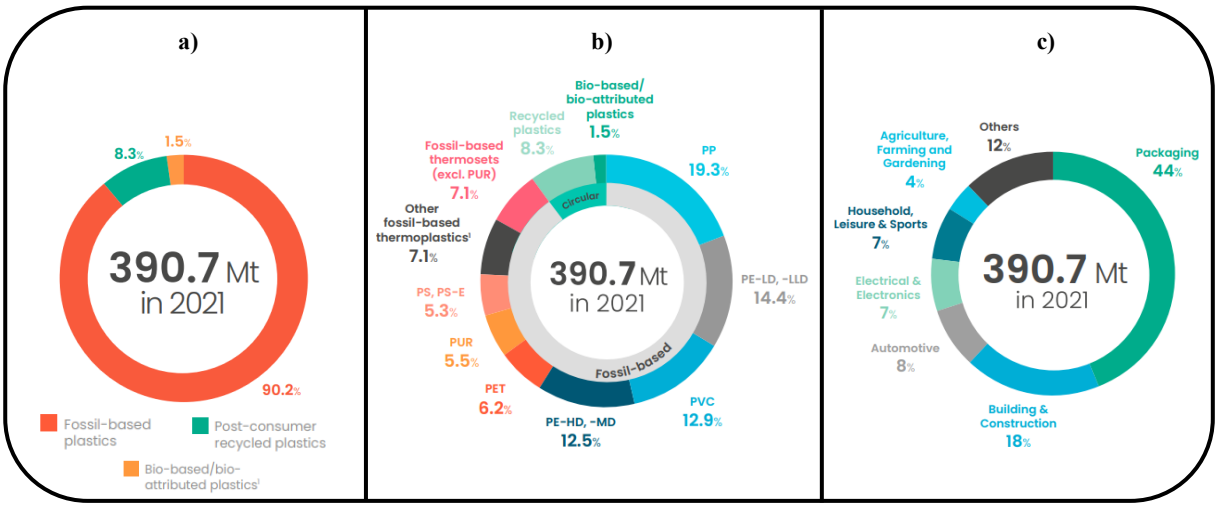

Figure 1.1 a) World plastics production in 2021, and its distribution b) by type and c) application. [1]

This system does not align with the directions imparted by the Sustainable Development Goals, adopted by The United Nations Member States in 2015, and particularly with Goal 12, which demands sustainable consumption and production patterns.[5] Nevertheless, in the last decade, several efforts have been made towards the development of sustainable polymers, and many scientists have accepted the challenge to make new materials starting from renewable bio-based resources.[6],[7]

Furthermore, in order to build a more circular material economy and reduce the disposal of plastic, new sustainable recycling strategies have been introduced, referring not only to mechanical recycling processes (secondary recycling) but also to chemical recycling methods (tertiary recycling).[8] The last approach can involve either the depolymerization of the polymer waste under specific conditions to subsequently repolymerize them into virgin-quality polymeric materials, or the conversion of the polymer waste into the starting building blocks (repurposing).[9]

In the described field is located this work, with the aim of contributing to the research on new sustainable bio-based thermosets.

1.2 Sustainable Thermosetting Polymers

Thermosets are polymer materials with covalently bonded repeating units in the three-dimensional network formed after crosslinking reactions during the polymerization process (curing).

The densely crosslinked structure prevents the material from reaching a fluid state upon heating. Therefore, once the starting resin, either in a liquid, soft or viscous state, is turned into an infusible and insoluble network after curing, the material cannot be reshaped or reprocessed any longer. This aspect makes the recycling process more difficult and challenging.

Because of their chemical structure, thermosets have outstanding properties: high modulus, high strength, hardness, dimensional stability and good both thermal and chemical resistances. They have been widely employed in different applications such as coatings, adhesives, electronic packaging, building and constructions, aerospace industry, composites etc.[10] Among all polymers produced, 18% is represented by thermosets,[11] with an annual production of ~65 million tons.[12]

This class of material is usually synthesized starting from fossil resources, but in the last few years, researches have been done on bio-based thermosetting resins, attracting a lot of attention as a step towards sustainability. Nevertheless, a lot of challenges are involved in their development: the need to transform biomass into simpler units (platform chemicals or building blocks); the necessity to establish the problematic relationship between chemical structure and performance for the bio-based polymers; endow bio-based thermosets with reuse and recyclability, increasing their service lifetime.[13]

1.3 Renewable building blocks

Renewable feedstock represents a green alternative to the dwindling petroleum resources for the synthesis of sustainable thermosetting materials. However, the direct usage of natural resources is not always possible, due to their complex structures: the transformation of biomass into versatile platform

chemicals is needed. This transition can involve three different pathways: biorefinery, chemical conversion, or extraction and purification. [13] Among the most valuable bio-based platform chemicals, two important classes can be identified: carbohydrate-derived compounds and lignin-based aromatic phenols. In this thesis, two different renewable building blocks belonging to these classes are employed to synthesize thermoset materials: isosorbide and vanillin.

1.3.1 Isosorbide

According to the U.S. Department of Energy, isosorbide is among the top 12 most prominent renewable platform chemicals.[14] It is obtained from glucose, one of the major carbohydrate-derived feedstocks available, generally produced through hydrolysis of cellulose or starch. Specifically, isosorbide can be yielded through the hydrogenation of glucose into sorbitol and its subsequent dehydration (Scheme 1.1).[13]

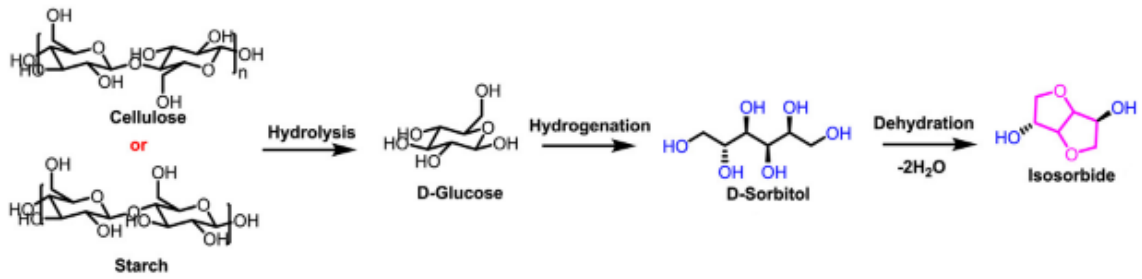

Scheme 1.1 Production flow of isosorbide.[13]

Because of its bicyclic ring structure and chiral diols, isosorbide imparts polymers with rigidity and high glass transition temperature.[15], [16] It has been widely employed for the development of thermoplastic materials such as polyesters, polyurethanes, and polycarbonates. Furthermore, it has been used in thermosetting applications to produce of precursors for unsaturated polyester resins and, soon after modification, as a reactive diluent.[14]

1.3.2 Vanillin

Vanillin is a promising aromatic platform chemical for a wide range of polymers. The most significant amount of vanillin supply in the world (85%) is produced using guaiacol and glyoxylic acid as (petroleum) intermediates in the process.[17] Nevertheless, despite the difficulties in the extraction and purification steps, nowadays, with the enhancement in wood biorefinery technology, 15% of the overall vanillin production derives from Kraft lignin. Lignin is the second most plentiful polymer in nature after cellulose: it represents 25% of the available biomass, [18] and it makes up ~30% of

wood.[19] Presently, vanillin is one of the only commercialized aromatic building blocks produced from biomass, able to replace the traditional fossil-based aromatic monomers. [17], [19]

A chemical modification of vanillin is required in order to enable the monomer's polymerization.[19] For instance, a methacrylation reaction can be performed, introducing double bonds in the structure, making the material a good fit for vinyl ester applications. Another approach could be coupling two vanillin derived compounds into a diaromatic monomer with the same functional groups at the ends of the chain.[20], [21], [22]

This vanillin derivative can be the basis for new sustainable polymers with interesting properties, due to their rigid aromatic structure.

1.4 Covalent Adaptable Network (CANs)

Recyclability has always been seen as an almost unreachable goal for thermosetting materials, due to their permanent crosslinked structure. Nevertheless, in the last years, steps have been made towards the design of reprocessable and chemically recyclable thermosets. Incorporating dynamic covalent bonds in the polymer network led to the development of a new class of material, coined by Bowman and coworkers as covalent adaptable network (CANs) polymers. CANs combine the excellent thermal and mechanical properties of thermosets with the reprocessability of thermoplastics, taking advantage of the reversible covalent bonds, which are able to undergo bond cleavage and reformation under the action of an applied stimulus.[8], [23] Depending on the exchange mechanism, CANs can be categorized into two different classes: dissociative and associative CANs.

In the dissociative CANs, a two-step crosslink exchange reaction takes place, with first the breakage and then the reformation of the linkages in a new position (Figure 1.2).

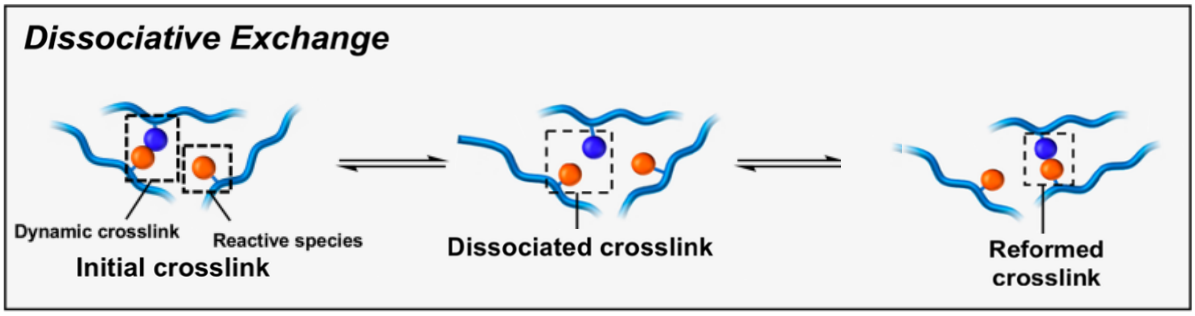

Figure 1.2 Depiction of dissociative bond exchange mechanism.[24]

This mechanism leads to a temporary decrease in the crosslinking density, with a significant change in the macromolecular structure that can enhance the sensitivity of the material to the action of solvents at high temperatures.[23]

The second class of covalent adaptable network polymers is the associative CANs. In these polymers, the crosslinking density is maintained during the exchange reaction, since the new bond formation precedes bond breaking through the formation of an associative intermediate (Figure 1.3).[24],[25] This helps to preserve the connectivity and the integrity of the polymer network even at high temperature and in the presence of solvents.[23], [24]

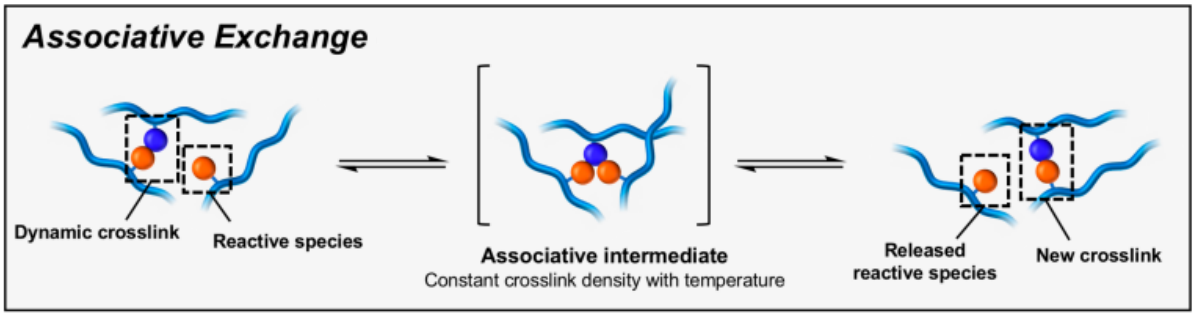

Figure 1.3 Depiction of associative bond exchange mechanism. [24]

In 2011 Leibler and coworkers developed associative CANs based on transesterification exchange reactions that exhibited a viscosity-temperature relationship similar to vitreous silica, reason for which these materials were named Vitrimers.[8],[24] Upon heating, vitrimers display a decrease in the viscosity, retaining the integrity of the network and imparting the material with reprocessability.

1.4.1 Transesterification reaction

In the last decades, a large variety of covalent adoptable networks has been developed by introducing multiple associative dynamic bonds, such as ester, disulfide, vinylogous urethane, imine and siloxane. The transesterification, shown in Scheme 1.2, is acknowledged as one of the most commonly used exchange reactions, due to the vast supply of compounds containing ester groups and hydroxyl moieties. [8]

Scheme 1.2. Transesterification reaction. [8]

The presence of a catalyst can help the rearrangement of the network at elevated temperatures, affecting the kinetics of the exchange reaction. The increase in the catalyst concentration does not impact the activation energy of the relaxation process. Furthermore, the addition of the catalyst can be avoided whenever the concentration of hydroxyl groups is high enough.

1.4.2 Schiff base reaction

The Schiff base reaction is one of the widely exploited processes for forming dynamic covalent bonds, specifically of imine bonds. The imine bonds can be synthesized with a dissociative mechanism through a condensation reaction between a primary amine and an aldehyde or a ketone (Scheme 1.3a). After the removal of water, imines can be further involved in two exchange reactions with associative dynamic character: imine methasis (Scheme 1.3b) or transimination (Scheme 1.3c). These dynamic covalent bonds impart the material with recyclability, reprocessability and self-healing properties. [8], [26]

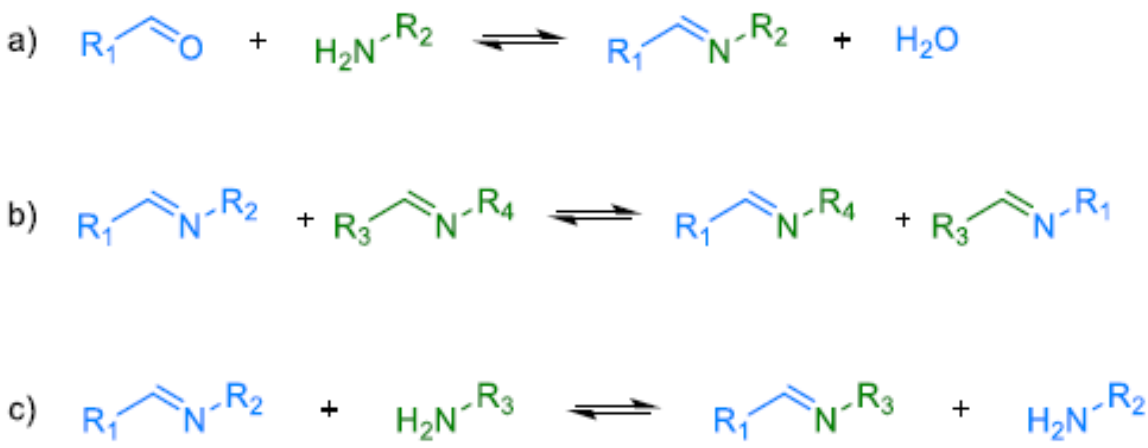

Scheme 1.3 Reversible reaction of imine: a) condensation reaction, b) imine methasis, c) transimination.[8]

1.5 Digital Light Processing 3D Printing

Additive manufacturing is a technology that produces three-dimensional objects by adding material layer by layer. This process is used for rapid prototyping and fabricating items with highly complex geometries. [27] Furthermore, the possible on-site manufacturing can reduce the waste production and the emissions due to the product's transportation from the factory to the facility, leading towards an environmentally friendly fabrication process. [28] In particular, in this work, a vat photopolymerization technique, such as digital light processing (DLP) 3D printing, was used to produce biobased thermosets. This method is known for its high printing efficiency and accuracy, together with its fast

printing speed and high resolution.[29] The main components of the Digital Light Processing (DLP) 3D printer are shown in Figure 1.4a. A UV light source is used as energy input for the polymerization of a photosensitive resin, stored in a resin tank. Thanks to a digital micromirror device (DMD), a sequence of UV images is projected on the resin surface, allowing the polymerization of a complete layer, with a single exposure. Therefore, multiple exposures are employed to build the object. It is important to specify that, a cured resin attached to the build platform is obtained after a first exposure, with a thickness defined as cured depth (C_d) (Figure 1.4b). During the printing process, the layer thickness is actually determined by the appointed slice thickness (S_t), decided by the user. When the cured depth is thicker than the slice thickness, an overcuring process takes place, since the UV light penetrates not only the uncured resin but also part of the formerly cured layer (Figure 1.4c, d). This phenomenon is fundamental for the crosslinking between layers and, therefore, for additive manufacturing. The described overlapping area is defined as the overcure depth O_d. [27]

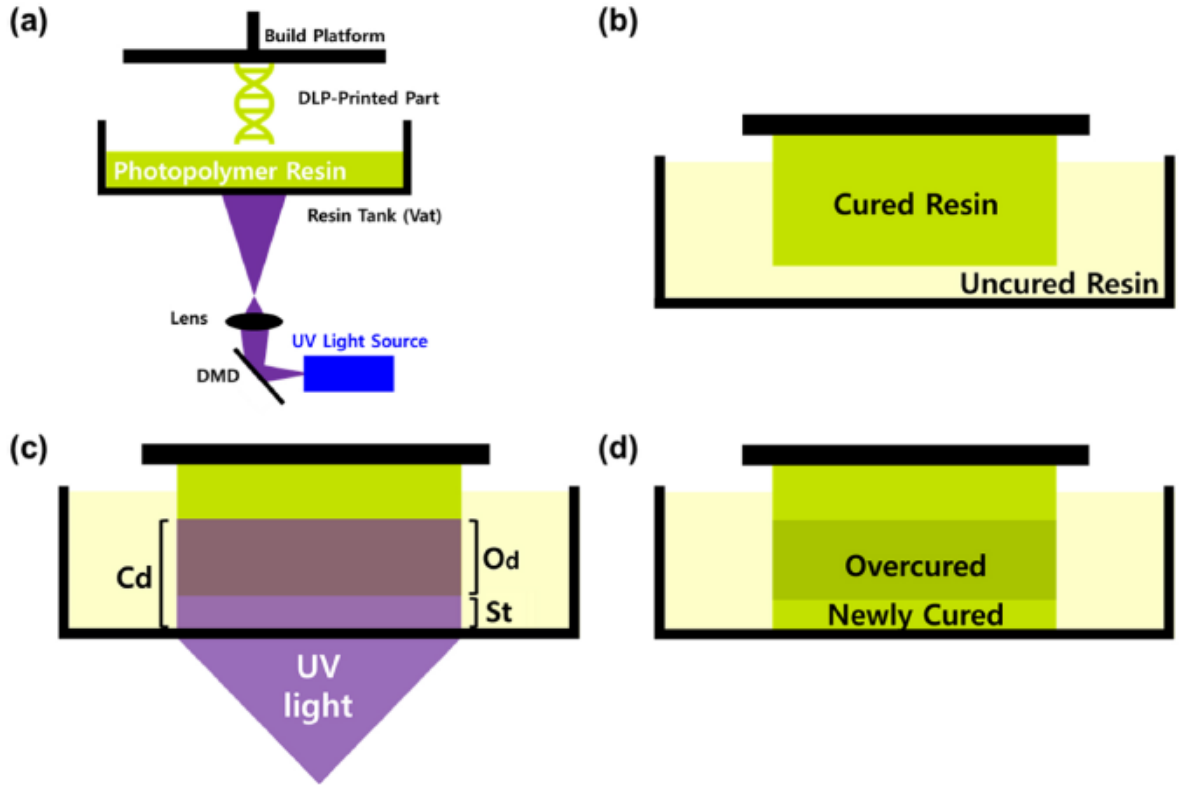

Figure 1.4. a) Main components of the Digital Light processing (DLP) 3D printer, b) Printing state before UV irradiation for adhesion of a new layer, c) As UV light penetrates to cured depth (Cd), the uncured fresh resin undergoes 'curing', whereas the already-cured resin undergoes additional polymerization, or 'overcuring', where the overcured depth (Od) is determined by the UV light energy, resin's absorption coefficient, and the slice thickness (St), d) Successful adhesion of a new layer as a result of sufficient crosslinking between the layers due to overcuring effect. [27]

Recently, with the increasing implementation of the DLP 3D printing technique, the development of sustainable photopolymer was required. New photocurable resins were designed starting from renewable resources such as soybean oil, starch, terpenes and lignin.[30],[31] Furthermore, the discovery of CANs represented an opportunity for thermosetting materials to solve the limit regarding their recycling and reuse. [32] Zhang and coworkers, for example, produced a sustainable acrylate resin for DLP 3D printing, with functional groups present in the polymer network, useful for both the photopolymerization and the dynamic exchange reactions, endowing the material with good repairability.[33]

In this field is located this thesis project, to print new biobased thermosetting materials, designed for circularity, thanks to the introduction of dynamic covalent bonds in the polymer network.

Materials and methods

2.1 Materials

Isosorbide (98%, Sigma-Aldrich), vanillin (99%, Sigma-Aldrich), 2,2'-(Ethylenedioxy)bis(ethylamine) (Dom) (≥97%, Thermo Fisher), methacrylic anhydride (MAA) (≥94%, Sigma-Aldrich), 4-(dimethylamino)pyridine (DMAP) (≥99 %, Sigma-Aldrich), sodium bicarbonate (≥99.7%, Sigma-Aldrich), sodium hydroxide (NaOH) (99%, VWR Chemicals), magnesium sulfate ($MgSO_4$) (≥99%, VWR), phenylbis(2,4,6-trimethylbenzoyl)-phosphine oxide (BAPO) (97%, Sigma-Aldrich), acetone (Ace) (≥99%, VWR), ethanol (EtOH) (100%, VWR), methanol (MeOH) (100%, Fisher Scientific), hydrochloric acid (HCl) (37%, Sigma-Aldrich), dichloromethane (DCM) (≥99%, Fisher Scientific), deuterated chloroform ($CDCl_3$) (99.8 atom % D, VWR), zinc acetate ($Zn(OAc)_2$) (99.99% , Sigma-Aldrich).

2.2 Synthesis of vinyl ester resins

2.2.1 Methacrylation of Isosorbide

Isosorbide (30.00 g, 205.28 mmol), MAA (63.28 g, 410.48 mmol), and the catalyst DMAP (1.44 g, 11.78 mmol) were added to a 250 mL round-bottom flask with a magnetic stir bar, and placed in a preheated oil bath. The reaction was carried out at 60°C for 24 h (Scheme 2.1). The resulting mixture was cooled to room temperature, diluted in DCM, and sequentially washed with a saturated aqueous solution of sodium bicarbonate (sat.aq. $NaHCO_3$), 0.5 M NaOH, 1M NaOH, and water. The washing procedure was performed twice, and the organic phase was dried over $MgSO_4$, and concentrated under reduced pressure using rotavapor, yielding isosorbide methacrylate (MI) as a pale-yellow oil (86% yield).

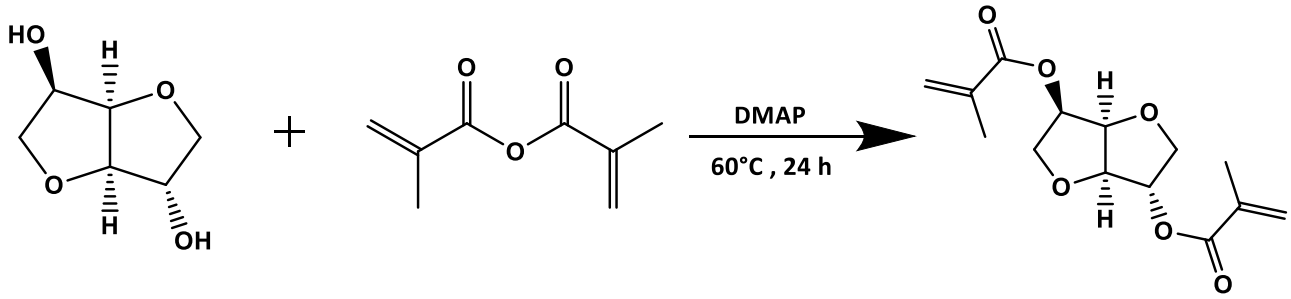

Scheme 2.1 Synthesis of MI from Isosorbide and MAA.

2.2.2 Methacrylation of Vanillin

Vanillin (30.43 g, 200 mmol) and methacrylic anhydride (33.95 g, 220.22 mmol) were added to a 250 mL round bottom flask, together with a catalyst, DMAP (0.17 g, 1.39 mmol). The reaction mixture was heated to 60°C and allowed to react for 24 h (Scheme 2.2). The resulting mixture was then diluted in DCM, and sequentially washed with a saturated aqueous solution of $NaHCO_3$, 0.5 M NaOH, 1.0 M NaOH and water. The washing procedure was performed twice, then the organic phase was dried over $MgSO_4$, and concentrated under reduced pressure, yielding methacrylated vanillin (MV) (white powder, 72% yield).

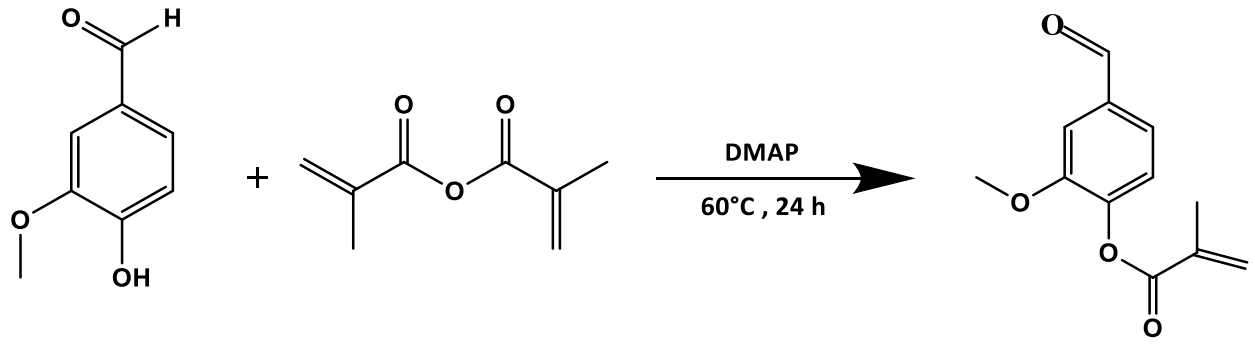

Scheme 2.2 Synthesis of MV from Vanillin and MAA.

2.3 Synthesis of vanillin-based imine resin

A Schiff-based resin was synthesized by performing a polycondensation reaction between methacrylated vanillin and a diamine. MV (8.8 g, 20 mmol) and Dom (1.78 g, 12 mmol) were placed in a 100 mL round-bottom flask, together with DCM, and put under stirring at room temperature for 4h (Scheme 2.3). The reaction mixture was then washed with 1 M NaOH and water, and the organic phase was dried over $MgSO_4$ and concentrated under reduced pressure by using rotavapor, yielding a product named SB (96.3% yield).

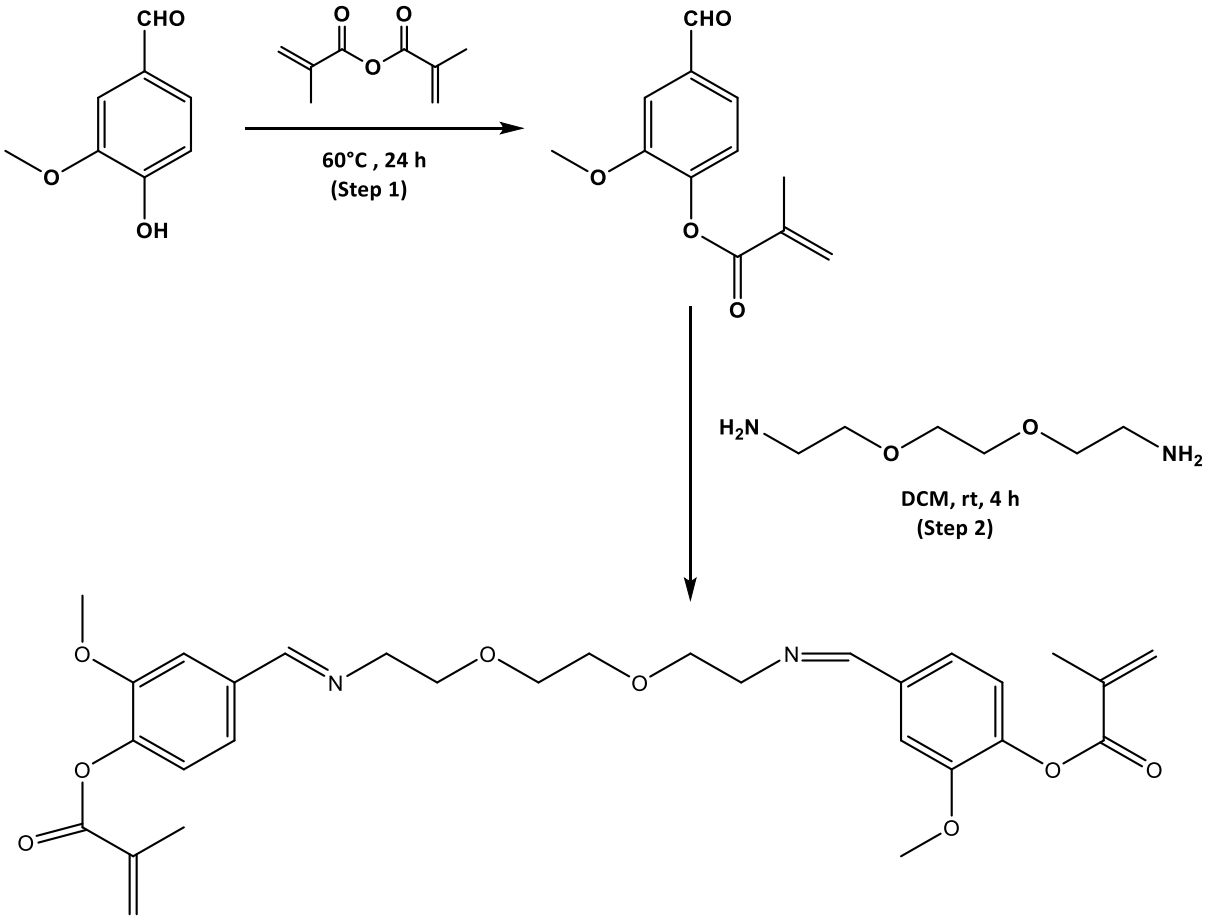

Scheme 2.3. Synthesis of vanillin-based imine resin SB.

2.4 Preparation of photocurable resins

Three vinyl ester resin formulations were prepared by mixing MI and MV, the starting monomers, in different ratios: 50-50 % w/w (MI50), 75-25 % w/w (MI75), and 100-0% w/w (MI100) of respectively MI and MV.

The imine resin formulation was prepared by mixing 50% w/w of MI and 50% w/w of SB, and it was named SB_MI50.

All the resins were diluted in DCM with a concentration of 100% w/v (weight of the resin with respect to the volume of the solvent). The solutions were stirred at room temperature, until obtaining a homogeneous mixture. The photo-initiator BAPO, with a concentration of 5% w/w (weight of BAPO with respect to the weight of the resin), was added and stirred until complete solubilization.

2.5 Jacobs working curves

The photocurability of the resins was evaluated by performing monotonous experiments, using an Asiga MAX UV DLP 3D printer, shown in Figure 2.1.

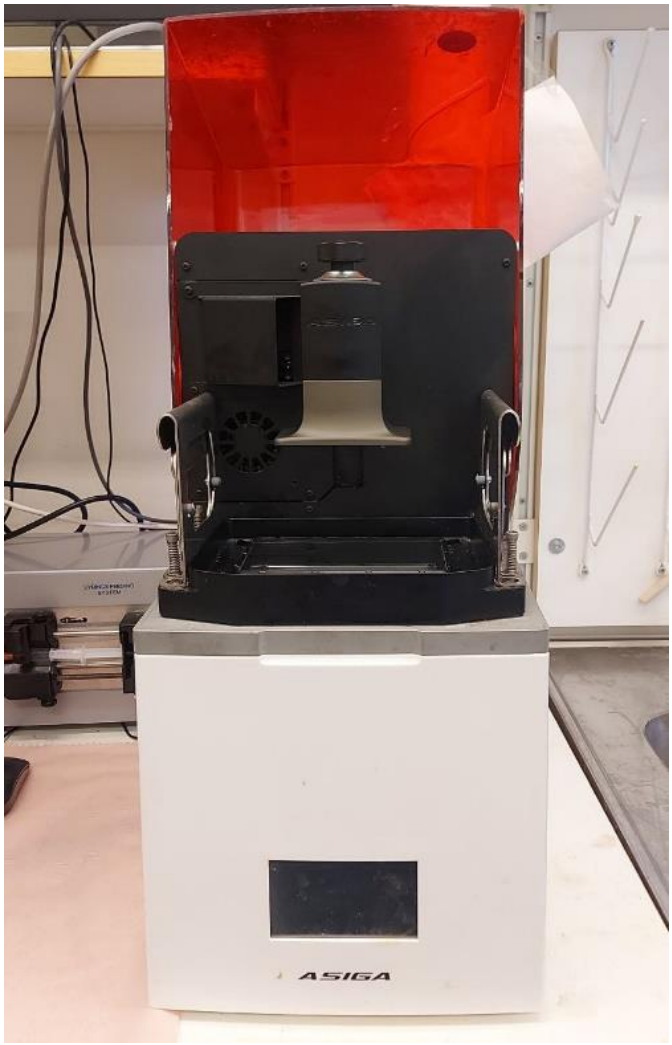

Figure 2.1 DLP 3D printer.

The resins solutions were poured in the vat, where the UV light was projected for one layer, using different exposure time. The obtained cured disks, where removed from the vat and cleaned with DCM. The cured thickness (C_d), defined as the thickness of the cured resin after the exposure of its surface to the UV dose, was measured with a thickness gauge. The cured depth C_d is directly proportional to the natural logarithm of the light irradiation dosage E_{max}, according to the following equation (Equation 2.1):

$$C_d = D_p \ln(E_{max}/E_c) \quad \textbf{(2.1)}$$

where D_p is the penetration depth at which the irradiance is reduced to 1/e of the surface intensity, E_{max} is the product of the UV light intensity per unit area and exposure time, and E_c is the critical energy required for the initiation of the polymerization, related to the gel point of the resin.[34], [27] These datasets were used to develop a semi logarithmic plot of C_d and E_{max}, resulting in a straight line, called Jacobs working curve.[25] Jacobs' study is based on three fundamental assumptions: the light absorption of the photopolymer resin follows the Beer-Lambert law, the laser irradiance distribution is Gaussian, and the transition of the resin from liquid to solid occurs at the gel point. [34] The Jacobs working curves for each tested resin were established. These curves are a powerful tool for the characterization of highly crosslinked photopolymers with fast curing behavior (digital curing behavior), giving information on the materials' curing characteristics, and specifically on the dose needed to cure a certain layer and the penetration depth for the resin of use. [35]

2.6 Digital Light Processing 3D Printing

The prepared photocurable resins (MI50, MI75, MI100 and SB_MI 50) were 3D-printed by using Asiga MAX UV DLP 3D printer (light emission at λ=385 nm, nominal xy pixel resolution of 27 μm). Specimens in the shape of both rectangular bars (26.00 mm x 1.53 mm x 0.75 mm) and films (31.71 mm x 19.77 mm x 0.75 mm) were fabricated. The UV light intensity and the slice thickness (thickness/layer) were set at 26.69 mW/cm^2, and 0.050 mm. The exposure times were 100, 94, 86, and 87 seconds for respectively MI 50, MI 75, MI 100, and SB_MI 50. The samples were printed at 385 nm wavelength and 25°C. The time required for the printing of one sample, in both cases, was close to 30 minutes. The photocured thermosets were subsequently immersed for a few seconds in DCM, in order to remove the remaining monomer residue. A post-curing treatment followed, using a 36 W UV-curing lamp (Asiga UV-lamp) (Figure 2.2), with a wavelength of 385 nm and an irradiation intensity of 2.6 ± 0.4 mW/cm^2, with a post-curing time of 3 min/side. The same procedure was adopted for printing the thermosets in a more complex geometry.

Figure 2.2 UV-curing lamp.

2.7 Characterization methods

2.7.1 Nuclear Magnetic Resonance

Nuclear Magnetic Resonance (NMR) spectroscopy is a powerful characterization tool used for the determination of the organic molecules' chemical structure. This technique is based on the absorption of electromagnetic radiation by the molecule's nuclei, in the radio-frequency region.[36] The most used nuclei are ^{1}H and ^{13}C. If a molecule is placed in an external magnetic field, the electrons surrounding the nuclei generate their own magnetic fields, that run antiparallel to the external one, leading to a reduction in the net magnetic moment. This difference between the magnetic fields is called nuclear shielding.[37] All protons are shielded by their electron clouds, to an extent that is directly proportional to the electron clouds' density, which depends on the chemical environment. These variations lead to a difference in the frequencies, referred to as chemical shifts (δ). The frequencies at which the nuclei resonate scale with the applied magnetic field's strength, and the higher the electron cloud's density of protons, the lower the resonance frequency will be. To elude these problems, the chemical shifts are expressed as the difference between the adsorption position of the tested proton and the one of a reference proton, following Equation 2.2:

$$\delta_{ppm} = 10^{6} * \frac{\upsilon_S - \upsilon_R}{\upsilon_{RS}} \quad (\mathbf{2.2})$$

where υ_S is the frequency of the signal, υ_R is the frequency of the reference, and υ_{RS} is the frequency of the spectrometer. [36] A one-dimensional (1D) NMR spectrum is a plot of the chemical shifts on the x-axis, versus the peak intensities on the y-axis, and it allows both the determination of the type of chemical groups within a molecule (via chemical shift), and the quantity of each type of nucleus present (via peak intensity).[38] All the samples were characterized by ^{1}H NMR. The instrument used is an Avance 400 (Brucker, U.S.A) spectrometer with a proton frequency of 400 MHz (Figure 2.3). The solvent selected, used as the reference compound, was deuterated chloroform ($CDCl_3$), showing a peak at 7.26 ppm.

Figure 2.3 NMR instrument.

2.7.2 Attenuated total reflection – Fourier-transform infrared spectroscopy

The analysis of a sample via Attenuated total reflection (ATR) – Fourier-transform infrared (FTIR) spectroscopy leads to the acknowledgment of the examined material's chemical structure. This technique plays an important role in determining the degradation effects on a compound. Additionally, it has the advantage of requiring a small amount of material, without the need for sample preparation. The analysis consists in pressing the sample against the ATR crystal (zinc selenide or germanium crystal), which has a higher refractive index. An IR beam, directed into the crystal, is internally reflected after the contact with the tested sample, creating an evanescent wave, whose

energy can be partially absorbed by the sample itself. The attenuated energy is returned to the detector, and used by the instrument for the creation of an IR spectrum.[39] All the ATR-FTIR spectra were recorded in the range of 4000 – 600 cm^{-1} with a resolution of 4 cm^{-1}, by using a PerkinElmer Spectrum 2000 Fourier Transform Infrared spectrometer (Norwalk, CT), equipped with an attenuated total reflection (ATR) sampling accessory, visible in Figure 2.4.

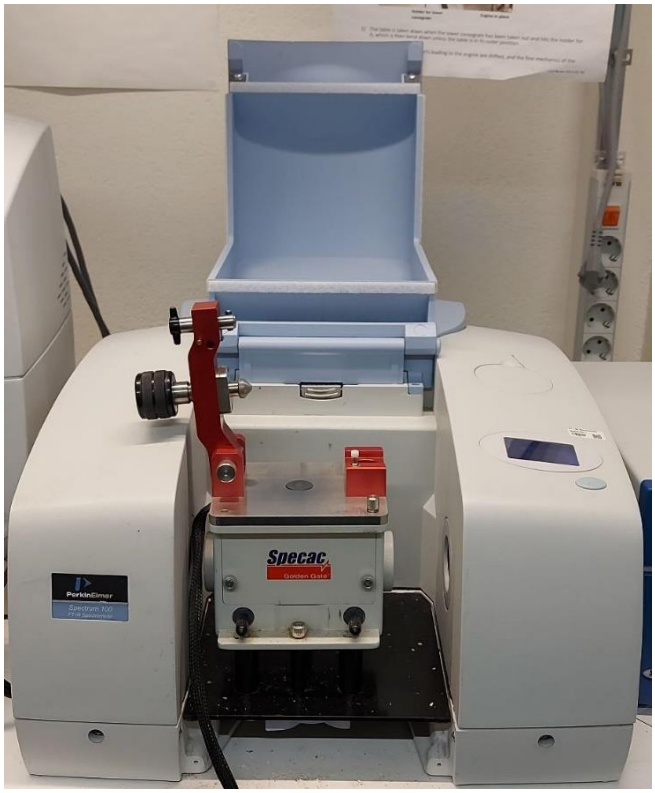

Figure 2.4 ATR-FTIR instrument.

2.7.3 Thermogravimetric analysis

Thermogravimetric analysis (TGA) is a quantitative analytical technique that estimates the material's thermal stability, giving valuable information about its decomposition. This method records the change in the mass of a sample when either subjected to a heating ramp (dynamic measurement) or held at a constant temperature (isothermal measurement).[40] The results are displayed in a graph, the so-called TGA curve, where the percentage weight, on the y-axis, is expressed as a function of temperature or time, on the x-axis. The experiments are performed in a controlled atmosphere, that can be reactive, oxidizing, or inert. In the measurements, the sample is placed in a ceramic crucible, over a pan that rests on the weighing arm of a microbalance. The sample pan is subsequently situated

in a sealed furnace, and a temperature programmer controls the operation of the furnace. A computer is connected to the machine, allowing the recording and saving of all the data. [41]

A complementary presentation of these data is given by the differential thermogravimetry curve (DTG), obtained as the first derivative of the weight with respect to temperature or time, providing information on the rate at which the mass changes. The loss of material produces steps in the TGA curves and peaks in the DTG curves. [40]

The thermal stability parameters evaluated in the analysis are the 5% and 30% weight loss degradation temperatures ($T_{5\%}$ and $T_{30\%}$ respectively), the temperature of the maximum decomposition rate (T_{max}), and the heat-resistance index (T_s), determined according to the following equation (Equation 2.3):[42], [14]

$$T_s = 0.49 \times [T_{5\%} + 0.6\,(T_{30\%} - T_{5\%})] \qquad (\mathbf{2.3})$$

The analysis was carried out in a TGA/SDTA851e Mettler Toledo (U.S.A) (Figure 2.5). Samples with a weight around 10 mg, were placed in 70 µL alumina crucibles. The experiments were performed under a nitrogen flow of 50 mL/min, with a temperature range from 30 to 600°C, at a heating rate of 10°C/min. TGA data were analyzed by Mettler Toledo STARe v. 15.00 software.

Figure 2.5 TGA instrument.

2.7.4 Differential scanning calorimetry

Differential scanning calorimetry (DSC) is an experimental technique widely employed in the polymer field for the determination of thermal characteristic properties, such as the glass transition temperature, heat capacity, crystallization, and melting temperatures. The differential scanning calorimeter, the instrument used for the measurement, consists of two solid pans, placed into two separate identical holders. One pan contains the sample, while the second one is empty and is used as a reference. Both the sample and the reference holders have their own heater and resistance sensor. The two calorimeters sit on a common block at a constant temperature. A temperature ramp is applied, and whenever the sensors detect a temperature difference between the two cells, a heating compensation is applied through computer control, in order to keep the same temperature rise between the sample and the reference.[43] The analysis requires a high sensitivity to the small changes in energy, related to the thermal processes, either exothermic or endothermic, that might occur during the measurement. To achieve this result, both the temperature and the scan rate are carefully controlled.[44] One of the advantages of DSC is the small quantity of material required for the measurement (order of milligrams). The difference in heat required to maintain the same temperature rise is displayed on the y-axis of a DSC curve, as a function of the temperature, plotted on the x-axis. The glass transition temperature (T_g) is a second-order endothermic transition, and for this reason, it appears in the DSC thermogram as a step and not as a peak.[45] It is also possible to establish the heat capacity (C_p), which shows a jump at the glass transition. Besides the crystallization and melting temperatures can be determined respectively by an exothermic and endothermic peak.

DSC experiments were performed on a Mettler Toledo DSC820 (Figure 2.6). Samples were weighed (5-7 mg) and sealed into 100 μL aluminum crucibles. Two heating ramps were performed from -10°C to 200°C, separated by a cooling ramp. Both heating and cooling ramps were realized with a rate of 10°C/min, under a nitrogen atmosphere, using a flow rate of 50 mL/min. The glass transition temperature was determined from the first heating cycle. DSC data were analyzed by Mettler Toledo STARe v. 15.00 software.

Figure 2.6 DSC instrument.

2.7.5 Tensile testing

The mechanical properties were investigated by means of an Instron 5944 universal testing machine (Figure 2.7). The synthesized samples had a uniform dimension of 26.00 mm x 1.53 mm x 0.75 mm. The reprocessed samples were obtained by cutting the film into different strips. The thickness for each tested sample, used for the measurement, was determined as the mean value of 3 different measurements performed along the specimen´s length. All tests were performed at 22°C and 50% relative humidity, and a crosshead speed of 0.1 mm/min was adopted.

Figure 2.7 Tensile test instrument.

2.7.6 Gel content test

The solvent resistance of all thermosets was measured in triplicates in three different solvents: acetone, ethanol, and dichloromethane. In detail, small fragments of the photopolymerized specimens (~ 10 mg) were immersed in the solvent (2 mL) at room temperature for 72 h. The solvent was removed with a syringe and the insoluble parts were collected and let dry. The gel content of the thermosets was calculated according to the following equation (Equation 2.4):

$$Gel\ content = \frac{m_{ae}}{m_{be}} * 100\% \qquad \textbf{(2.4)}$$

where m_{ae} and m_{be} are the sample weight before and after the extraction of the thermosets, respectively.

2.7.7 Mechanical Recycling

For mechanical recycling by thermal reprocessing, different strategies were adopted. The first attempts involved only MI50 and MI75. The original thermosets were cut into small pieces and processed into new films by hot-pressing, varying the process parameters (pressure, temperature, and time) to find the optimum conditions. Since, in most cases, it wasn't possible to obtain compact films,

a different approach was embraced. The virgin samples were ground to a fine powder with a mortar, and zinc acetate, a transesterification catalyst, with a concentration of 5% w/w was added. The mixed powders were then transferred to a square-shaped mold (25 mm x 25 mm x 0.5 mm) and hot-pressed for 1h at 180°C under a low pressure of 270 kN (3 MPa); a minor hot-pressing time of 30 min was also employed. With regard to SB_MI50, the same procedure as for MI50 and MI75 was adopted: the ground thermoset was added with $Zn(OAc)_2$ (5% w/w) and hot pressed at 180°C for 30 min under 3 MPa. Another attempt was further made, lowering both temperature and time up to 150°C and 15 min.

All samples underwent a second recycling cycle, using the same procedure and the same parameters as above. The one and twice-reprocessed samples were renamed respectively as MR1 and MR2. The instrument used for the reprocessing was the hot press, shown in Figure 2.8.

Figure 2.8 Hot-press machine.

2.7.8 Chemical Recycling

The chemical degradation of MI50, MI75, and MI100 thermosets was tested in methanol, 0.5 M NaOH, and 1 M NaOH. In detail, small fragments of the sample (~ 100 mg) were immersed into vials with the solvent (5 mL), and heated at 100°C under reflux, until complete solubilization was reached. The chemical recycling of MI50 was performed by dissolving fragments of the cured samples (1.2 g) in 1 M NaOH (25 mL) for 4 h at 100°C. The mixture was then acidified, adding HCl dropwise to the solution, until a pH of 2 was reached. The resulting product was subsequently heated at 100°C, in order to evaporate the solvent. After yielding some dried powders, ethanol was added, and the mixture was put under stirring at room temperature overnight. This step was performed to dissolve the organic molecules and precipitate NaCl. The salt formed was removed via filtration. The solution was then reduced under pressure, to remove most of the solvent. A powder was subsequently collected and, after the addition of zinc acetate (5% w/w), reprocessed via hot pressing at 120°C, for 30 min under 3 MPa. The same procedure was adopted for the chemical recycling of MI75. The chemical degradation of SB_MI 50 thermoset was evaluated in 0.1 M HCl, 1 M NaOH, and excess of Dom. Fragments of thermoset were immersed in 5 mL of both 0.1 M HCl and 1 M NaOH, while a smaller amount of solvent was used in the case of the diamine Dom (3 mL). The samples were heated at 80°C. The chemical recycling of SB_MI 50 was performed. Fragments of thermoset (290 mg) were dissolved after immersion in excess of diamine (6 mL) for 6 h at 80°C. The resulting product was precipitated in water, subjected to suction filtration, and dried in the oven at 60°C for 30 min. The collected polymer was mixed with MV, with a stoichiometric ratio of 1:3 (MV : polymer), and BAPO (5% w/w). Zinc acetate was then added with a concentration of 2% w/w, and mixed to the powder that was subsequently transferred to a square-shaped mold (25 mm x 25 mm x 0.5 mm) and hot-pressed at 140°C for 30 min, under 3 MPa.

Results and discussion

3.1 Synthesis of vinyl ester resins

Methacrylic anhydride was used, in the presence of a small amount of catalyst DMAP, to introduce photocurable functional groups both on isosorbide and vanillin, following a procedure employed in previous work.[46] DCM was used as a solvent to maximize the reaction yield as previously reported.[47]

The chemical structure of the synthesized monomers methacrylated isosorbide (MI) and methacrylated vanillin (MV) was characterized by ^{1}H NMR analysis (Figure 3.1).

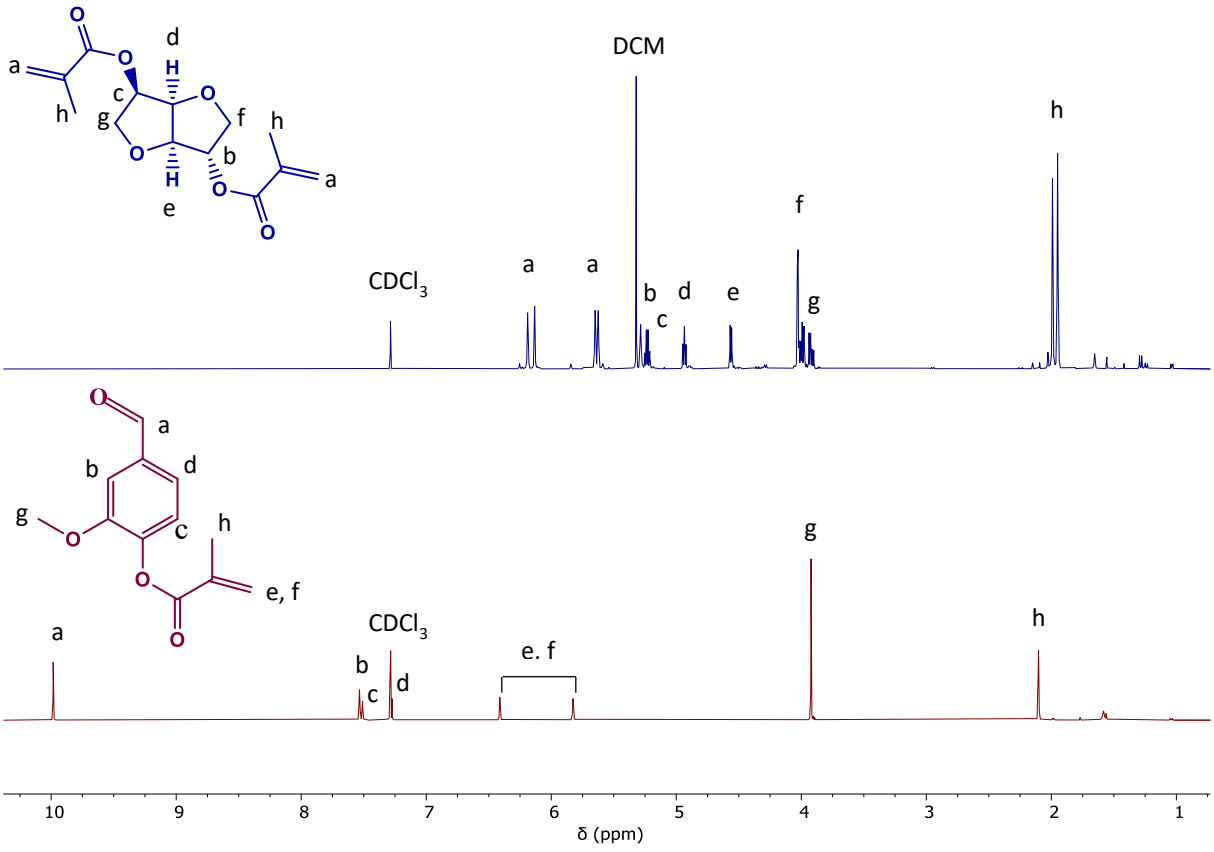

Figure 3.1 ^{1}H NMR spectra of MI and MV monomers.

Methacrylated isosorbide spectrum showed the characteristic chemical shifts for 6.22, 6.13, 5.65, and 5.62 ppm methylene protons of vinyl groups (C=C**H$_2$**) (a). The appearance of these peaks proved that the methacrylation occurred properly, introducing crosslinking sites that will allow the formation of the thermoset´s network. The signals of the methine protons next to the ester group (O=C-O-C**H**)

were detected at δ 5.29 and 5.23 ppm (b, c). Peaks at δ 4.94, 4.56 ppm, and δ 4.01 and 3.92 ppm correspond respectively to the methine protons (O-C**H**) (d, e) and the methylene protons (O-C**H₂**) (f, g) of the isosorbide ring. Finally peaks at δ 2.01 and 1.95 for the methyl protons of the methacrylate group (O=C(O)-C(CH₂)-C**H₃**) (h) were observed.

Methacrylated vanillin spectrum showed characteristic chemical shifts for 9.98 ppm methine protons of the aldehyde group (O=C**H**-C-) (a), 7.51, 7.28, and 7.53 ppm methine protons of the vanillin aromatic ring (-C**H**-C-C**H**-C**H**-) (b, c, d). The appearance of the peaks at δ 6.41 and 5.83 ppm for the methylene protons of the vinyl group (C=C**H₂**) (e,f) proved the successful methacrylation of vanillin. The signal at δ 3.92 ppm for the methyl protons of the ether group (C**H₃**-O-C) (g) was detected, together with the peak at δ 2.10 ppm for the methyl protons of the methacrylate group (C**H₃**-C=CH₂) (h).

Next, MI and MV monomers were further investigated via FTIR spectroscopic analysis (Figure 3.2). In the case of MI monomer, the peak at 1716 cm^{-1} was associated with the C=O ester bond, while the signals of the C=C vibration peaks were observed at 1637 and 813 cm^{-1}. In MV spectrum, the characteristic peaks were visible at 1721 cm^{-1} for the C=O ester bonds, 1698 cm^{-1} for the C=O bonds from the aldehyde group, and 1595 cm^{-1} for the aromatic bonds. Furthermore, the adsorption bands at 954 and 856 cm^{-1} were both ascribable to the C=C bending vibrations.

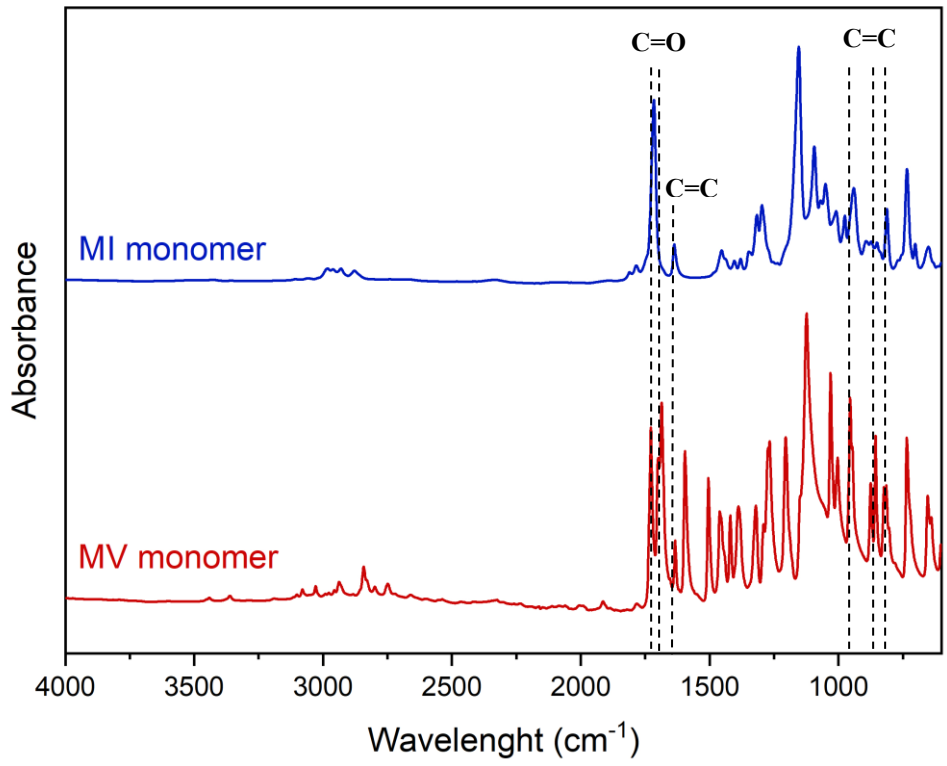

Figure 3.2 FTIR spectra of MI and MV monomers.

Therefore, vinyl bonds were successfully introduced into MI and MV resins networks, as confirmed by spectroscopy analysis such as ^{1}H NMR and FTIR. This step made the synthesized vinyl ester resins suitable for DLP 3D printing.

3.2 Synthesis of vanillin-based imine resin

The Schiff base resin was synthesized through a two-step reaction. First, vanillin was functionalized with methacrylate moieties, providing crosslinking sites for the monomer. Next, a Schiff base reaction between the aldehyde group of the previously synthesized MV and the diamine Dom was performed. A vanillin-based vinyl ester resin containing imine bonds was obtained, and named SB. Because of the high reciprocal reactivity of MV and Dom, there was no need to use a catalyst, and the reaction was carried out at room temperature.[48],[49]

The chemical structure of SB monomer was confirmed by a ^{1}H NMR analysis (Figure 3.3).

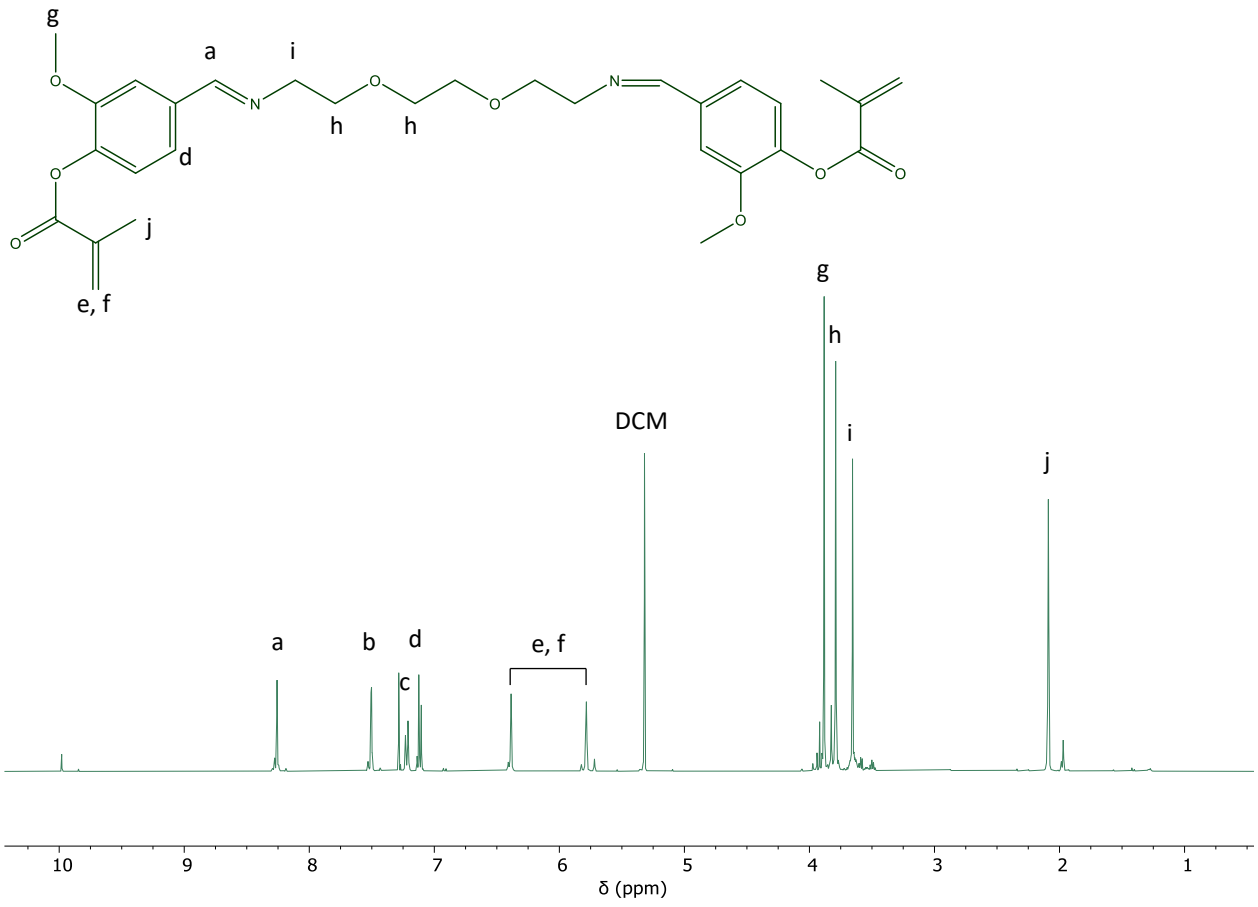

Figure 3.3 ^{1}H NMR spectra of SB monomer.

SB monomer spectrum exhibited the imine peak (C**H**=N) at δ 8.26 ppm (a). The signals at δ 7.50, 7.21, and 7.12 ppm were ascribable to the methine protons of the vanillin aromatic ring (C**H**-C-C**H**-

C**H**) (b, c, d). Peaks at δ 6.39 and 5.79 ppm for the methylene protons of the vinyl group (C=C**H₂**) (e,f) were detected. The methyl protons of the ether group (C**H₃**-O-C) (g) were observable at δ 3.88 ppm, while the methylene protons of the ether group (C**H₂**-O-C**H₂**) (h) were detected at δ 3.79 ppm. Peaks at δ 3.66 ppm for the methylene protons next to the imine bond (CH=N-C **H₂**) (i) were observed, and at δ 2.09 ppm the peak for the methyl protons of the methacrylate group (C**H₃**-C-=CH_2) (j) was present. The almost complete disappearance of the signal at δ 10.0 ppm, ascribable to the vanillin aldehyde group, and the appearance of the new peak at δ 8.26 ppm, documented the successful imination of MV.

The product was then analyzed using FTIR spectroscopy, and the spectrum in Figure 3.4 showed features consistent with the expected SB resin structure. The C=N imine peak was observed at 1645 cm^{-1}, and the absence of signals for both the aldehyde (~ 2750 cm^{-1}) and the primary amine groups (~ 3500 cm^{-1}) was detected, confirming the success of the reaction.

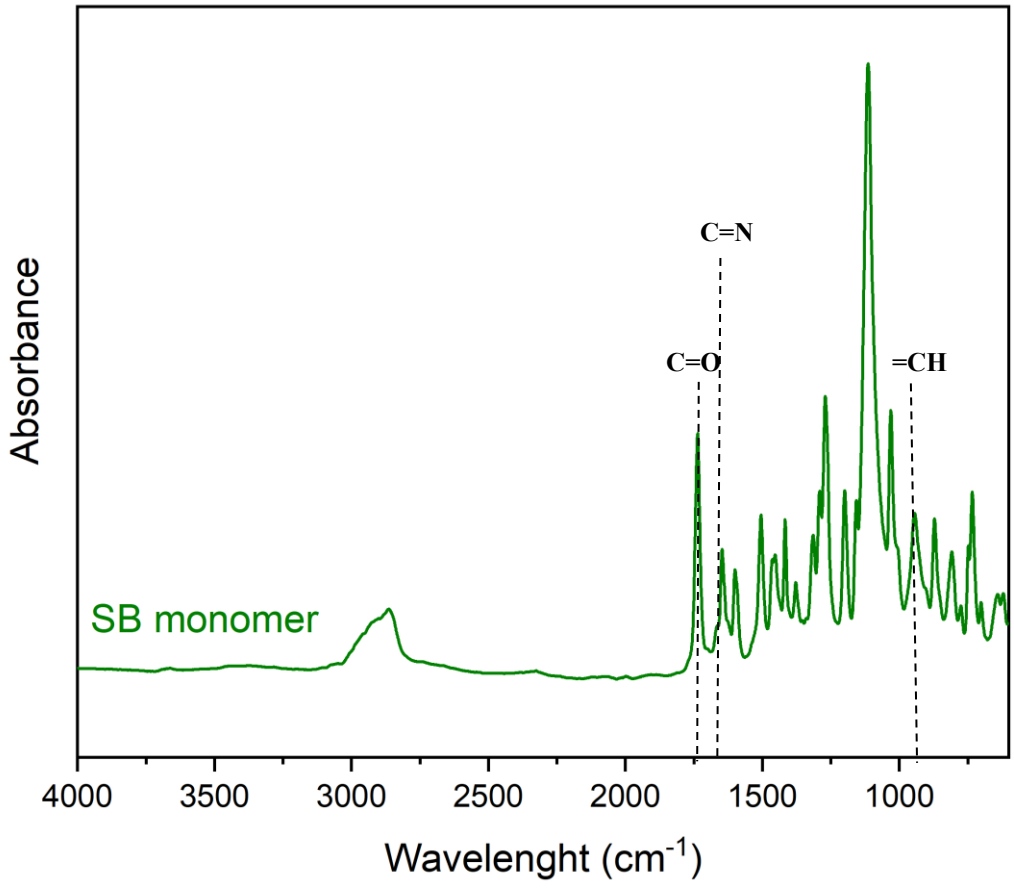

Figure 3.4 FTIR spectra of SB monomer.

3.3 Jacobs working curve

The building blocks derived monomers adopted in this work, synthesized as described in the previous section, were combined to design new photocurable biobased resins, applicable to digital light processing three-dimensional printing. Specifically, MI50, MI75, MI100, and SB_MI50 were prepared by mixing the starting monomers at different concentrations. Next, the solvent DCM and the photoinitiator BAPO were added to the reaction mixture.

The resin cure parameters were deduced by implementing Jacobs working curve. This model determines the optical properties of a resin, such us the penetration depth (D_p) and the critical dose required to induce polymerization (E_c).[34], [27] For this purpose, samples for each tested resin, shaped into small disks, were cured using different exposure times that were 90, 95, 98, and 100 seconds (Figure 3.5). The final curing time that led to the formation of the relatively transparent compact circular disks was 100 seconds.

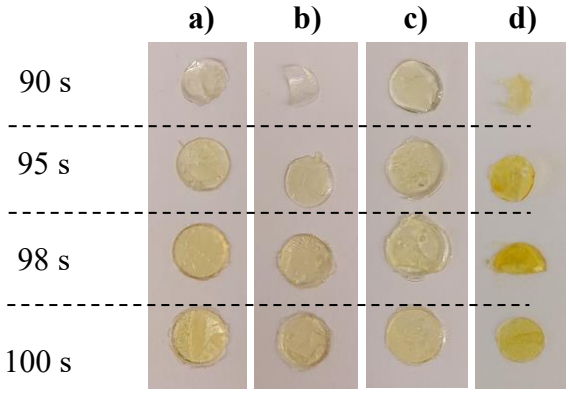

Figure 3.5 Cured disks of a) MI50, b) MI75, c) MI100 and d) SB_MI50 after different curing times.

Next, the thickness of the cured disks (C_d) was measured, the data were analyzed, and a semilogarithmic plot of the cured thickness (C_d) as a function of the light irradiation dosage (E_{max}) was generated (Figure 3.6).

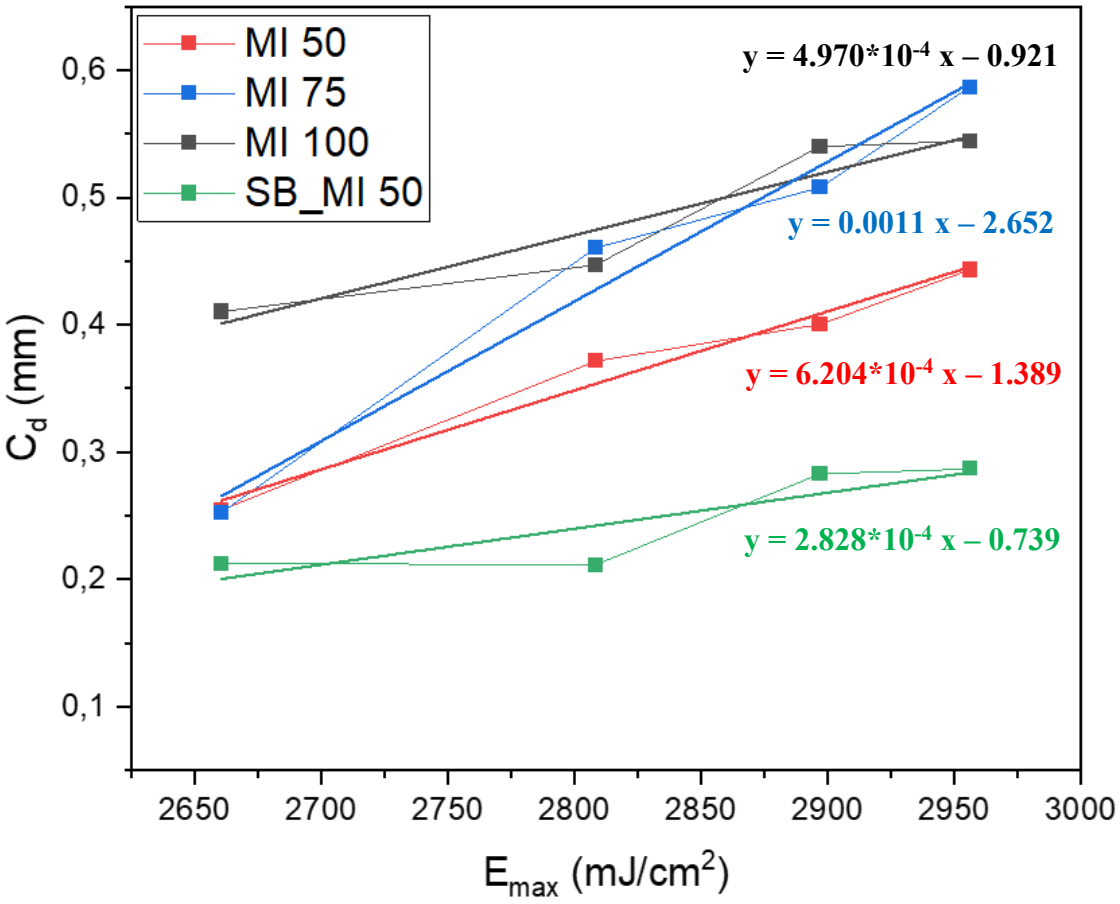

Figure 3.6 Jacob´s working curves of the resin formulations.

The slope of the best-fit line in Jacob's curve analysis signifies the penetration depth (D_p) of the material. SB_MI50 showed the lowest slope among all the tested resins (Table 3.1). A smaller D_p is correlated to a lager confinement of the applied irradiation light to the designated layers, ensuring an accurate layer-by-layer fabrication during 3D printing and thus enhancing print resolution.[50] With regard to the vinyl ester resins and the influence of the increased concentration of MI, no general trend embracing all resin formulation was observed. However, MI75 exhibited a significantly larger D_p than MI50, which led to a larger overcure and a lower print quality, as discussed in later sections. Another critical parameter that was considered in the evaluation of the resin behaviors is the critical dose E_c. This value is defined as the amount of irradiation light necessary to form a non-flowable material, related to the gel point of the resin, and it is used to measure the efficiency of polymerization. On Jacob's working curves this metric corresponds to the intersection of the best-fit line with the x-axis. A resin with a smaller E_c has a higher efficiency of polymerization.[35],[27],[50] Comparing all the tested resins, SB_MI50 showed the lowest E_c after MI100, while MI75 exhibited the highest E_c among all resins (Table 3.1).

	D_p (mm)	E_c (mJ/cm^2)
MI50	0.0006	2238
MI75	0.0011	2410
MI100	0.0005	1853
SB_MI50	0.0003	1952

Table 3.1 Penetration Depth (D_p) and Critical dose (E_c) values of resins formulations.

3.4 Digital Light Processing 3D Printing

The prepared photocurable formulations were printed via digital light processing (DLP) 3D printing in the shape of rectangular bars and films (Figure 3.7a, b). The resins with higher MI content were prone to breaking more easily, suggesting that the MI content increases fragility. The reason for this characteristic is connected to the isosorbide chemical structure, whose bicycling ring and chiral diols imparted the formed thermosets with stiffness.[14],[51] Amongst all the printed compounds, MI100 was the most brittle to the point that it wasn´t possible to print an unbroken specimen. On the other hand, SB_MI50 demonstrated greater flexibility and good printability, likely thanks to the introduction of the diamine Dom employed in the synthesis process. This not only allowed the formation of a Schiff-base thermoset, but also played the role of spacer between the more rigid aromatic vanillin units.

The print accuracy of the tested resins was further investigated through the fabrication of clover-shaped samples (Figure 3.7c). Because MI100 failed in the previous experiments, the clover structure was not attempted. MI75 showed a tendency for overcuring, according to Jacob´s working curves: the higher penetration depth D_p resulted in bleeding of light into preceding layers.[50] To evaluate the quality of the prints, we used the presence of a loop between the upper leaves of the clover structure and compared it to the CAD model. Great print quality was observed for MI50 and SB_MI50 samples, both of which had a lower D_p than MI75, and produced clear details in the printed clover shapes (Figure 3.7c). In comparison, MI75 resin produced a clover structure with a much less clear lop structure.

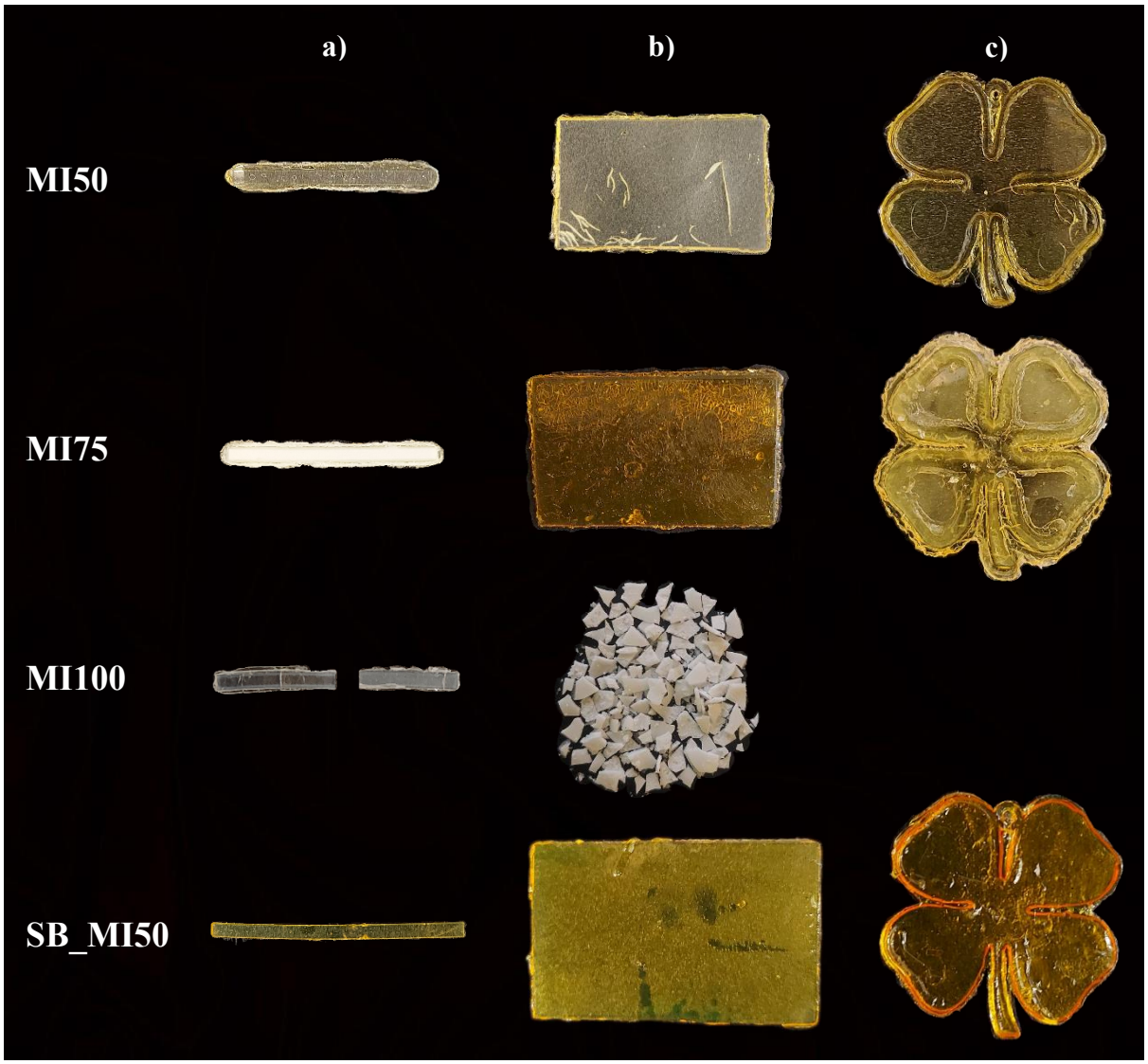

Figure 3.7 3D printed samples: a) bars, b) films, c) clovers.

In order to investigate the chemical structure of the resins after curing, a comparative ATR-FTIR analysis was performed (Figure 3.8). There was a significant reduction of the C=C vibration peaks (at 1637 and 813 cm^{-1} for the MI moieties, and 954 and 856 cm^{-1} for the MV moieties) observable after curing in MI50, MI75 and MI100 thermosets. This proved that the double bonds were crosslinked and confirmed the successful photopolymerization of the resins. Nevertheless, the peak at 1637 cm^{-1} was still detected in MI100 spectrum, implying an incomplete curing reaction. Additionally, the adsorption bands at 1716 and 1721 cm^{-1}, ascribable to the C=O ester bond and the aldehyde group respectively were also observed. These two signals overlapped in MI50 and MI75, resulting in two co-peaks in the MI50 spectrum, and into one peak with a small shoulder in the MI75 spectrum.

In the case of SB_MI50 a noticeable reduction of the peak at 945 cm^{-1}, ascribable to the =CH functional group, was detected, indicating the formation of a crosslinked network. The ester bonds were preserved, as confirmed by the presence of the peak at 1723 cm^{-1} in SB_MI50 spectrum. Furthermore, the imine peak at 1645 cm^{-1} was also detected in this thermoset. The preservation of this group is important in imparting the polyimine network with reprocessability and recyclability properties.

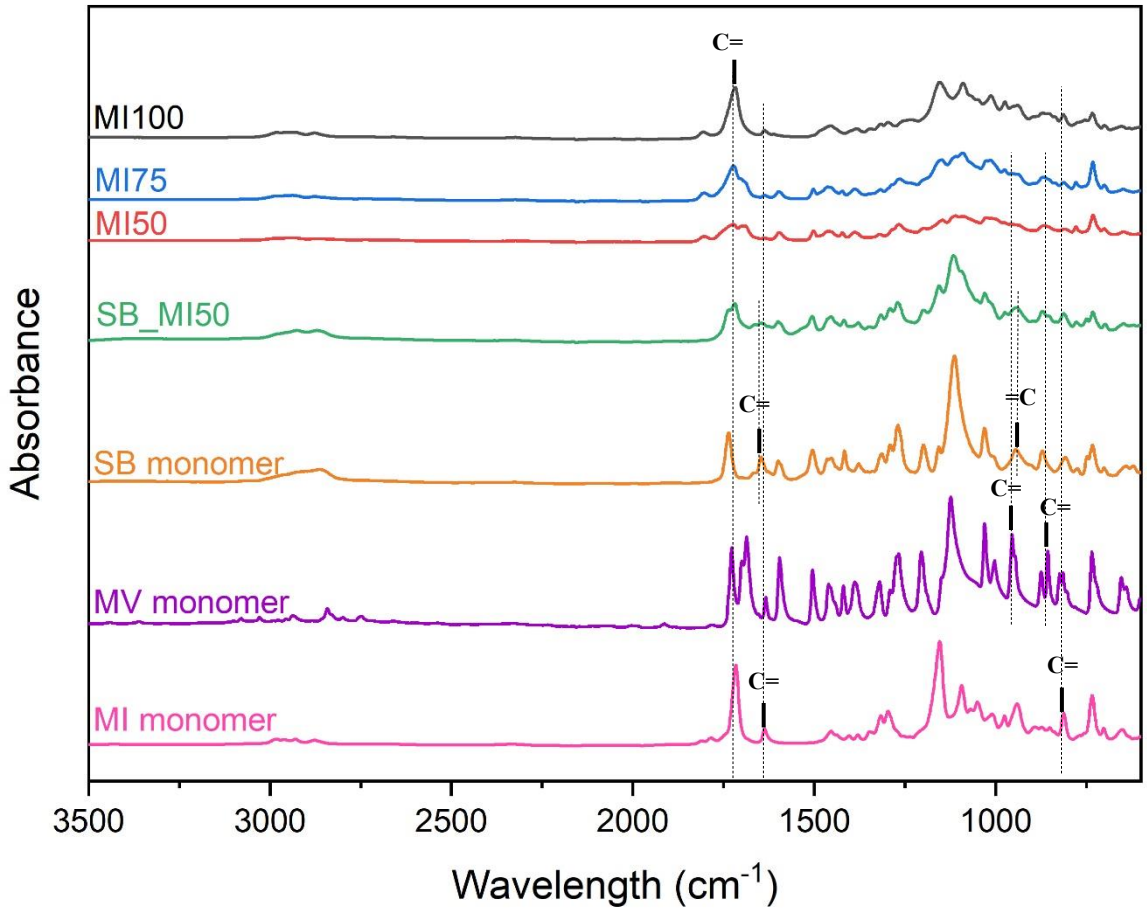

Figure 3.8 FTIR spectra comparison between monomers and cured thermosets.

3.5 Thermoset properties

3.5.1 Thermogravimetric analysis

The thermogravimetric analysis (TGA) was carried out in the attained thermosets to determine their thermal properties (Figure 3.9a, Table 3.2). All thermosets turned out to be thermally stable, with the onset of degradation above 150°C. Thermal stability correlated with the increased MI content with M100 being the most thermally stable (Table 3.2). To further evaluate the overall thermal stability of the photocured samples, the statistic heat resistant index (T_s) was calculated. The decrease in the

isosorbide content affected the final T_s values. The reason could be related not only to the crosslinking density, but also to the chemical structure of the resin. The presence of vanillin units, along with the aldehyde group, imparted the thermoset with lower thermal stability. With increasing vanillin content, the thermal resistance would decrease. As a matter of fact, while MI monomer $T_{5\%}$ was at ~ 177°C, MV monomer showed the onset of the degradation at ~ 138°C. SB_MI50 showed a slightly lower thermal stability than the other tested thermosets ($T_{5\%}$ of 159.4°C). the thermogravimetric analysis we observed a larger residue remaining at higher temperatures with the vanillin-based imine thermoset. This was probably due to the higher density of aromatic units in the network structure. The derivative TGA curves were also determined (Figure 3.9b), showing the same trend in the maximum weight loss Temperature (T_{max}) for all samples.

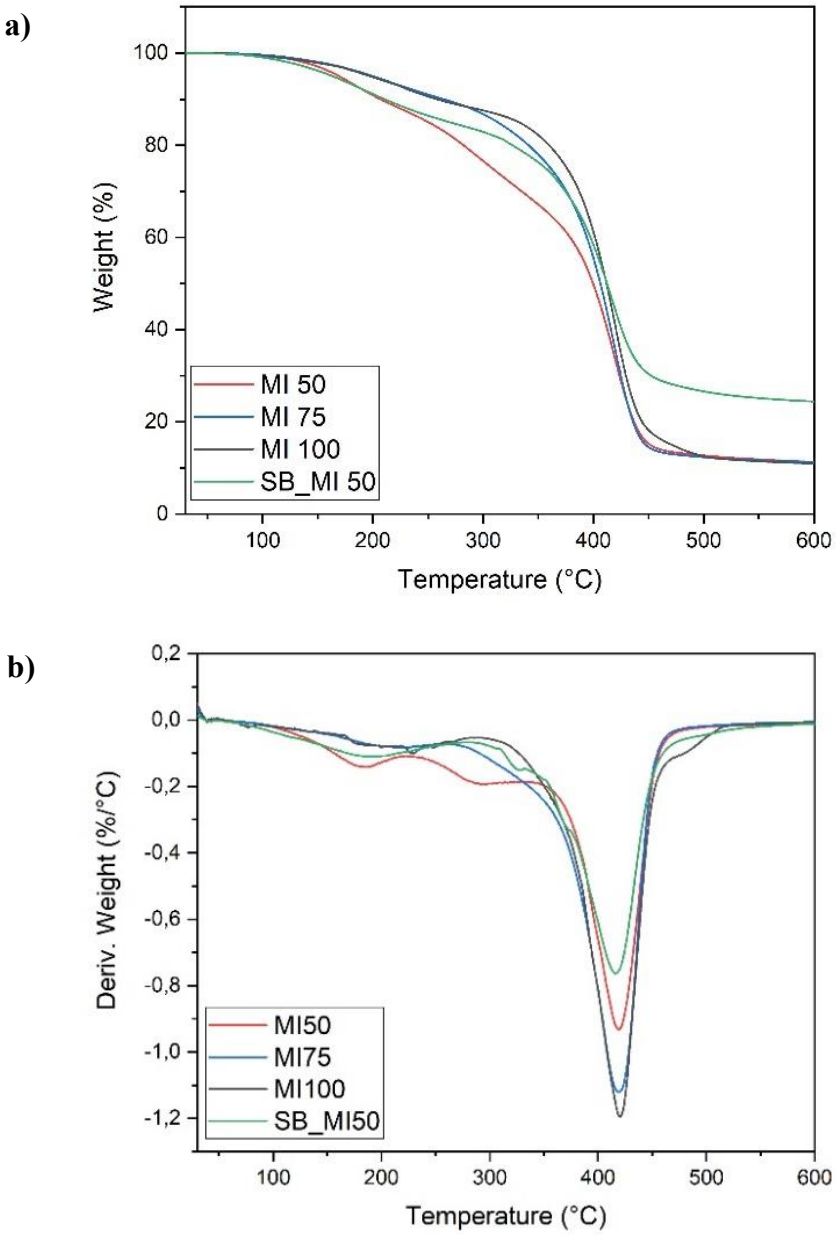

Figure 3.9 a) TG and b) DTG curves of the virgin thermosets.

Sample	$T_{5\%}$ (°C)	$T_{30\%}$ (°C)	T_{max} (°C)	T_s (°C)	Residue (%)
MI 50	167.2 ± 3.9	337.3 ± 1.5	422.7 ± 0.47	131.9 ± 0.7	12.8 ± 1.9
MI 75	199.9 ± 1.8	376.6 ± 3.4	423.0 ± 0	149.9 ± 1.4	10.9 ± 2.5
MI 100	203.9 ± 5.1	386.9 ± 1.6	424.3 ± 0.5	153.7 ± 1.2	10.4 ± 2.0
SB_MI 50	159.4 ± 6.7	375.7 ± 2.7	421.6 ± 0.6	141.8 ± 1.6	23.8 ± 1.7

Table 3.2 Thermal properties of virgin thermosets.

3.5.2 Differential scanning calorimetry

The differential scanning calorimetry (DSC) analysis was carried out on the virgin samples. The DSC curves allowed for the identification of the glass transition temperature (T_g). The first heating cycle was measured and recorded (Figure 3.10, Table 3.3). Amongst MI50, MI75 and MI100, the latter thermoset showed the highest T_g of 64.1°C, concordantly with previous work. As a matter of fact, it has been proved that the presence of isosorbide blocks in the polymer network could increase the glass transition temperature of some thermosetting resins, imparting the final material with stiffness.[52],[53],[54] Furthermore, SB_MI50 exhibited a T_g of 93°C, the highest glass transition temperature of all thermosets. This was likely due to the major flexibility of its starting monomer, which led to a more crosslinked structure after curing. This result is in line with the high solvent resistance observed for SB_MI50, as described in the following section.

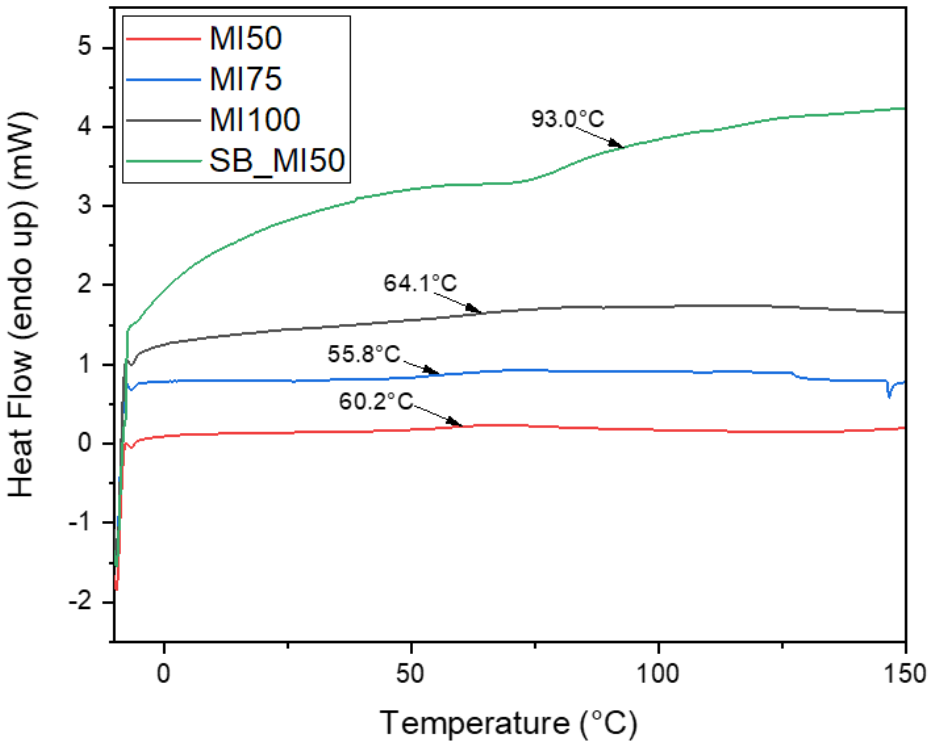

Figure 3.10 1st heating DSC curves of virgin thermosets.

	MI 50	MI 75	MI 100	SB_MI50
Tg (°C)	60.2 ± 2.8	55.8 ± 0.6	64.1 ± 2.6	93.0 ± 11.2

Table 3.3 Glass transition temperatures of virgin thermosets.

3.5.3 Gel content test

The gel content measurement was performed for all samples in three different solvents: acetone (Ace), ethanol (EtOH) and dichloromethane (DCM). The thermosets were submerged in the solvents and evaluated after three days. The result of this test documented excellent solvent resistance for all samples, with an average gel content above 87% (Table 3.4). Of the four tested thermosets, only MI100 was slightly affected by the solvents. In all other cases, the solvents did not change color which is indicative of no or minimal dissolution (Figure 3.11). The robustness of thermosets is due to a high degree of crosslinking. Surprisingly, even though MI50 has a higher content of MV, it also yielded a high gel content (>92.8%). On the other hand, the lower stability of MI100 (between 87.6 and 91.8%) was interesting. This outcome could be explained by assuming that a higher MI content may lead to a lower mobility of the resin, thus yielding a lower gel content.[14] The steric hindrance could also be a factor. Additionally, MI100 appeared to have an incomplete network despite the low viscosity of the MI monomer. This could be due to the fact that during its polymerization, one

methacrylic group bonded to the growing network, imparting the end chain, with an available reactive site (C=C), with restricted mobility. The higher the conversion, the more stationary the unreacted sites are, reaching the point where the system is locked.[55],[56]

Finally, SB_MI50 showed the highest insoluble fractions (>96.5%), indicating a high curing degree, with values similar to the ones obtained in the case of a thermoset formed just with SB units [44], suggesting that the MI moieties did not affect the overall solvent resistance.

Sample	**Average gel content (%)**		
	in **Ace**	in **EtOH**	in **DCM**
MI50	92.8 ± 1.4	92.8 ± 3.7	95.3 ± 1.4
MI 75	90.4 ± 1.7	94.1 ± 2.0	96.0 ± 1.2
MI 100	91.1 ± 3.8	87.6 ± 4.7	91.8 ± 1.4
SB_MI 50	96.5 ± 1.5	96.8 ± 1.2	98.2 ± 1.4

Table 3.4 Gel content of thermosets in Ace, EtOH and DCM.

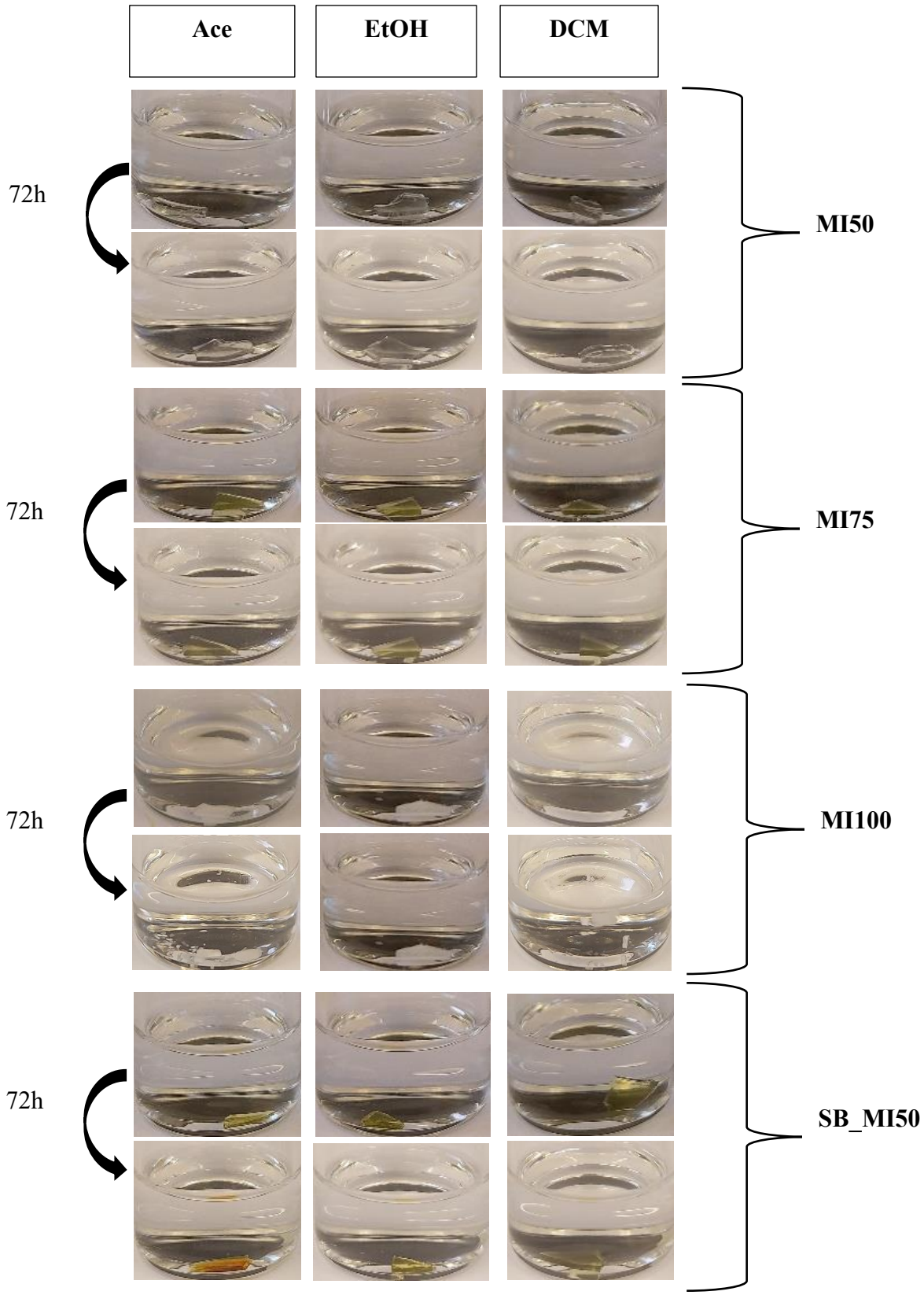

Figure 3.11 Thermosets in Ace, EtOH and DCM, start and after 72h.

3.5.4 Testing of mechanical properties

The mechanical properties of the cured biobased thermosets were investigated by tensile testing. The measurements involved different samples. Table 3.5 contains the values of Young´s modulus, as well as stress at break and elongation at break. Figure 3.12 depicts a single test for each sample as a representative curve. High elastic modulus values were obtained for all samples, particularly for MI50 and MI75 (2026.8 and 1925.0 MPa respectively). The mechanical properties of CANs can be defined as a function of crosslinking density, monomer structure, and the nature of the dynamic covalent bonds incorporated in the network.[23] Therefore, the more rigid monomers of MI50 and MI75 provided higher mechanical strength to the material (47.0 and 58.2 MPa respectively), together with higher Young´s moduli values. Moreover, the chemical structure of SB_MI50, and in particular the higher flexibility of this thermoset imparted by the diamine-derived chain during the synthesis process, could be held responsible for the lower Young´s modulus achieved (1163.8 MPa). Additionally, SB_MI50 showed a slightly higher extension at break, also ascribable to its higher flexibility.

Sample	Elastic modulus [MPa]	Stress at break [MPa]	Elongation at break [%]
MI 50	2026.8 ± 250.2	47.0 ± 13.7	4.9 ± 1.4
MI75	1925.0 ± 484.9	58.2 ± 8.8	5.9 ± 1.8
SB_MI50	1163.8 ± 215.6	41.8 ± 4.0	7.3 ± 1.8

Table 3.5 Mechanical properties of cured thermosets.

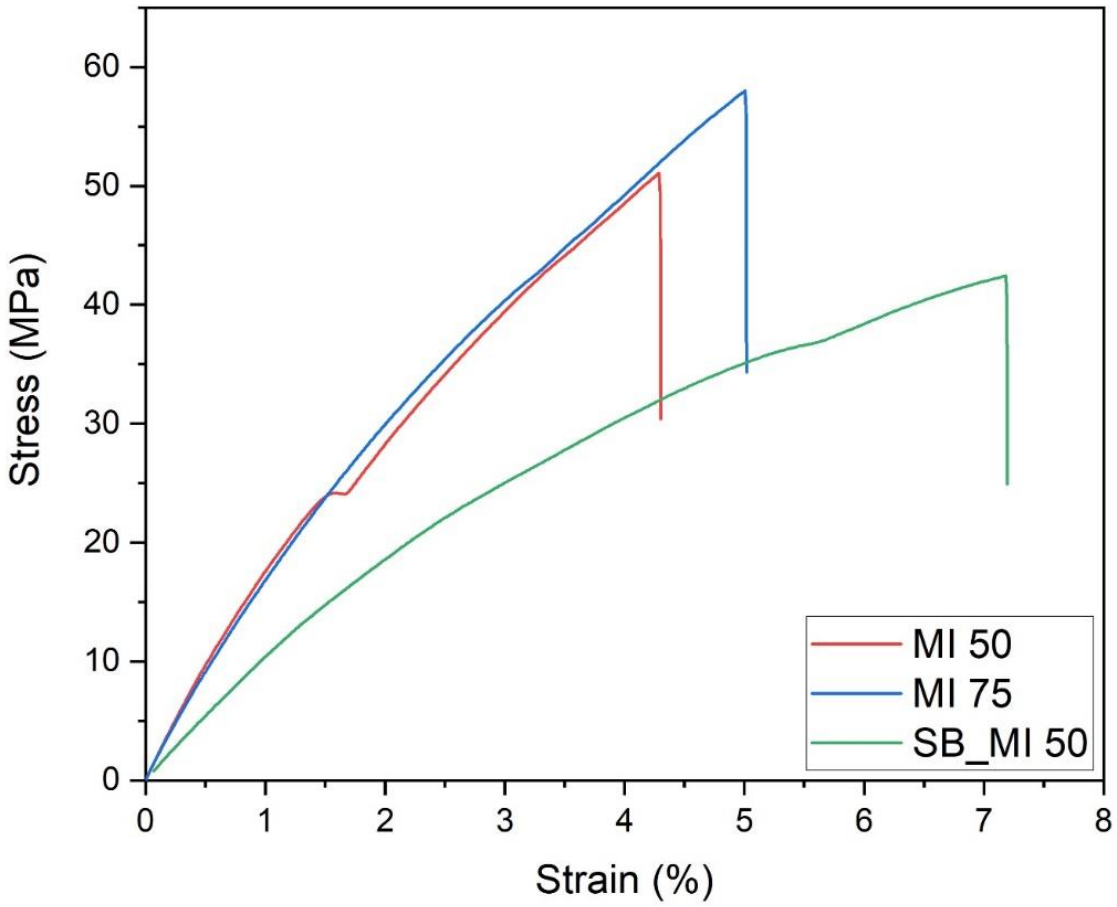

Figure 3.12 Representative stress-strain curves of cured thermosets.

3.6 Mechanical recycling

3.6.1 First cycle

The tested thermosets were mechanically recycled via hot-pressing. Different attempts were required before finding the optimum parameters (temperature, pressure, and time). The adopted mechanical recycling procedure and the reprocessed samples are shown in Figure 3.13. Results indicate that adding a catalyst in reprocessing is an important parameter to achieve compact films. In the tested materials, the presence of ester bonds in MI50 and MI75 networks allowed the occurrence of transesterification reactions following an associative pathway, accomplishing the redistribution of polymer chain connectivity. [23] The exchange mechanism was facilitated by incorporating $Zn(OAc)_2$, a non-toxic and highly efficient transesterification catalyst, in the system, enhancing the efficiency of the vitrimerization. Furthermore, the absence of free hydroxyl groups did not appear to prevent the transesterification reaction from occurring, as demonstrated in previous work.[57] In the case of

SB_MI50, the imine bonds are instead the ones to enable this material to be reprocessed, following a metathesis pathway.

Considering the strategy using $Zn(OAc)_2$ to reprocess MI50 and MI75, two different conditions were tested, reprocessing the samples at the same temperature and pressure (180°C, 3 MPa), and using different processing times (1h vs 30 min). The shorter processing time was tested to evaluate the possibility of forming a compact film in a short period of time while decreasing the risk of degradation. The results showed that the color of the films obtained after 30 min was lighter than the ones after 1h of reprocessing, suggesting minor damage to the material with a shorter processing time. Additionally, with a shorter processing time, the entire recycling process became less energy-consuming, which is an essential improvement to the process.

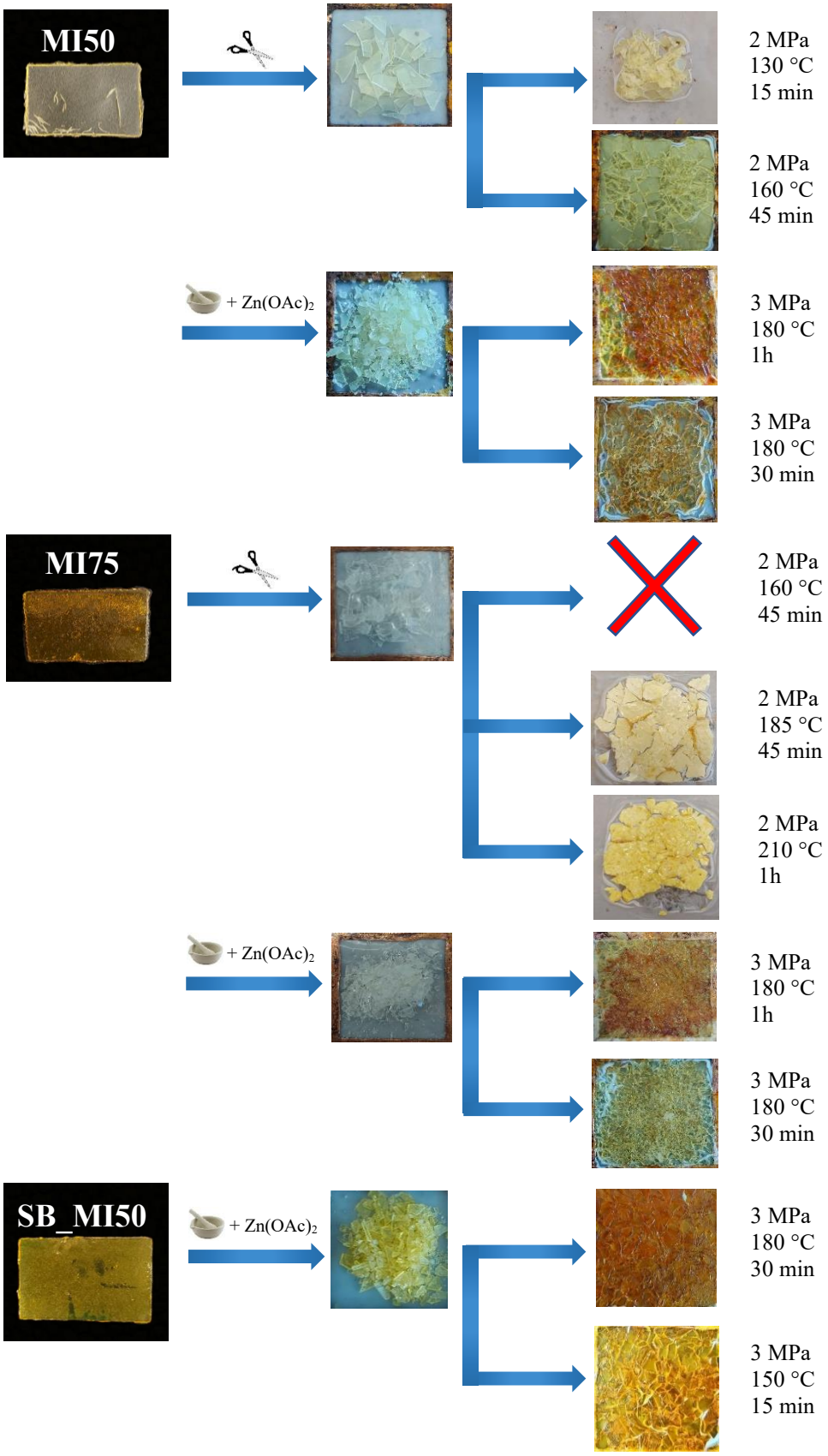

Figure 3.13 Mechanical recycling procedure for the once-reprocessed thermosets MI50, MI75 and SB_MI50.

The mechanical behavior of the reprocessed samples at 180°C for 1h and 30 min was investigated by tensile testing and compared with the virgin (original) thermosets MI50 and MI75 (Figure 3.14). After reprocessing a significant decrease in the mechanical properties was observable for all samples. The reduction of the processing time from 1h to 30 min led to an increase in the elastic modulus of MI50 from 392.7 to 624.3 MPa. Higher stress values at break and elongation at break were also reached for all samples. For this reason, these conditions (180°C, 3 MPa, 30 min) were also adopted for the mechanical recycling of SB_MI50.

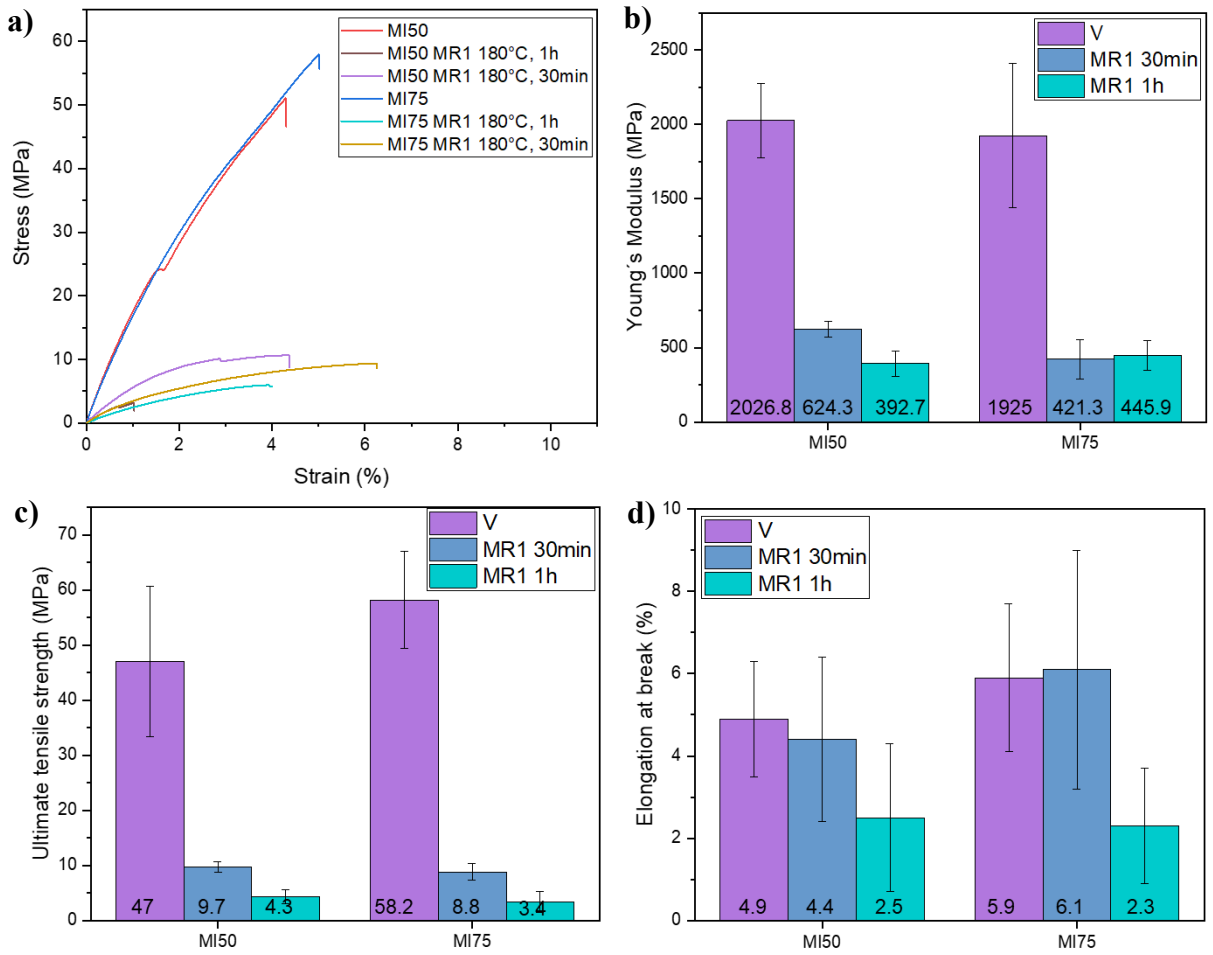

Figure 3.14 a) Representative stress-strain curves of MI50 and MI75 virgin, MR1 1h, and MR1 30min, and b) Young´s modulus (MPa), c) tensile strength (MPa), d) elongation at break (%).

The mechanical recycling of SB_MI50 was performed at 180°C, but a lower temperature of 150°C was also tested. The material´s original color was kept with the employment of the lower temperature, suggesting a greater preservation of the network chemical structure, while a darker color was obtained after reprocessing at 180°C (Figure 3.13). The success in yielding a compact film with both conditions, suggests the possibility of activating the imine exchanged at a lower temperature; the

same thing cannot be said for the transesterification exchange reaction, since the attempts to reprocess MI50 and MI75 at a lower temperature failed. This result is supported by previous work, according to which elevated temperatures are needed for the polymer network to undergo transesterification reactions.[58] The comparison of the mechanical properties between the original thermoset SB_MI50 and the once-reprocessed samples is shown in Figure 3.15. In both cases, it was possible to observe values of elastic modulus for the once reprocessed samples rather similar to the virgin material, exhibiting a vitrimer behavior. In particular, for the mechanically recycled thermoset at 150°C, a Young´s modulus of 1229.7 MPa was reached. Nevertheless, a reduction of both the ultimate tensile strength and the elongation at break was observable after reprocessing.

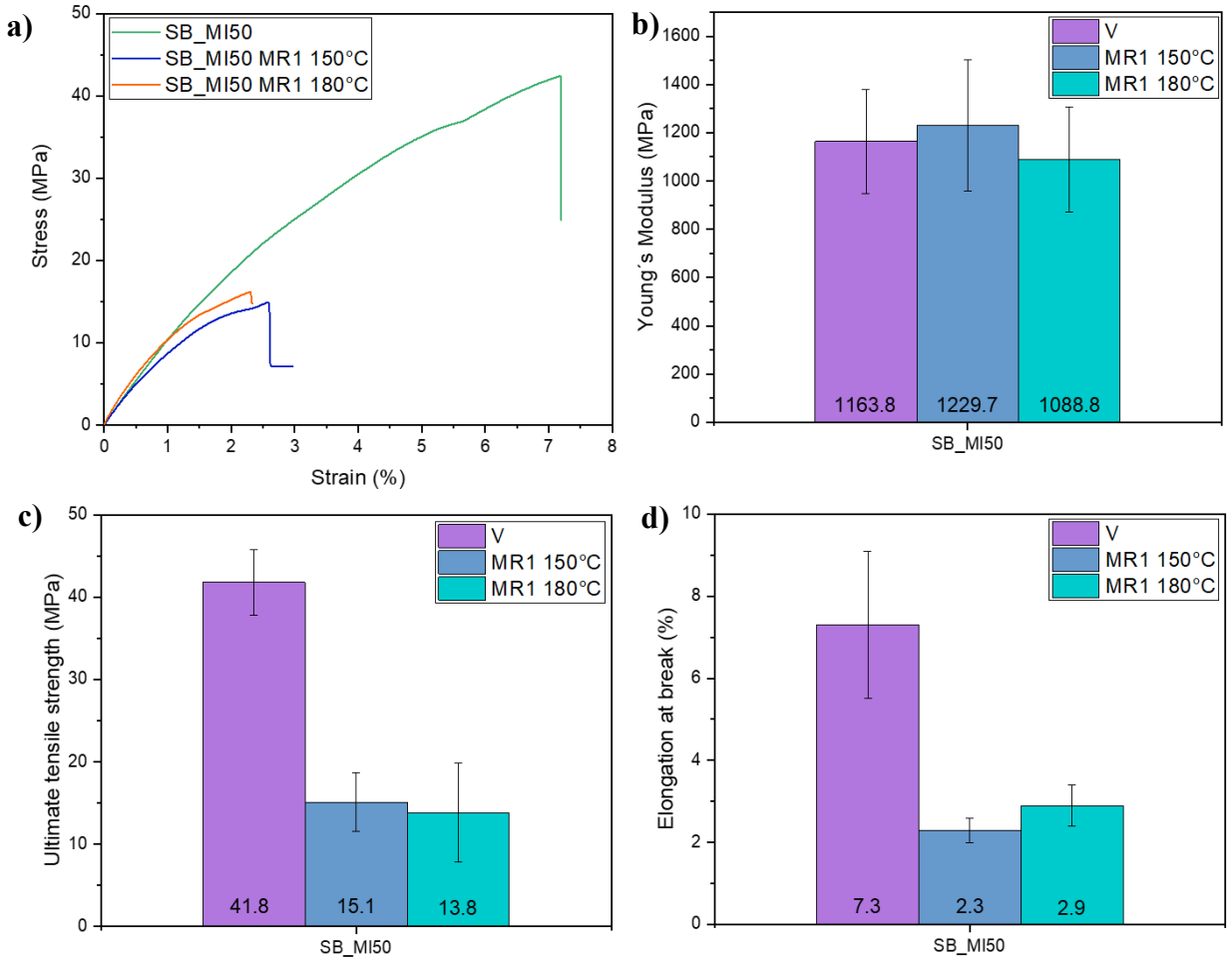

Figure 3.15 a) Representative stress-strain curves of SB_MI50 virgin, MR1 150°C, and MR1 180°C, and b) Young´s modulus (MPa), c) tensile strength (MPa), d) elongation at break (%).

An additional comparison between MI50, MI75, and SB_MI50 thermosets and the samples reprocessed in the same conditions (180°C, 3 MPa, 30 min) can be made. After reprocessing, SB_MI50 was not only the thermoset with the higher elastic modulus among the mechanically recycled samples (1088.8 MPa), but also the material that retained better its mechanical properties.

SB_MI50 showed a 6 % reduction of the Young´s modulus, against the 69 and 78% reduction for MI50 and MI75 respectively. The drop in the mechanical properties for MI50 and MI75 could be caused by the more restricted chain mobility, resulting in an inadequate fusion of all grinded fragments together, as noted in other systems.[59],[60] On the other hand, the higher flexibility of SB_MI50 and the likely lower activation energy, correlated to the nature of its chemical exchange reaction, could be considered responsible for the lower starting elastic modulus and its higher retention after reprocessing.

3.6.2 Second cycle

A second mechanical recycling was performed on the samples. The ground thermosets were added with $Zn(OAc)_2$ and reshaped into new films, visible in Figure 3.16, by hot pressing. Since the mechanical performances of MI50 and MI75 after one reprocessing cycle at 180°C for 1h turned out to be less mechanically performing (with lower mechanical properties), these samples were not furtherly reprocessed.

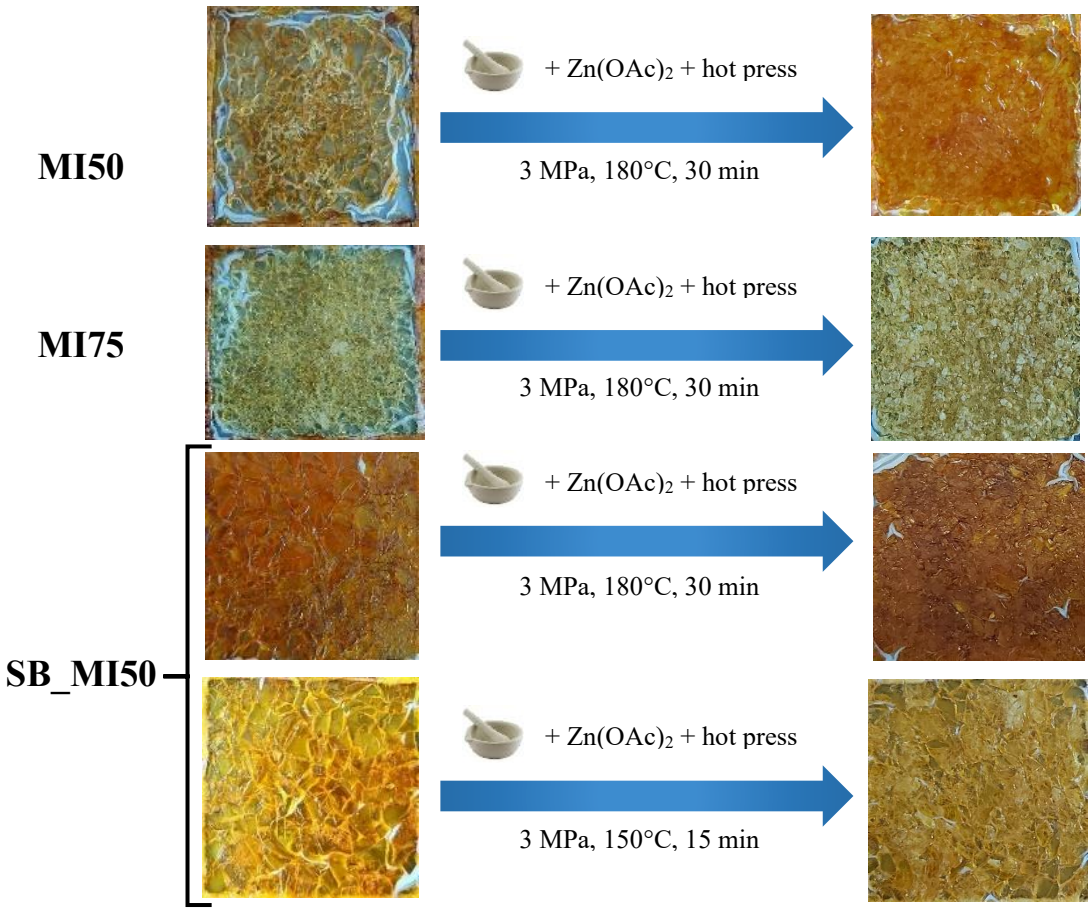

Figure 3.16 Mechanically recycling procedure for the twice-reprocessed thermosets MI50, MI75 and SB_MI50.

Tensile testing assessed the mechanical properties of the twice-reprocessed thermosets. The representative curves of the reprocessed samples and their tensile properties are shown in Figure 3.17. After the second reprocessing, the thermosets illustrated a further reduction in the elastic modulus with respect to the original photocured resins, but values very close to the first reprocessed samples. In the case of MI50 and MI75, a slight increase after the second reprocessing was observable. A reason for this change could be due to post-curing during the reprocessing via hot-pressing, since the presence of a small number of unreacted sites that were detected in the virgin thermosets. All samples exhibited stress values at break comparable to the once-reprocessed thermosets. A decrease in the elongation at break was more apparent as a feature specifically for the twice-reprocessed samples. However, SB_MI50 was an exception, because when hot pressed at 150°C for 15 min, it still retained its strain.

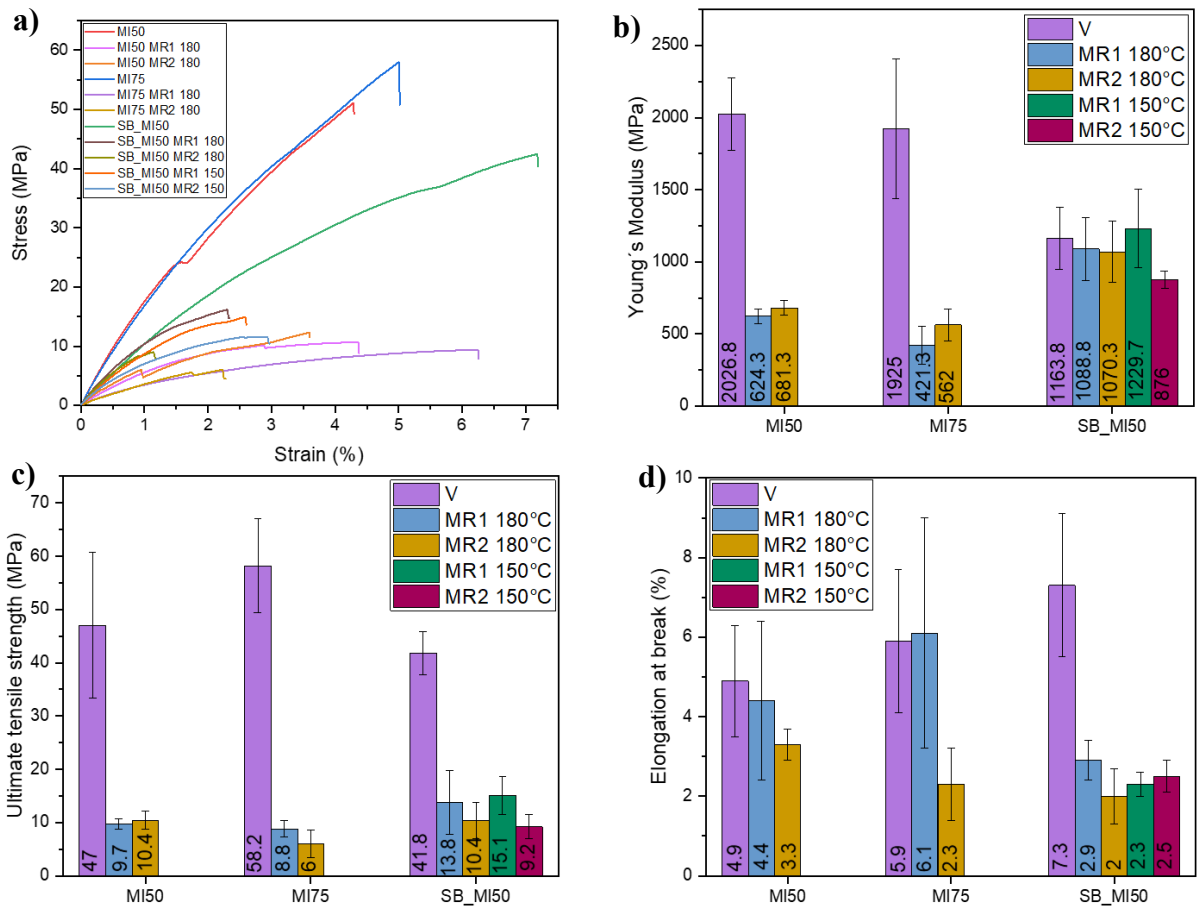

Figure 3.17 a) Tensile stress-strain curves of MI50, MI75, and SB_MI50 virgin thermosets, one and twice reprocessed samples, and b) Young´s modulus (MPa), c) tensile strength (MPa), d) elongation at break (%).

An FTIR analysis was performed on the twice reprocessed samples. The spectra of the mechanically recycled thermosets (Figure 3.18) were compared with the ones of the virgin materials. In the case of

both MI50 and MI75 (Figure 3.18a, b), the signal at 1721 cm^{-1} belonging to the ester bonds (C=O) was detected. Furthermore, some changes ascribable to the presence of zinc acetate were also observable. The peak at 1595 cm^{-1}, associated with the C=C aromatic bonds, showed a small shoulder, probably due to the formation of a zinc-carboxylate complex (Figure 3.19), with an adsorption band between 1560 and 1520 cm^{-1}. This result could be explained by the fact that grinding the thermosets before reprocessing led to some bond breaking, and mixing the obtained fragments with zinc acetate helped mobilize the catalyst in the thermoset network. Carboxylate-zinc vibrations were also attributed to the peak at 1408 cm^{-1}.[61],[57] Besides, after two cycles of mechanical recycling the appearance of the OH adsorption band, together with the reduction of the ester signal, was observed for these thermosets (MI50 and MI75). For the reprocessed SB_MI50 at 180 and 150°C, both the signals for the ester bonds and the C=C aromatic vibrations were detected (Figure 3.18c). Although, some changes are noticeable, including the appearance of a high peak at 1674 cm^{-1} that might be come from a shift in the imine signal, or to the aldehyde group, suggesting the probable opening of only a small fraction of material.

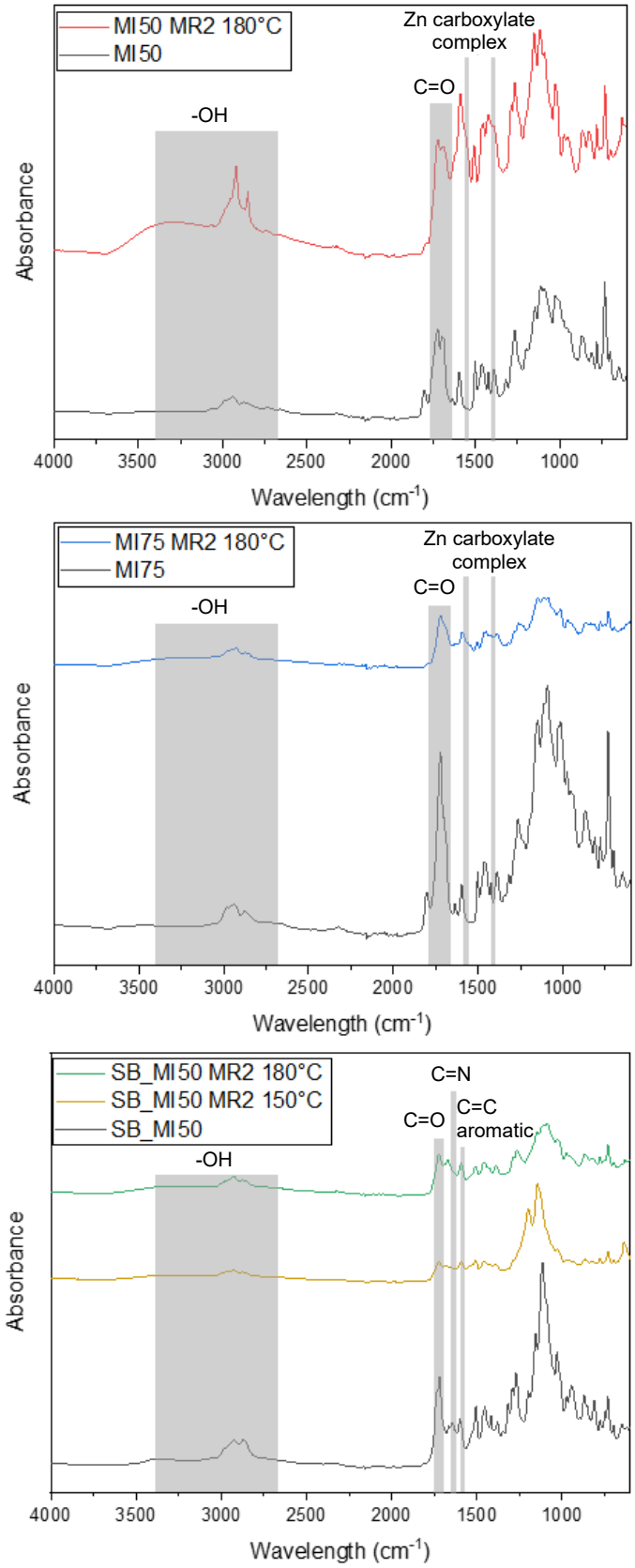

Figure 3.18 ATR-FTIR spectra of a) MI50, b) MI75 and c) SB_MI50 before and after reprocessing.

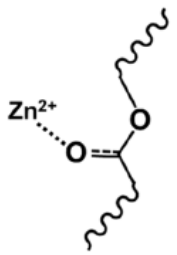

Figure 3.19 Zinc carboxylate complex.

3.7 Chemical recycling

Degradation experiments were performed by immersing MI50 and MI75 at 100°C in various solvents, such as methanol, 0.5 M NaOH, and 1 M NaOH. The 1 M NaOH showed the best results in the shortest time, reaching solubilization after 3h. The ideal degradation mechanism is one based on the use of an appropriate reactive solvent. In this case, an alkaline solution (1 M NaOH) depolymerized the material by cleavage of covalent bonds. In this set of tested thermosets, the secondary esters act like heat-cleavable linkages.[62] The oligomers obtained were recovered by evaporation of the solvent after acidification of the solution, reaching a pH of 2. This last step was necessary since a base-catalyzed reaction of ester groups leads to the formation of stabilized carboxylate anions and alcohols, as shown in Equation 3.1, making the degradation of esters thermally irreversible.

$$RCOOR' + OH^- \rightarrow RCOO^- + R'OH \qquad (\mathbf{3.1})$$

In an acidic solution instead, protons can promote the reformation of ester function, making the degradation of esters reversible. [63],[64]

Ethanol additional and the mixing of the mixture at room temperature was performed overnight. A filtration was then performed to remove the salt in the previous steps, and the solution was reduced under pressure. A powder was finally collected for both MI50 and MI75 and after the addition of zinc acetate (5% w/w) it was reprocessed via hot pressing at 120°C, for 30 min under 3 MPa. In the case of the chemically recycled MI50 since the powder proved to be quite sticky it wasn´t possible to form a homogeneous film. A compact film was instead obtained for the chemically recycled MI75. The procedure followed for the chemical recycling of the vinyl ester thermosets MI50 and MI75 is summarized in Figure 3.20.

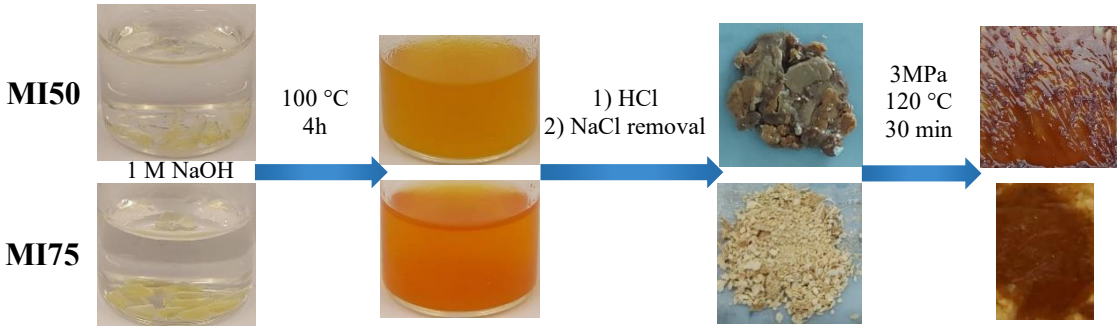

Figure 3.20 Summary of the chemical recycling procedure for MI50 and MI75.

An FTIR analysis was performed on MI75 chemically recycled film (MI75 CR), and its spectrum was compared with the ones of the chemically recycled powder (MI75 deg) and the virgin thermoset (Figure 3.21). Both MI75 deg and MI75 CR showed the characteristic peak at 1721 cm^{-1} ascribable to the ester bond. Besides the formation of an adsorption band around 3000 cm^{-1}, ascribable to the OH groups, was observable, confirming the depolymerization of the network.

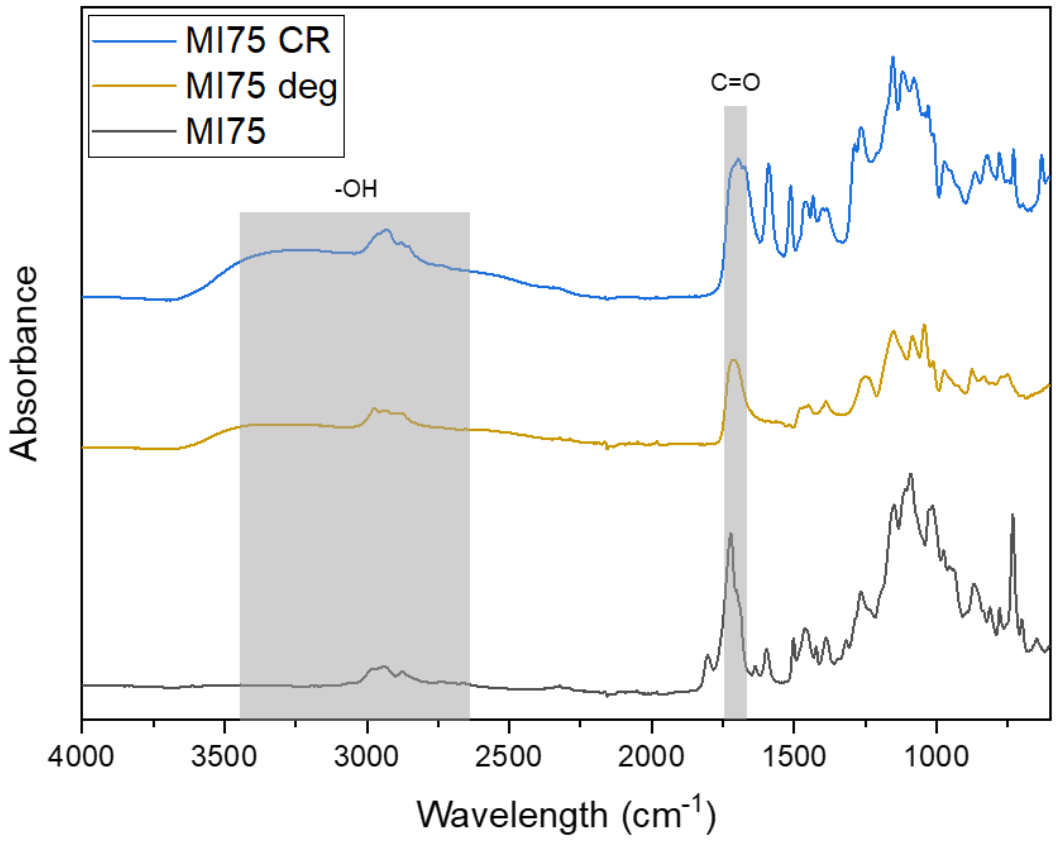

Figure 3.21 ATR_FTIR spectra of MI75, its degraded powder (MI75 deg) and the chemically recycled film (MI75 CR).

Next, the chemical structure of MI50 degraded powder was investigated via FTIR spectroscopy. The FTIR analysis was performed twice on the tested material, and resulted in two different spectra (MI50 deg1 and MI50 deg2), shown in Figure 3.22, and compared with the virgin thermoset, the monomers MI and MV and the starting building blocks vanillin (V) and isosorbide (IS). In the MI50 deg1 spectrum, the presence of peaks in the same adsorption bands as for vanillin was detected, such as the peak at 1694 cm^{-1} ascribable to the aldehyde group, suggesting the presence of this building block. Nevertheless, the appearance of other picks was detected. Both in MI50 deg1 and MI50 deg2 spectra, an adsorption band between 3600 cm^{-1} and 2350 cm^{-1}, ascribable to OH groups, was observed. However, the ester peaks are not easily detected (either absent or present in a low concentration). This implies an almost complete depolymerization of this thermoset in alkaline solution. The inability of MI50 to be chemically recycled into a new homogeneous film could be due to the lower content of MI, and so a lower number of reactive sites available for reprocessing.

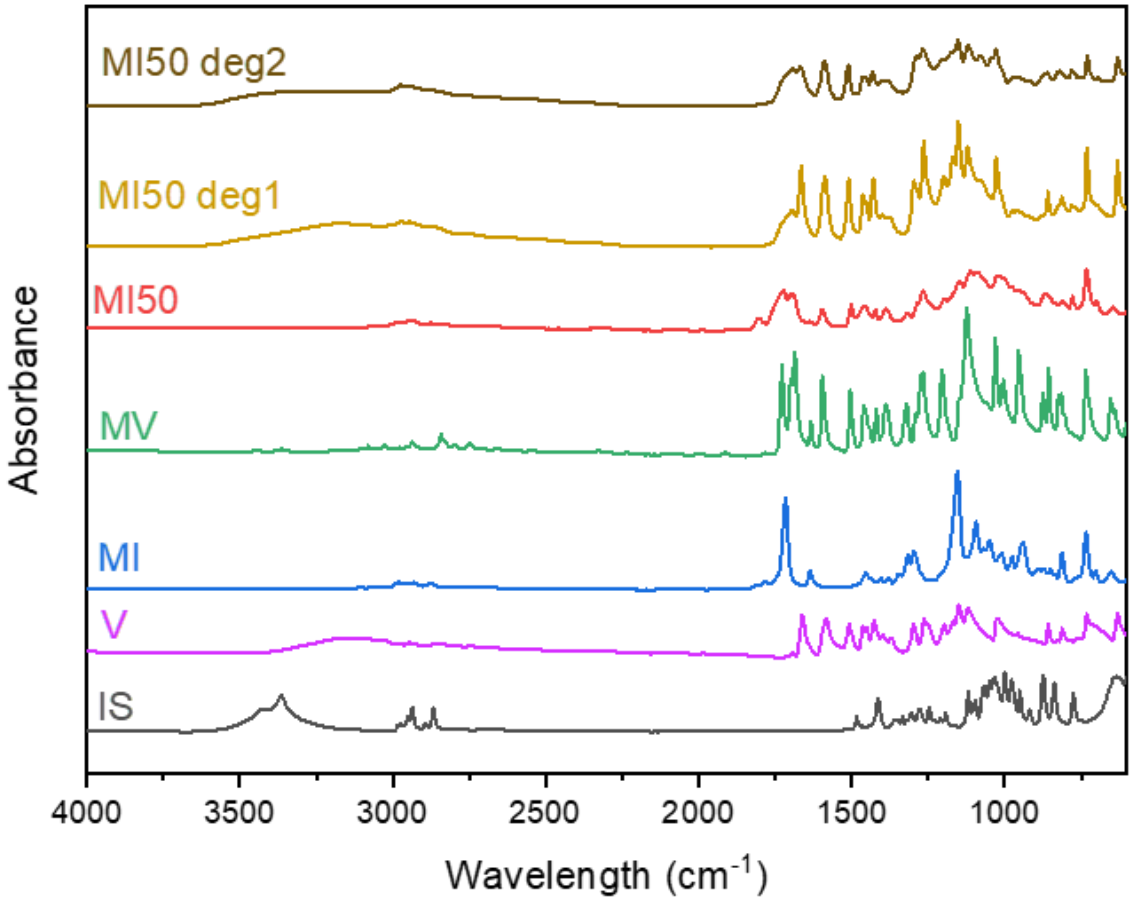

Figure 3.22. ATR_FTIR spectra of MI50 degraded powder (MI50 deg1 and MI50 deg2), the virgin thermosets (MI50), the monomers MI and MV, and the starting building blocks.

Tensile testing was employed to investigate the mechanical properties of the chemically recycled MI75. The representative stress-strain curves of the virgin thermoset MI75 and all the reprocessed samples and their tensile properties are shown in Figure 3.23.

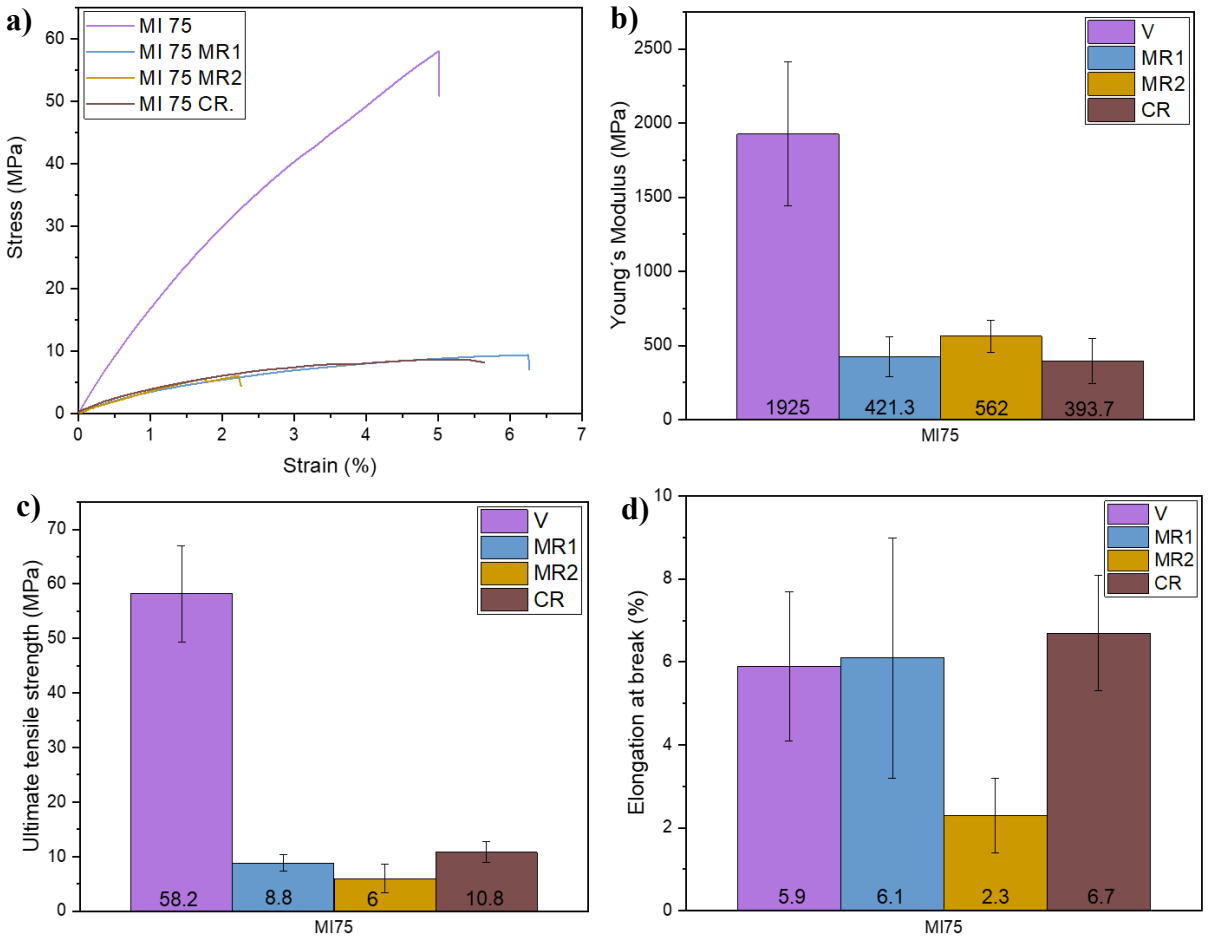

Figure 3.23 a) Tensile stress-strain curves of MI75 and all the reprocessed samples, and b) Young´s modulus (MPa), c) tensile strength (MPa), d) elongation at break (%).

A decrease in Young´s modulus was observed after the chemical recycling, reaching a value of 393.7 MPa with respect to 421.3 and 562 MPa for once and twice-reprocessed samples respectively. Nevertheless, the reduction in the elastic modulus was not as significant as the one gained after the first reprocessing. Besides, an increase in both stress and elongation at break was noted. The lower mechanical properties of the chemically recycled MI75 could be due to a not complete esterification reaction, confirmed by the presence of the OH adsorption band in the FTIR spectrum (Figure 3.21), and therefore the presence of OH functions in the recycled polymer network.

Focusing instead on the vanillin-based imine thermoset SB_MI50, the chemical degradation was tested by immersing the samples into vials with 0.1 M HCl, 1 M NaOH and an excess of diamine (Dom). Specimens soon after immersion in the solvents and after 24 h are shown in Figure 3.24a, b. No degradation was visible in 0.1 M HCl solution, despite the presence of imine bonds in the network

that in previous work turned out to be susceptible to acidic solvents.[65],[66] Imine bonds can be hydrolyzed in mildly acidic conditions, and the sensitivity of these linkages to water should facilitate the degradation. Nevertheless, in this study no degradation either swelling was observed, probably because of the high degree of crosslinking and the high content of aromatic groups in the network.[48] The alkaline environment led instead to a partial but not significant degradation of the samples; as a matter of fact, the benzoic imine bond is known to be stable in alkaline solution[67], and the obtained limited dissolution could be ascribable to the effect of the solvent on the ester bonds, also present in the network. Finally, the thermoset was dissolved after immersion in excess of diamine for 6 h at 80°C. The complete solubilization in the diamine was reached because of the susceptibility of imine bonds to amine. A transamination reaction between the imine bonds in the thermoset network and the amino groups in the solvent, with an associative dynamic character, took place, leading to total depolymerization of the network.[68] The solubilized material was then precipitated in water, and after vacuum filtration, a powder was collected (Figure 3.24c).

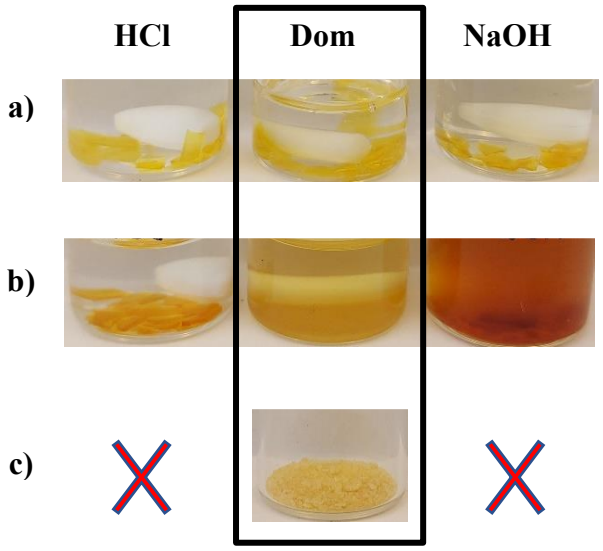

Figure 3.24 (a, b) Photo of specimens in 0.1 M HCl, Dom and 1 M NaOH a) soon after immersion and b) after 21 h. c) Chemically recycled powder after vacuum filtration.

The good chemical solvent resistance shown by this thermoset in common solvents, combined with its selective solubility in a specific chemical such as a diamine, is a promising start towards chemical recycling.

The collected powder was subsequently analyzed via ATR-FTIR spectroscopy. A comparison between the spectra of the chemically degraded material and the virgin SB_MI50 is shown in Figure 3.25. After the depolymerization step, the characteristic peaks at 1721 and 1645 cm^{-1}, ascribable to

the ester and the imine bonds respectively, were detected. Nevertheless, a change in the spectra was visible, and the appearance of the adsorption band at 3500 cm^{-1}, related to the formation of amine bonds (-NH) confirmed the occurrence of the transimination reaction.

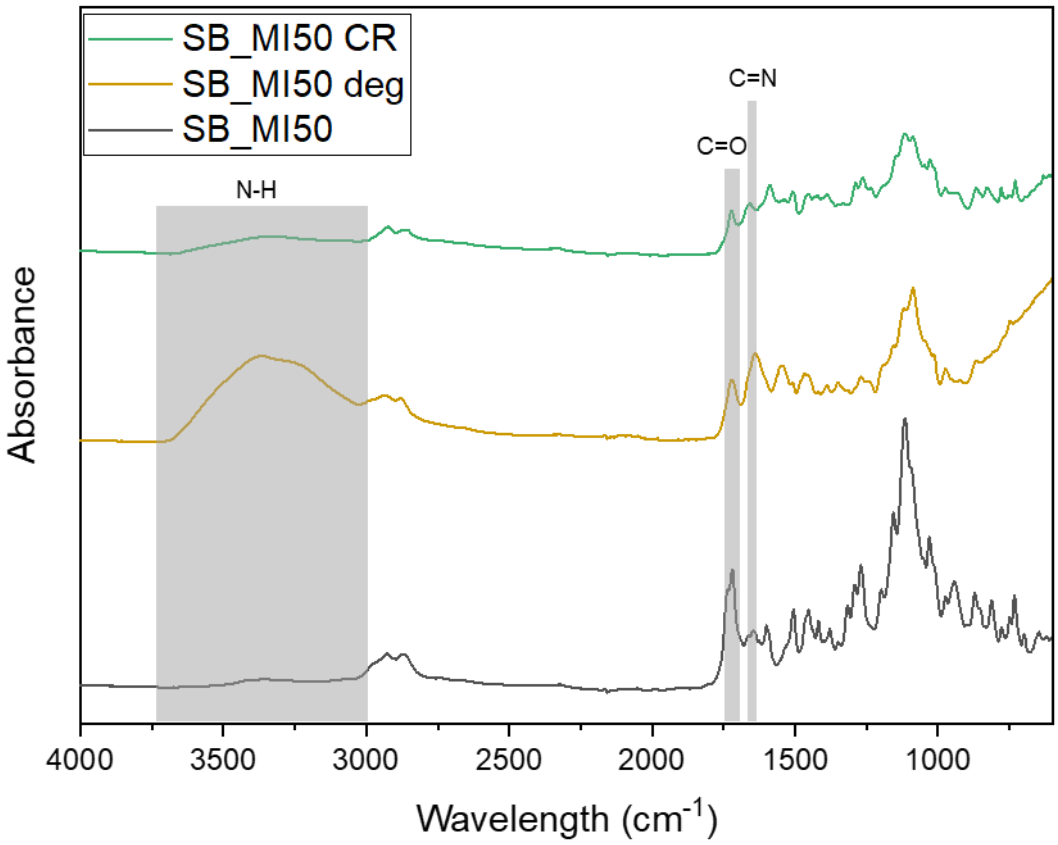

Figure 3.25 ATR-FTIR spectra comparison between SB_MI50 chemically degraded powder and the virgin thermoset.

The obtained oligomers including amino end groups were used to prepare a new resin, by adding MV and BAPO. Zinc acetate was also added to the mixture that was reprocessed via hot pressing at 140°C for 30 min, under 3 MPa, yielding a new homogeneous film. The addition of MV and the photo-initiator was realized to induce, during the thermal reprocessing, the imine exchange in the solid state. The chemical recycling process adopted for SB_MI50 is summarized in Figure 3.26.

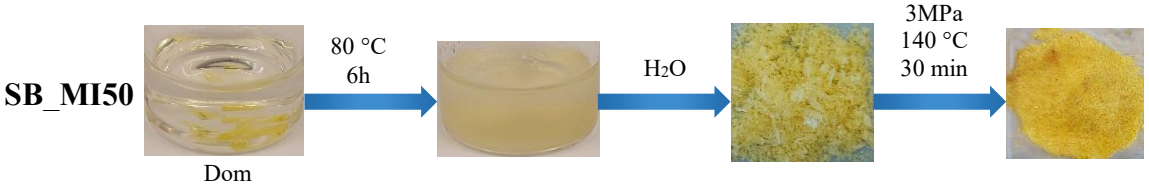

Figure 3.26 Summary of the chemical recycling procedure for MI50 and MI75.

The chemical structure of the chemically recycled film was investigated via FTIR (Figure 3.22). No peaks were detected for the aldehyde group, proving that MV, added to the chemically recycled powder just before reprocessing, reacted with the amine groups. Nevertheless, the adsorption band at 3500 cm^{-1} was still detected, meaning that additional amine groups were available for further reaction. The mechanical properties of the chemically recycled SB_MI50 were investigated by tensile testing. The representative curves of the virgin thermoset SB_MI50 and all the reprocessed samples, both mechanically and chemically, are shown in Figure 3.27, together with their mechanical properties. The elastic modulus of the chemically recycled SB_MI50 (1045 MPa) proved comparable with Young´s modulus of both the mechanically recycled samples and the virgin material. Besides, an increase in both the ultimate tensile strength was the elongation at break was noticed.

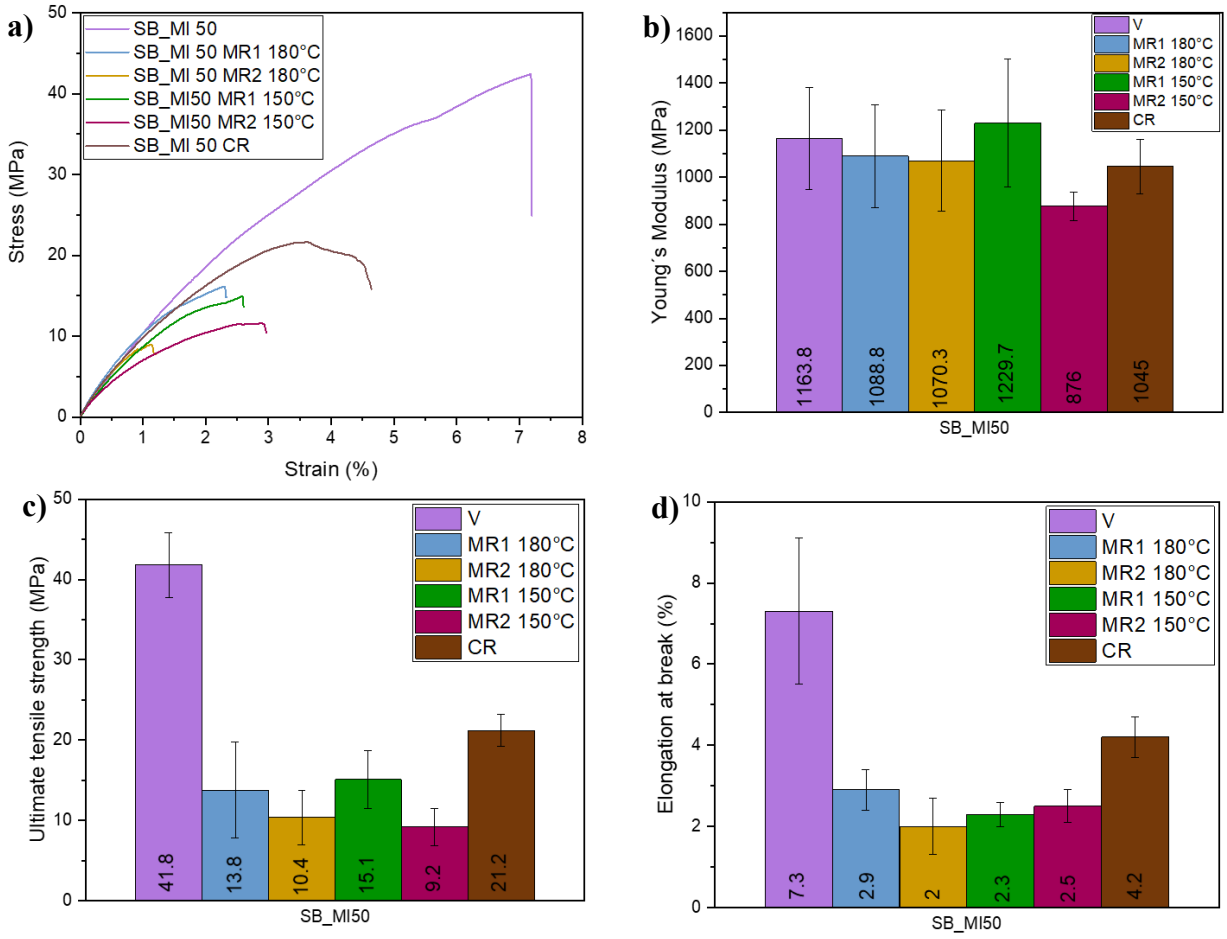

Figure 3.27 a) Tensile stress-strain curves of SB_MI50 and all the reprocessed samples, and b) Young´s modulus (MPa), c) tensile strength (MPa), d) elongation at break (%).

Conclusion

This work has focused on the design and testing of four photocurable, thermally reprocessable, and chemically recyclable biobased thermosetting resins, synthesized using isosorbide and vanillin as renewable building blocks. A methacrylation reaction was performed on the starting components. The introduction of vinyl bonds in the network, confirmed by FTIR spectroscopic analysis, endowed the final resins with photocurability, making them suitable for digital light processing (DLP) 3D printing. Methacrylated isosorbide (MI) and methacrylated vanillin (MV) were mixed in different ratios, resulting in three vinyl ester resins: MI50, MI75, and MI100. A fourth imine resin, SB_MI50, was formulated by mixing MI with a Schiff base resin, where the latter was synthesized through a reaction between the aldehyde group of MV and the amino group of a diamine. Next, the resins MI50, MI75, and SB_MI50 were successfully 3D printed into thermoset films, a process that was confirmed using FTIR analysis showing the reduction of vinyl bonds after UV irradiation. MI100 did not result in a coherent film likely because of the stiffness imparted by the higher content of the isosorbide bicycling ring. All cured thermosets exhibited good thermal stability, with an onset of degradation above 150°C. Thermosets also demonstrated excellent solvent resistance properties (average gel content above 87%), indicating a high degree of cross-linking. The more rigid monomers, MI50 and MI75, resulted in final thermosets with high mechanical strength and high Young´s moduli values (2026.8 and 1925.0 MPa respectively) indicating high stiffness. On the other hand, the Schiff base thermoset SB_MI50 showed a lower Young´s modulus (1163.8 MPa) and a higher extension at the breakpoint, likely due to the higher flexibility of the monomer used. MI100 didn´t undergo tensile testing because of its fragile behavior.

The incorporation of dynamic covalent bonds into the polymer networks allowed for the mechanical recycling of all thermosets following a simple procedure of their grinding, consecutive addition of zinc acetate, and final thermal processing via hot pressing. Analytical results suggest that MI50 and MI75 thermosets were able to rearrange the network topology via transesterification reactions, which was triggered by the application of heat as an external stimulus. On the other hand, in the case of SB_MI50, imine bonds were used for the redistribution of the network connectivity, following a metathesis pathway. Furthermore, the ability of SB_MI50 to be thermally reprocessed at a lower temperature than the ester-containing thermosets MI50 and MI75, suggested imine bonds require lower energy in order to be activated, conferring the material with easier recyclability.

A decrease in the mechanical properties, such as elastic modulus and ultimate tensile strength, was observed for MI50 and MI75 after the first recycling cycle. This is likely due to the limited chain mobility resulting in an inadequate fusion of the ground fragments. However, the twice-reprocessed

samples still showed a surprisingly small increase in Young´s modulus. The likely reason for this is the presence of unreacted monomer and its post-curing during reprocessing. The mechanical properties of SB_MI50 remained similar after two mechanical recycling cycles. This behavior could be related to higher flexibility and lower bond exchange activation energy of SB_MI50.

The presence of labile bonds in the network also conferred the tested thermosets with chemical recyclability. The ester-containing MI50 and MI75 were easily depolymerized in alkaline solutions, and the recovered powders could be reprocessed via hot pressing, following the previously described procedure. Unfortunately, only MI75 chemical recycling allowed for the generation of a new homogenous film. This is likely due to the higher content of MI in MI75, which consequently contributes to the higher number of reactive sites as compared to MI50. SB_MI50 was able to be chemically recycled in the presence of an excess of diamine, thanks to an associative exchange mechanism following the transimination pathway. The collected recycled oligomers including amino end groups were successfully used to prepare a new resin, that was subsequently cured via hot pressing.

A decrease in MI75 Young´s modulus was observed after chemical recycling (393.7 MPa), however, the chemically recycled SB_MI50 retained its elastic modulus (1045 MPa), demonstrating better stability in comparison with other thermosets.

In conclusion, here described are new photocurable, reprocessable, and chemically recyclable thermosets with novel designs consisting of isosorbide and vanillin as starting platforms. These derivatives of naturally abundant bio-materials (glucose and lignin) exhibit promising properties that make them attractive alternatives to petroleum-based polymers. Exploring their properties and potential uses in the future will surely aid in helping us overcome the issues of the overuse and depletion of fossil fuels and plastic pollution.

Bibliography

[1] PlasticsEurope, Plastics – the Facts 2022, October 2022, https:// s://plasticseurope.org/knowledge-hub/plastics-the-facts-2022/.

[2] Statista, Cumulative plastic production volume worldwide from 1950 to 2050, March 2023, https://www.statista.com/statistics/1019758/plastics-production-volume-worldwide/#:~:text=Published%20by%20Statista%20Research%20Department%2C%20Mar%2024%2C%202023,increase%20to%2034%20billion%20metric%20tons%20by%202050.

[3] L. Parker, The world's plastic pollution crisis explained, June 2019, National Geographic, https://www.nationalgeographic.com/environment/article/plastic-pollution.

[4] J. McGlade, I. S. Fahim, D. Green, P. Landrigan, A. Andrady, , M. Costa, A. Turra, From Pollution To Solution: a global assessment of marine litter and plastic pollution, *United Nations Environment Programme* **2021**.

[5] UN, *UN Sustain. Dev. Knowl. Platf.*

[6] A. Gandini, T. M. Lacerda, From monomers to polymers from renewable resources: Recent avances. Prog. Polym. Sci. **2015**, *48*, 1− 39.

[7] A. Gandini, T. M. Lacerda, A. J. F Carvalho, E. Trovatti, Progress of Polymers from Renewable Resources: Furans, Vegetable Oils, and Polysaccharides. Chem. Rev. **2016**, *116*, 1637−1669.

[8] F. Gamardella, S. De la Flor, X. Ramis, À. Serra, Towards the Recyclability of Thermosetting Polymers*,* Tarragona, **2020**.

[9] M. Hong, E. Y.-X. Chen, Chemically recyclable polymers: a circular economy approach to sustainability, *Green Chem.*, **2017**, *19*, 3692.

[10] S. Agarwal et al.,Thermosets: Structure, Properties, and Applications, Elsevier, **2018**.

[11] L. Shen, J. Haufe, M. K. Patel, Product overview and market projection of emerging bio-based plastics PRO-BIP 2009, **2009**, 43.

[12] S. Wang, S. Ma, Q. Li, B. Wang, J. Zhu, Robust, Fire-Safe, Monomer-Recovery, Highly Malleable Thermosets from Renewable Bioresources, *Macromolecules* **2018**, *51*, 20, 8001–8012.

[13] J. Liu, S. Wang, Y. Peng, J. Zhu, W. Zhao, X. Liu, Advances in sustainable thermosetting resins: From renewable feedstock to high performance and recyclability, *Progress in Polymer Science* **2021**, *113*, 101353.

[14] Y. Xu, G. Hua, M. Hakkarainen, K. Odelius, Isosorbide as Core Component for Tailoring Biobased Unsaturated Polyester Thermosets for a Wide Structure−Property Window, *Biomacromolecules* **2018**, *19*, 3077−3085.

[15] D. Juais, A. F. Naves, C. Li, R. A. Gross and L. H. Catalani, *Macromolecules*, 2010, **43**, 10315–10319.

[16] N. Azizi, Y. Chevalier and M. Majdoub, *Ind. Crops Prod.*, 2014, **52**, 150–157.

[17] M. Fache, B. Boutevin, S. Caillol, Vanillin Production from Lignin and Its Use as a Renewable Chemical, *ACS Sustainable Chem. Eng.* **2016**, 4, *1*, 35–46.

[18] T. T. Vu, Y.I. Lim, D. Song, K.R. Hwang, D.K. Kim, Economic analysis of vanillin production from Kraft lignin using alkaline oxidation and regeneration, Biomass Conversion and Biorefinery **2023**, *13*, 1819–1829.

[19] C. Zhang, S. A. Madbouly, M. R. Kessler, Renewable Polymers Prepared from Vanillin and Its Derivatives, Macromol. Chem. Phys. **2015**, *216*, 1816−1822.

[20] C. Aouf, J. Lecomte, P. Villeneuve, E. Dubreucq, H. Fulcrand, Chemo-enzymatic functionalization of gallic and vanillic acids: synthesis of bio-based epoxy resins prepolymers, *Green Chem.*, **2012**, *14*, 2328-2336.

[21] M. Fache, E. Darroman, V. Besse, R. Auvergne, S. Caillol, B. Boutevin, Vanillin, a promising biobased building-block for monomer synthesis, *Green Chemistry* **2014**, *16*, 1987-1998.

[22] S. Wang, S. Ma, C. Xu, Y. Liu, J. Dai, Z. Wang, X. Liu, J. Chen, X.Shen, J. Wei, J. Zhu, Vanillin-Derived High-Performance Flame Retardant Epoxy Resins: Facile Synthesis and Properties, *Macromolecules* **2017**, *50*, 5, 1892–1901.

[23] Y. Jin, Z. Lei, P. Taynton, S. Huang, W. Zhang, Review Malleable and Recyclable Thermosets: The Next Generation of Plastics, *Matter* **2019,** *1*, 1456–1493.

[24] G. M. Scheutz, J.J. Lessard, M. B. Sims, B. S. Sumerlin, Adaptable Crosslinks in Polymeric Materials: Resolving the Intersection of Thermoplastics and Thermosets, *J. Am. Chem. Soc.* **2019**, 141, 41, 16181–16196.

[25] B. R. Elling, W. R. Dichtel, Reprocessable Cross-Linked Polymer Networks: Are Associative Exchange Mechanisms Desirable, *ACS Central Science* **2020**, *6*, 9, 1488-1496.

[26] A. Liguori, M. Hakkarainen, Designed from Biobased Materials for Recycling: Imine-Based Covalent Adaptable Networks, *Macromol. Rapid Commun.* **2022**, *43*, 2100816.

[27] Jiho Lee, Hoon Kim, Hyoungsoo Kim, Taehyub Lee, Jeong-Hwan Kim, Alberto Andreu, Sanglae Kim, Yong-Jin Yoon, Average-Accumulated Normalized Dose (A-AND) predicts ultimate tensile strength and elastic modulus of photopolymer printed by vat photopolymerization, *Additive Manufacturing* **2022**, *55*, 102799

[28] G. Chyr, J. M. DeSimone, Review of high-performance sustainable polymers in additive manufacturing, Green Chem., 2023, 25, 453.

[29] Digital Light Processing 3D Printing of Gyroid Scaffold with Isosorbide-Based Photopolymer for Bone Tissue Engineering, *Biomolecules* **2022**, *12*(11), 1692.

[30] V. S. D. Voet, Closed-Loop Additive Manufacturing: Dynamic Covalent Networks in Vat Photopolymerization, *ACS Mater. Au* **2023**, *3*, 18−23.

[31] V. S. D. Voet, J. Guit, K. Loos, Sustainable Photopolymers in 3D Printing: A Review on Biobased, Biodegradable, and Recyclable Alternatives, *Macromol. Rapid Commun.* **2021**, *42*, 2000475.

[32] E. Morici, N. T. Dintcheva, Review Recycling of Thermoset Materials and Thermoset-Based Composites: Challenge and Opportunity, *Polymers* **2022**, *14*, 4153.

[33] B. Zhang, K. Kowsari, A. Serjouei, M. L. Dunn, Q. Ge, Reprocessable thermosets for sustainable three-dimensional printing, *Nat.Commun.* **2018**, *9*, 1831.

[34] P.F. Jacobs, Fundamentals of stereolitography, International Solid Freeform Fabrication Symposium **1992**.

[35] C. Hofstettera, S. Ormanb, S. Baudisb, J. Stampfla, Combining cure depth and cure degree, a new way to fully characterize novel photopolymers, *Additive Manufacturing* **2018** 24, 166–172.

[36] R. K. Mishra, J. Cherusseri, A. Bishnoi, S. Thomas, "Nuclear Magnetic Resonance Spectroscopy" *Spectroscopic methods for nanomaterials characterization*, Elsevier **2017** (13), 369-415.

[37] M. K. Singh, A. Singh, Nuclear Magnetic Resonance Spectroscopy, *Characterization of Polymers and Fibres*, The Textile Institute Book Series, **2022** (14), 321-339.

[38] A. J. Simpson, M. J. Simpson, R. Soong, Nuclear Magnetic Resonance Spectroscopy and Its Key Role in Environmental Research, *Environmental Science & Technology* **2012** *46* (21), 11488-11496.

[39] L. Barbeş, C. Rădulescu, C. Stihi, ATR-FTIR spectrometry characterisation of polymeric materials, *Romanian Reports in Physics*, **2014** 66(3), 765-777.

[40] P. Gabbott (ed.) *Principles and applications of thermal analysis*. John Wiley & Sons, **2008**.

[41] T. Hatakeyama, F. X. Quinn, *Thermal analysis: fundamentals and applications to polymer science*. [sl], **1999**.

[42] S. Ma, Y. Jiang, X. Liu, L. Fan, J. Zhu, Bio-based tetrafunctional crosslink agent from gallic acid and its enhanced soybean oil-based UV-cured coatings with high performance, *RSC Adv.* **2014**, *4*, 23036.

[43] J. D. Menczel, R. B. Prime, (Eds.). *Thermal analysis of polymers: fundamentals and applications*. John Wiley & Sons. **2009**.

[44] C. H. Spink, Differential Scanning Calorimetry. *Biophysical Tools for Biologists: In Vitro Techniques*, **2011**, 115.

[45] Web site - https://arlonemd.com/wp-content/uploads/2020/05/Measuring-and-Understanding-Tg.pdf, [online], **2011**.

[46] A. Liguori, S. Subramaniyan, J. G. Yao, M. Hakkarainen, Photocurable extended vanillin-based resin for mechanically and chemically recyclable, self-healable and digital light processing 3D printable thermosets, *European Polymer Journal* **2022,** *178*, 111489.

[47] S. Shin, B. Kim, E. Chang, J. K. Chobd, D. H. Suh, A biobased photocurable binder for composites with transparency and thermal stability from biomass-derived isosorbide, *RSC Adv.* **2014**, *4*, 6226.

[48] Y. Xu, K. Odelius, M. Hakkarainen, Photocurable, Thermally Reprocessable, and Chemically Recyclable Vanillin-Based Imine Thermosets, *ACS Sustainable Chem. Eng.* **2020,** *8*, 17272−17279.

[49] Belowich, M. and Stoddart, J., **2012**. Dynamic imine chemistry. *Chemical Society Reviews*, 41(6), p.2003.

[50] E. Fleck, A. Sunshine, E. DeNatale, C. Keck, A. McCann, Joseph Potkay, Advancing 3D-Printed Microfluidics: Characterization of a Gas-Permeable, High-Resolution PDMS Resin for Stereolithography, Micromachines **2021**, *12*, 1266.

[51] P. A. Wilbon, J. L. Swartz, N. R. Meltzer, J. P. Brutman, M. A. Hillmyer, J. E. Wissinger, Degradable Thermosets Derived from an Isosorbide/Succinic Anhydride Monomer and Glycerol, *ACS Sustainable Chem. Eng.* **2017**, *5*, 9185−9190.

[52] Yin, B.; Hakkarainen, M. Oligomeric isosorbide esters as alternative renewable resource plasticizers for PVC. J. Appl. Polym. Sci. 2011, 119 (4), 2400−2407.

[53] Sadler, J. M.; Toulan, F. R.; Nguyen, A.-P. T.; Kayea, R. V.; Ziaee, S.; Palmese, G. R.; La Scala, J. J. Isosorbide as the structural component of bio-based unsaturated polyesters for use as thermosetting resins. Carbohydr. Polym. 2014, 100, 97−106.

[54] Jasinska, L.; Koning, C. E. Unsaturated, biobased polyesters and their cross-linking via radical copolymerization. J. Polym. Sci., Part A: Polym. Chem. 2010, 48 (13), 2885−2895.

[55] W. Liu, T. Xie, R. Qiu, Biobased Thermosets Prepared from Rigid Isosorbide and Flexible Soybean Oil Derivatives, *ACS Sustainable Chem. Eng.* **2017**, *5*, 774−783.

[56] J. M. Sadler, A.T. Nguyen, F. R. Toulan, J. P. Szabo, G. R. Palmese, C. Scheck, S. Lutgend, J. J. La Scala, Isosorbide-methacrylate as a bio-based low viscosity resin for high performance thermosetting applications, *J. Mater. Chem. A*, **2013**, *1*, 12579.

[57] A. Bandegi, M. Amirkhosravi, H. Meng, M. K. R. Aghjeh, I. Manas-Zloczower, Vitrimerization of Crosslinked Unsaturated Polyester Resins: A Mechanochemical Approach to Recycle and Reprocess Thermosets, *Global Challenges* **2022**, *6*, 2200036.

[58] Montarnal, D., Capelot, M., Tournilhac, F., and Leibler, L. (2011). Silica-like malleable materials from permanent organic networks. Science 334, 965–968.

[59] R. Hajj, A. Duval, S. Dhers, L. Avérous, Network Design to Control Polyimine Vitrimer Properties: Physical Versus Chemical Approach, *Macromolecules* **2020**, *53*, 3796−3805.
[60] M. Guerre**,** C. Taplan, R. Nicolaÿ, J. M. Winne, F. E. Du Prez**,** Fluorinated Vitrimer Elastomers with a Dual Temperature Response, *J. Am. Chem. Soc.* **2018**, 140, *41*, 13272–13284.
[61] L. Yue, H. Guo, A. Kennedy, A. Patel, X. Gong, T. Ju, T. Gray, I. Manas-Zloczower, Vitrimerization: Converting Thermoset Polymers into Vitrimers, *ACS Macro Lett.* **2020**, *9*, 836−842.
[62] S. Ma, D. C. Webster, Degradable thermosets based on labile bonds or linkages: A review, *Progress in Polymer Science* **2018,** *76*, 65–110.
[63] M. Partini, R. Pantani, FTIR analysis of hydrolysis in aliphatic polyesters, *Polymer Degradation and Stability* **2007** *92*, 1491-1497.
[64] D. Raghavan, K. Egwim, Degradation of Polyester Film in Alkali Solution, *J. Appl. Polym. Sci.* **2000** *78* (14), 2454-2463.
[65] S. Zhao, M. M. Abu-Omar, Recyclable and Malleable Epoxy Thermoset Bearing Aromatic Imine Bonds, *Macromolecules* **2018**, *51*, 9816−9824.
[66] X. Liu, L. Liang, M. Lu, X. Song, H. Liu, G. Chen, Water-resistant bio-based vitrimers based on dynamic imine bonds: Self-healability, remodelability and ecofriendly recyclability, *Polymer* **2020,** *210*, 123030.
[67] J. Wang, X. Chen, W. Cui, S. Yi, pH-responsive vesicles from supra-amphiphiles based on dynamicimine bond, *Colloids and Surfaces A: Physicochem. Eng. Aspects* **2015,** *484*, 28–36.
[68] A. Liguori, M. Hakkarainen, Designed from Biobased Materials for Recycling: Imine-Based Covalent Adaptable Networks, *Macromol. Rapid Commun.* **2022**, *43*, 2100816.